Adaptive Control and Cooperative Learning of Symbiotic Behavior of Human-Machine-Interaction

by

Ker-Jiun Wang

B.S, National Taiwan University, 2001

M.S. National Cheng Kung University, 2005

M.S, Carnegie Mellon University, 2012

Submitted to the Graduate Faculty of the

Swanson School of Engineering in partial fulfillment

of the requirements for the degree of

Doctor of Philosophy

University of Pittsburgh

2019

UNIVERSITY OF PITTSBURGH

SWANSON SCHOOL OF ENGINEERING

This dissertation was presented

by

Ker-Jiun Wang

It was defended on

October 9, 2019

and approved by

Zhi-Hong Mao, PhD, Professor, Department of Electrical and Computer Engineering, and Bioengineering

Patrick Loughlin, PhD, Professor, Department of Bioengineering, and Electrical and Computer Engineering

George Stetten, PhD, Professor, Department of Bioengineering

Mingui Sun, PhD, Professor, Department of Neurological Surgery, Bioengineering, and Electrical and Computer Engineering

Dissertation Director: Zhi-Hong Mao, PhD, Professor, Department of Electrical and Computer Engineering, and Department of Bioengineering

Adaptive Control and Cooperative Learning of Symbiotic Behavior of Human- Machine-Interaction

Ker-Jiun Wang, PhD

University of Pittsburgh, 2019

Building a Human-Robot Symbiotic environment that robots could live side-by-side with humans, perform joint actions to achieve common goals, and further augment human's existing capabilities is always our dream. Besides numerous benefits, it poses many challenges as well. Most importantly, the robot should have learning and adaptability to coordinate its actions with the human. It should take Human-in-the-Loop co-learning, co-adaptation, and the prediction of mutual consensus behaviors into account to foster a stable closed-loop interaction, such that the robot can have more flexibility to perform a broader range of sensorimotor skills in diverse interaction contexts. Moreover, human and robot need to have a seamless communication interface, with which it can identify a wide spectrum of interaction features, from kinematic trajectories and dynamics profiles, to eye gazes, facial expressions and emotion states, etc., to effectively convey multi-modal intentions.

In this dissertation, we tried to address these challenges by developing a biomimic learning and adaptive control framework, which allows wearable robots to cooperate with humans seamlessly. We used Co-Adaptive Optimal Control and Nonzero-Sum Differential Game to describe the human-machine neuromuscular coordination skills, and utilized iterative Inverse Optimal Control and Inverse Differential Game theory to model the cerebellum cooperative learning procedures. The mathematical derivations of theorems as well as the real human subject research on simulated double-inverted pendulum for human-exoskeleton

cooperative balancing task were conducted, where we demonstrated promising results that our decentralized cooperative learning and control model is comparable to the centralized optimal control strategy. In the meanwhile, we have developed a compact, non-obtrusive and ergonomic wearable Human-Machine Interface, which observes the physiological gestures (i.e., eye/facial expressions, hand/body movements, somatosensory stimulations, etc.) with over 95% accuracy, based on our developed Deep Multi-Spectrogram Convolutional Neural Network decoder, to interpret and communicate multi-modal human intentions with the machines. It allows the end-users to interact with the machines seamlessly using nature and intuitive commands with engaging and immersive experiences. Hopefully our developments can lead to the next generation intelligent symbiotic machines that enable us to go beyond existing cognitive and physical limitations, achieving superior performance in motor generation and perceptual capabilities in the near future.

Table of Contents

List of Tables

List of Figures

1.0 Introduction

In the evolution of human civilization, humans are constantly developing tools to empower themselves. Starting from the Stone Age, our ancestors knew how to use materials to build various tools as extensions of our body powered by muscles. During the Industrial Revolution in the 18th century, we invented steam engines and used the external power to fabricate useful machines under human control. Later in the 19th century, we understood how to use electricity. It paved the ways for the transformative invention of computer-controlled automation processes in the last century, with which it created a new frontier for the humans to interact with the smart machines. Until now in our daily life, think about how many times we use our smartphones to "Google" a piece of information everyday. When we do this, we are extending our brain's memory and knowledge by using a prosthetic device without giving it a second thought. In the next decade or so, even the robots will enter into our homes and workplaces, complementing human abilities and skills in many application domains. A good example is the development of exoskeleton robots as rehabilitation tools and human power augmentation devices. In such scenario, the traditional one-way unilateral interaction will gradually transit to the bilateral interaction architecture, and therefore the humans and machines will constantly monitor and adapt each other's behaviors in all aspects. In the near future, with the advancement of Brain-Computer Interface (BCI), it further outlines the possibility of the unification of human and machines in a single entity by mind. As a result, we are slowly entering into Human 2.0 and we are doing this through a symbiotic relation with our surrounding intelligent environment.

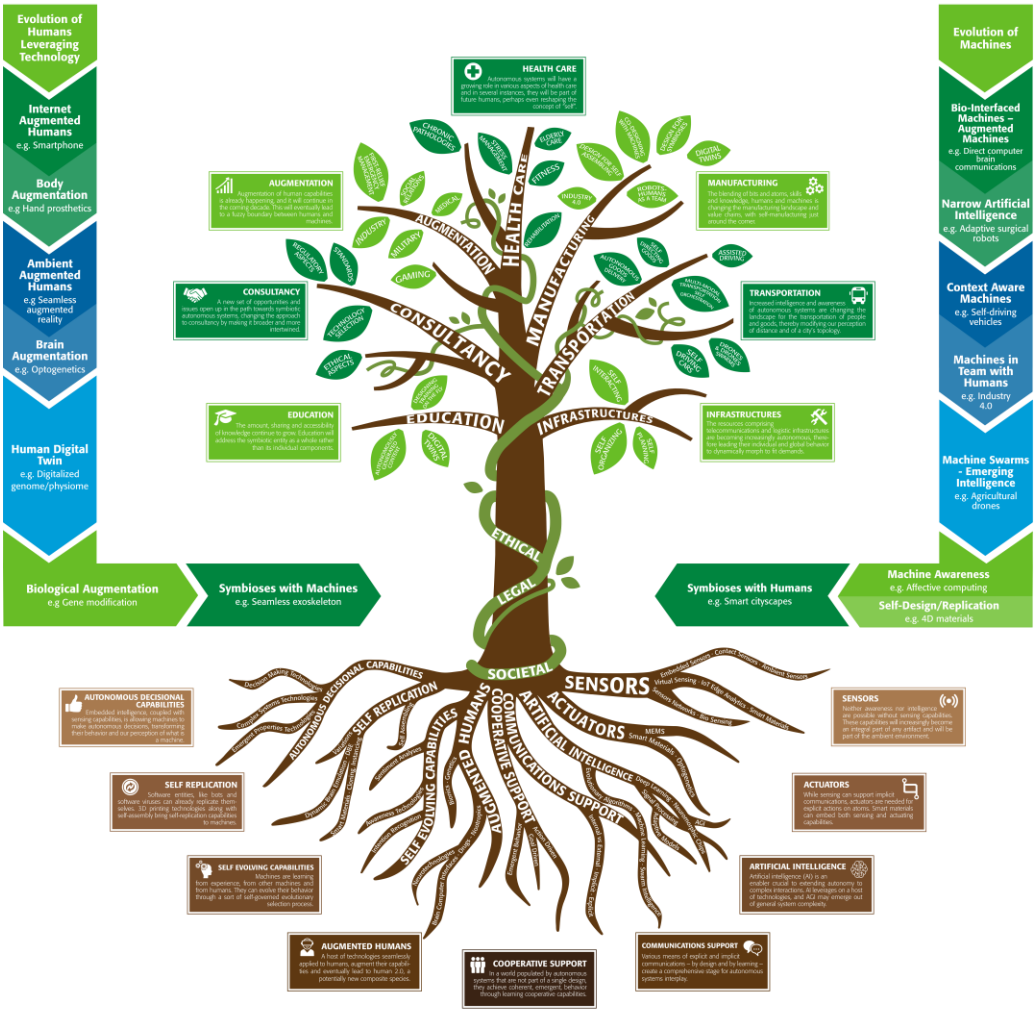

Figure 1.1. Infograph of Symbiotic Autonomous System (adapted from IEEE). The Symbiotic Autonomous Systems (SAS) initiative fosters studies and applications focused on the convergence of human augmentation with the increasing intelligence and awareness of artifacts, leading towards a symbiosis of humans and machines. This will have significant implications for human society as a whole, affecting culture and the economy and prompting new questions about our place on Earth.

There are several grand challenges associated with the dawning of this new era: (1) Since the humans and machines are living together closely, we will be responding to the behaviors of machines and the machines will react to our behaviors in a continuous adaptation fashion. (2) Based on our mother nature, the symbiosis behaviors are deeply inherited in all biological

creatures, from the miniature-scale multicellular organisms to the large-scale human society. How to find the fundamental principles governing the human-human collaboration behavior, with a distributed, bottom-up approach, and transfer such rules and knowledge onto the intelligent machines, so as to enable seamless human-machine physical interactions. (3) How to design a human-centered interaction interface, which is extremely compact, portable, and can easily capture human intentions to communicate with the surrounding smart environment effectively.

The objective of this human-machine symbiosis project is to investigate the possible solutions to address these grand challenges by designing an adaptive system that can optimize the collaboration between human and machine based on modeling and learning of human motor behaviors in human-machine interaction. To achieve this goal, the researches we conducted in this dissertation have the following three contributions:

Contribution 1 - Theoretical development of the human-machine co-learning and adaptive control framework: We propose that the next generation physical Human-Robot Interaction (pHRI) control technique should be like two persons cooperatively living together, constantly finding each other's intentions, and adapting/conforming to each other's behaviors. To model this way of interaction, our objective is to develop a learning and control framework that describes the physical-level human-robot interaction using biomimic cerebellum learning and the neuromuscular control approach, which is similar to our motor cortex and spinal cord (central nervous system (CNS)) neural control. The co-learning and adaptive cooperation model will be synthesized in the cerebellum and then used to generate "predictive" feed-forward controls to work with the reactive neuromuscular feedback gains to stabilize the dynamical

system. The Co-Adaptive Optimal Control and Inverse Differential Game Theory will be used to formulate this cerebellum co-learning and adaptive control architecture.

Contribution 2 - Verify the proposed method in a simulated exoskeleton platform with human subjects testing to prove its feasibility: To validate our proposed algorithm, we have picked one of the most promising human-robot interaction scenario as our evaluation testbed – the cooperative balancing task between human and robot. The simplified exoskeleton model (double-inverted pendulum) was utilized to implement the hip-ankle balancing strategies among human and robot. Remarkably, the tasks described here are conducted in a parallel distributed control architecture between human, robot and the controlled dynamical system.

Contribution 3 – Explore the possibility of using human-centered wearable platform, user experience design, and Deep Machine Learning technology to build a simple and intuitive Human-Machine Interface (HMI): In the future, human-smart tech interaction will not confine only on the 2D surface of our personal computers, or cellphone touch screens. The traditional stand-alone computation devices will gradually disappear. Instead, with the power of IoTs and Cloud Computing, more and more AI services are hidden in the background of the environment and process our daily information without being noticed. It outlines a futuristic multi-modal interaction strategies for the human to communicate with the ubiquitous AI, partially already being deployed in our living environment, such as AMAZON Alexa and Goggle Assistant, with which you can use voice command to retrieve relevant information or generate control. We envision that the wearable technologies that constantly monitor body physiological signals can become the next wave of universal human-machine control interface. As we can collect the signals from the wearable devices and transmit the data to the remote computers or cloud servers to do more advanced processing, so human can do more implicit

control using their daily activities, current body physiological signals, even mind and emotions to change the environment, and the environment will understand what the people want and further adapt to satisfy their needs. It requires more futuristic interaction experience (UX) design to let people feel natural, useful and powerful when using these devices, to interact with the surrounding smart technologies. To facilitate the human-machine interaction and better communicate each other's intent, we will develop an ergonomic, compact, earbud-like wearable platform that classifies brainwaves, eye movements, facial expressions and body gestures to generate intuitive commands and interact with the smart machines.

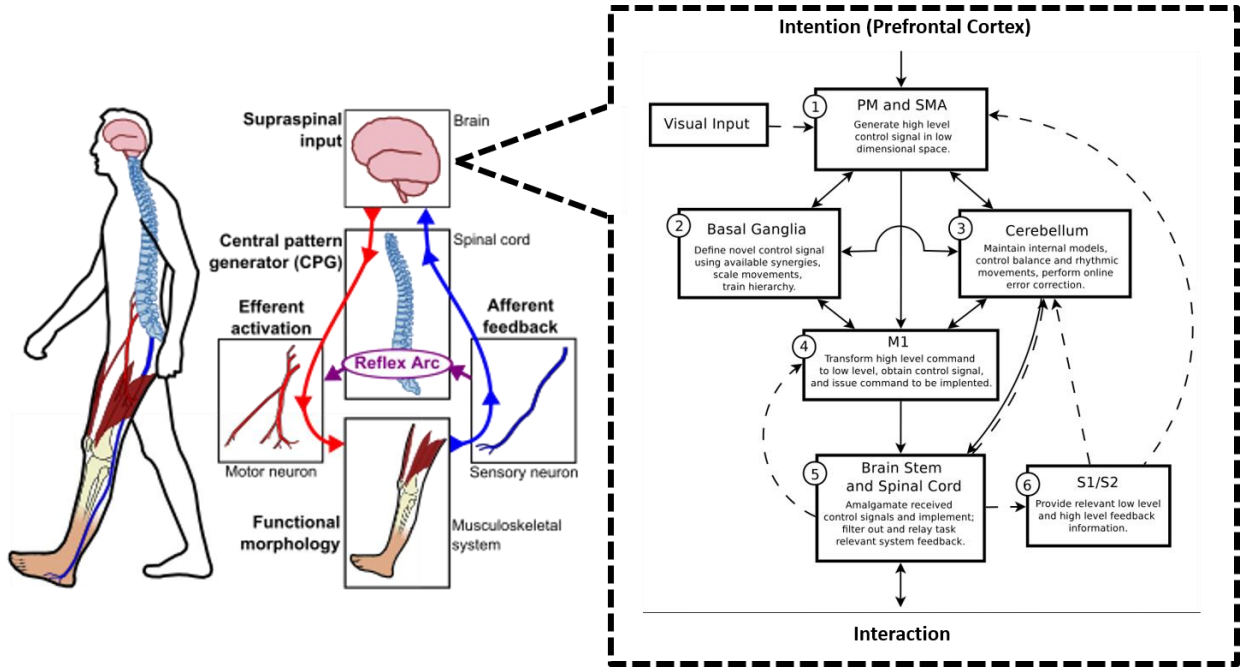

Figure 1.2. Nominal sensory-motor control loop for human locomotion, and the hierarchical organization of motor function in the brain.

1.1 Research Significance

1.1.1 Biomimic Human Learning and Control of Movement Strategy, which Provides a Seamless and Safe Physical Human-Robot Interaction

Since the robots closely work with the human partners, it is beneficial to build biomimick, human-like physical interaction skills on the robots. As such, the human can easily discover and predict the robots' behaviors, and consequently collaborate with them seamlessly and safely. The related approaches using Optimal Control and Cerebellum Feeforward and feedback control (Fig. 3.5 (a)) as theories of human motor coordination have been studied for many years [1]-[7]. However, the current theories [8] are still just unilateral control of a single dynamical system, they do not consider the interactions between two entities, which take the mutual learning and co-adaptive behaviors into account to exploit the benefit of cooperative stabilization. This research project is going to investigate the fundamental principles governing the human-human interactions using Co-Adaptive Optimal Control and Cooperative Differential Game theory. And by combining the cerebellum feedforward and feedback control, we will establish a biomimick cooperation and predictive control strategy, and transfer the related skills onto the robot in order to enable seamless human-robot interactions. The benefit of this bio-inspired approach is evident in the situation when two people cooperatively perform one common task, the overall performance will be better than just a single person [9].

1.1.2 Bilateral Control Structure with Mutual Learning, Prediction and Optimal Behavior Coordination Ability, which Allows Arbitrary Master-Slave Role Switching Between Human and Robot

As we have mentioned before, current robots are still one-way control (i.e., hierarchical supervised control). This type of control structure only has one top-level intelligent decision maker (i.e., either human or robot). For instance, like human-power-augmentation exoskeletons, the able-bodied users give intelligent commands to the robots so that the robots can passively compensate human's movements [10]. Another example is the rehabilitation robot, where a disabled user has to passively follow the predefined robot trajectories in order to exploit neuroplasticity of the brain [11]. In all these situations, human and robot's functionalities are fixed. They cannot arbitrarily switch roles between master (active role) and slave (passive role). This type of controller would not be useful when a patient wants to maximize the rehabilitation outcome, where he/she has to gradually increase the active participation of the entire neuro-rehabilitation procedure (i.e., from passively following the trajectories to actively initiating motion commands [12]).

Based on our bilateral co-learning and adaptive control structure, human and robot are both intelligent decision makers. They can constantly learn each other's intention/behavior, predict future consensus movement, and make optimal motor coordination (See Chapter 3) (Fig. 3.3). By properly modulating the interaction stiffness through changing the parameter values of the cost/reward functions, we can arbitrarily switch the roles between master and slave. (Here, we assume human and robot control behaviors are implicitly defined in the structure of cost/reward functions, and performed as feedback control gains – stiffness). Sometimes, when the robot generates improper movements, the human can become "stiffer" and take the lead to

guide the “softer” robot. Also, when the human is tired and makes a wrong decision, the robot can also change its cost value and become a stiffer master to dominate the entire control procedure. Moreover, since the human controller can share workload with the robot controller, both human and robot will spend much less energy on controlling the device. Therefore, we will have a power efficient design with small batteries, light-weight actuators and maximal entire performance.

1.1.3 A Novel Wearable Intention Detection Device and Co-Adaptive HMI Decoder Provide an Easy-to-Use Human-Machine Interface to Help People with Motor Impairments

Current assistive technologies to help people with disabilities interact with the environment are complicated, cumbersome, and expensive, e.g., head tracking control [13], sip-and-puff system [14], camera-based eye tracker, and wheel-mounted joystick, etc., where users still need to apply a lot of body/lung strength and/or extensive fine motor control to operate the device, which is not user-friendly, not portable, and usually confines the time when the users are sitting in the wheelchair. In the meanwhile, Brain-Computer Interfaces (BCIs) have been developed for a long time, which provide an alternative approach to solve the above problems. Ideally, if we have a perfect BCI, we can directly translate brainwave signals into feasible commands and operate external devices simply by thinking. However, many issues face the development of BCIs, such as the low classification accuracy of brain signals and the tedious human-learning procedures [15], which usually cause the BCI illiteracy problem. Also, current non-invasive BCIs use Electroencephalogram (EEG) caps where many electrodes must be

attached on the user's head to identify imaginary motor commands. It brings a lot of inconvenience too.

As a part of this human-machine symbiosis project, we have developed a wearable device that is extremely compact, non-obtrusive, and comfortable to be worn for long hours to help disabled people easily generate actionable commands. Here, we look at the word – "Symbiosis" in a different perspective: if the machine is worn on human's body, not only the ways of physical interactions should be similar to human beings, but the mechanical structures also have to be ergonomically compatible with the human body. For this demand, we used only two non-invasive electrodes attached on top of the user's ears (temple positions) to collect physiological signals related to brainwaves, eye movements and facial expressions. And through proper UI/UX design, we will give the user a very intuitive and engaging experience by the combination of these physiological gestures while interacting with the smart environment (Here again, the "Symbiosis" means the cognitively smooth interaction, i.e., the ways of interactions must be compatible with human nature interactions in daily activities). At the same time, we used our developed human-machine co-learning, co-adaptive decoder, to address the BCI illiteracy problem due to the unstable collected signal quality. Overall, we hope the research we conducted can provide a seamless wearable HMI interface that brings a lot of convenience for not only the people with disabilities, but also for the general public to improve the quality of life.

1.2 Innovation

The innovative works conducted in this dissertation are focusing on the mission of solving the Human-Machine Symbiosis challenges. Based on our vision, all the devices and

automation processes, as long as they are interacting with the human, should follow the principle of human-centered design. As a result, all the technologies we developed in this research have considered human-in-the-loop in every section, such as biomimic learning and control of pHRI, human-like communication interfaces, ergonomic wearable devices, and smooth cognitive-level human-machine interaction designs, etc. We believe that by following this principle, human could live with the developed intelligent technologies seamlessly and meaningfully. More precisely, our main contributions of this project can be illustrated in the following innovations:

(1) Our proposed biomimic co-learning and adaptive control framework can address the unsolved fundamental problems of physical human-robot interaction. Based on our control framework, human- robot interactions are just like the scenarios of human-human interactions. It endows the robot with a human-like behavior to constantly learn, adapt, predict future movement and optimally coordinate with the human partner. This strategy can make the exoskeleton become a completely intelligent entity that works symbiotically with the human being. Whenever one is weak, the stronger one can take the lead and change its role.

(2) Another key innovation that makes our framework superior is the prediction of future consensus movement (See. **Chapter 3 - Section 3.5**). As we know, there are other types of adaptive-optimal control algorithms [16]-[18] that can learn and make optimal decisions of the system with unknown dynamics, and therefore are used as cooperative controllers to work with the human. However, these types of controllers just treat human as disturbances with changing dynamics. And the only thing they do is to iteratively estimate the instantaneous controlled system dynamics and adapt their feedback gains to stabilize the system at the same time. The drawback of these

approaches is that they do not have the learning capabilities to understand the long-term behavior of how the human will change his/her feedback gains as a reaction to the changing dynamics of the robot adaptive controller. It turns out that the entire stabilization procedure takes a long time, and they cannot guarantee whether the robot and the human will eventually reach to a consensus behavior. On the contrary, our predictive control strategy can learn the human adaptive behavior as a response to the robot adaptive controller, and anticipate the mutual agreement after the iterative human-robot co-adaptive gain adjustment. As a result, the robot can directly send out the future consensus control protocol to cooperate with the human. This method can dramatically reduce the task execution time and ensure the system stability.

(3) To enable a human-machine symbiosis environment, we will develop a novel, human-centered, wearable HMI interface that is extremely compact, non-obtrusive and comfortable to be worn for long hours, so as to generates intuitive command to communicate with the smart environment. Particularly, our development can facilitate the accessibilities of those surrounding assistive technologies for the people who have motor disabilities. Our innovation uses simple earbud design with only two electrodes, which makes the device compact, ergonomic and sleek. And by our co-adaptive machine learning algorithm, human and machine can cooperatively adjust his/her collected signal waveforms and the machine decoder structures respectively, to minimize the uncertainties of the collected data with always drifting signal qualities, so as to get higher classification accuracies. And through Design Thinking approach, we have designed engaging, immersive and intuitive human-machine interaction strategies that allow people to interact with the smart home, play video

games, or operate telepresence robots by natural eye movements and facial expressions, totally “Hands-Free”.

1.3 Organization of the Dissertation

This dissertation will be arranged in the following organization: In **Chapter 2**, we will have an overview of the relevant backgrounds and the previous works conducted in Human-Machine Symbiosis areas, such as the emerging fields of physical human-robot collaborations, the use of Optimal Control to model the human motor control functions and its application on exoskeleton devices, and the use of Cooperative Differential Game to model human-robot cooperative co-adaptation behavior, followed by the state-of-the-art HMI interface technology of neurophysiological signal sensing and its promising applications on human–smart environment interaction and emotion measurement.

In **Chapter 3**, we will have a thorough study on our investigation of biomimic cooperative learning and adaptive control framework by using **Co-Adaptive Optimal Control** and **Differential Game Theory**, including the justifications and reasoning on how we arrived at our framework from observing the Human-Human collaboration tasks. The mathematical derivations of Co-Adaptive Optimal Control and **Nonzero-Sum Differential Game** to formulate the human-robot co-adaptation behavior, and the use of **Inverse Optimal Control** and **Inverse Differential Game** to model the cerebellum predictive learning mechanisms will be provided. It is accompanied by the real human subject experimental evaluations on human-robot cooperative balancing task on a simulated exoskeleton testbed of double-inverted pendulum. The results have shown and demonstrated the feasibility of our distributed cooperative control approach.

In **Chapter 4**, a novel human-centered HMI system for seamless Human-Machine Interaction will be introduced. The hardware design, bio-signal processing and Machine Learning, with its cell phone App development and Cloud Computing being provided. We will also illustrate how we use our identifies physiological gestures (i.e., eye movement, facial expressions, body movements) from our wearable platform in various real interactive scenarios, such as smart home control, telepresence robot operation, VR/AR gaming control, and the help for people with disabilities control the wheelchairs in order to recover their daily basic operation functions, etc. The detailed Machine Learning algorithm, using **Deep Multi-Spectrogram Convolutional Neural Network (Deep MS-CNN)**, to identify high-accuracy physiological gestures can be found in the **Appendix**. In addition, the **Appendix** also illustrates a preliminary study on using EEG to classify emotion mental states under affective touch stimuli. The potential application can be the use of wearable haptic interface to provide users touch simulations and regulate their emotions, especially for the people with mental stress or under serious depressions.

2.0 Backgrounds and Related Works

2.1 Human-Robot Cooperation in Optimal Control Framework on Exoskeleton Devices

Annually, about 795,000 people experience new or recurrent strokes in the United States [19]. These patients and others with neurological disabilities, e.g., spinal cord injury (SCI) and traumatic brain injury (TBI), or elderly people who gradually lose brain and muscle functions, may suffer from ataxia or lack of coordination of volitional movement. All this may significantly deteriorate life quality. Fortunately, with the advancement of robotics technology, scientists and engineers have actively sought the development of exoskeletons and orthotic devices to complement, substitute, or enhance human motor functionalities [20] (Fig. 2.1).

(a) (b) (c) (d)

Figure 2.1. Illustration of current state of the art exoskeletons. (a) ReWalk [25] from ReWalk Robotics. (b) EKSO [23][24] from EKSO-bionics (a spin-off company from Berkeley's BLEEX project). (c) SARCOS [26] from Raytheon. (d) HAL [29] from Cyberdyne.

Although great progress has been made in recent years [20], there are still lots of challenges associated with the current design [20], [21]. First of all, a lightweight, portable and energy efficient exoskeleton with minimum battery power consumption and maximum torque

output is expected. An intelligent controller is highly desirable to solve this problem. In addition, since exoskeletons are worn on and move synchronously with human body, designing and controlling these devices should consider physical Human-Robot Interaction (pHRI) and deal with unknown coupled dynamics between the wearer and robot. Exoskeletons need to have capabilities to learn different end-user's body dynamics. Most importantly, due to intrinsic coupling , pHRI is a human-in-the-loop control system. Human and robot are no longer two separate controllers that make their own decisions. In contrast, they are jointly reacting to the world according to their mutual behaviors and control strategies. Instead of unilateral control, intelligent decision making of each controller has to consider the other one's changing dynamics as part of its feedback loop, which is a two-way bilateral control structure. To our best knowledge, no existing exoskeleton uses this bilateral control strategy [c4-22]. Finally, current exoskeletons that can assist stroke or hemiplegia patients to walk again, like BLEEX [23], [24] or ReWalk [25], lack the ability to maintain balance. Patients wearing these devices have to use crutches as auxiliary supports to move their legs forward, which make exoskeletons bulky and clumsy. The design of balance controller for exoskeleton devices is the first priority and future trend if we really want to endow dexterous movement capabilities onto the patients or elderly people.

In this research, we propose a human-robot symbiosis control framework to address the above issues. The proposed framework is achieved by pursuing the following three specific research procedures:

Firstly, we model the human-human physical interaction behavior and transfer the interaction skills onto the robot. This way can help build a biomimic human-robot mutual learning, prediction and coordination control structure. The benefit of this bio-inspired approach

is manifested by that when two people cooperatively perform a common task, the overall performance will be improved [28]. Meanwhile, the cooperation is achieved in a dual optimal control paradigm, which is similar to the cooperative differential game [29], where each person is trying to minimize his or her own and counterpart's cost functions [30]. As a consequence, we develop a human-robot co-adaptive control strategy to realize this interactive behavior. It composes two parallel adaptive controllers constantly learning and interacting with each other (Fig. 3.3). Under this control structure, pHRI is just like two persons symbiotically living together, constantly finding each other's intention, and adapting, conforming to each other's behavior (Fig. 2.2). In addition, this strategy can ensure arbitrary role-switching between the master (active role) and slave (passive role). When one (i.e., either human or robot) is weak, the stronger one can take the lead and guide the weaker one's movement. Moreover, since the human controller can share workload with the robot, both human and robot will spend less energy on controlling the device. Therefore, we will have an energy efficient design with small battery, light-duty actuator to maximize the performance.

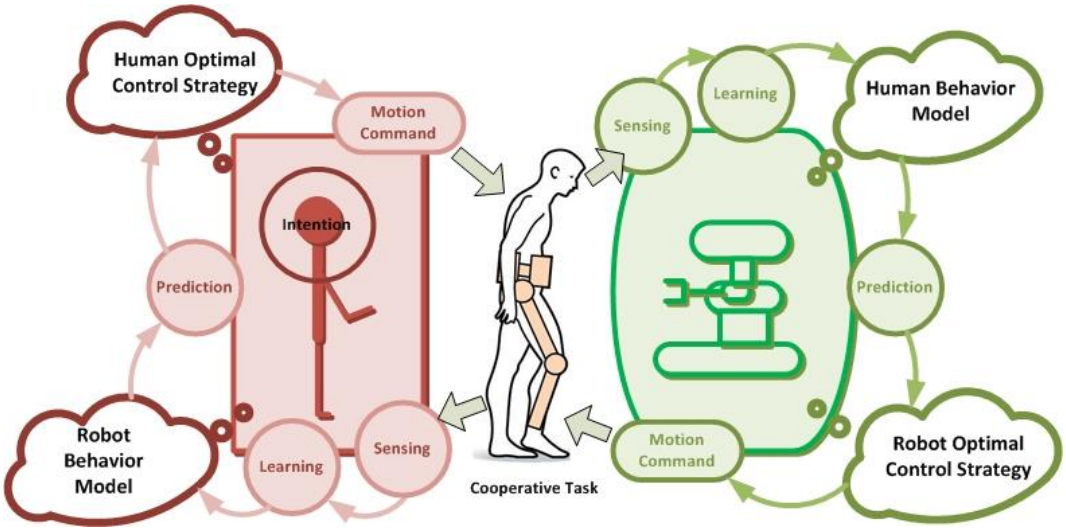

Figure 2.2. Physical human-robot symbiosis where human and robot are constantly learning each other's behavior and making predictive adjustment.

Secondly, recalling that when two people perform interactive activities, like dancing or playing Chinese Tai Chi Chuan [31], humans can easily find each other's intention and behavior simply by force and proprioceptive sensing. They can use this information to predict their partner's future movements. We call this ability as "listen to the force" according to Chinese Tai-Chi Chuan's interpretation [31]. We will also let the robot biomimic this behavior. It constitutes the major learning mechanism of our human-robot co-adaptive control. To realize this behavior, we use inverse optimal control method [32] to estimate human optimal cost function and intended goal states. The cost function implies human control strategy and the intended goal states represent the human intention. This approach can also solve the low S/N ratio problem of current bioelectrical signal detector to find the human's motion intention while using the exoskeleton devices.

Finally, to validate the feasibility of our proposed framework, a simplified double-inverted pendulum model will be used to simulate the human-robot cooperative balancing task without crutches. The upper-link represents the body torso while the lower-link represents the leg wearing exoskeleton. Through human and robot controlling the hip and ankle joints respectively, we can examine the feasibility of our approach by maintaining the double-inverted pendulum at upright position. We hope this research can establish a fundamental theoretical framework to support future pHRI studies.

2.2 Human-Robot Cooperation as Cooperative Differential Game

Physical human–robot interaction is an emerging research field due to the urgent need of robotics in unstructured environments and ad hoc human inaccessible tasks [33], [34]. In general,

humans and robots have complementary advantages: the former excel in reasoning and problem solving, while the latter are good in execution with a guaranteed performance [35], [36]. The combination of these advantages in a common task is found to be useful and in many applications necessary, such as teleoperation [37], co-assembly [38], and co-transportation [39].

To develop a natural and efficient human–robot interface is nontrivial. On the one hand, analysis of interactive behaviors of two agents is difficult, which can be very complex in different tasks and in different phases within a task. Abundant research effort has been made to address this issue, in the fields of multiagent systems and distributed intelligence [40]. Most of the works in this direction focus on robots themselves, instead of considering both humans and robots. On the other hand, human-in-the-loop robotic applications introduce inevitable problems of uncertainties and unobservable states, not to mention the consideration of ergonomics and human factors [41]. Many solutions have also been proposed to cope with these problems in the literature, including intention recognition based on different cues, e.g., haptic and visual cues [35], [42]. While how to address these two issues individually is still an open problem, a general framework is required to take both of them into account simultaneously. Therefore, adaptive frameworks/models for human–robot interaction have been proposed in recent studies [39], [43], [44], beyond a simple yet robust passive leader–follower model [45]. These studies point out that the robot should play an adaptive role to lead a task or to follow based on the human's intention or a specific circumstance, where the role is usually relevant to the balance of contributions of the human and the robot in a task [46].

Despite the aforementioned research effort, there have been few works done on rigorous analysis of interactive behaviors under an adaptive framework/model. In this research, we aim to achieve it by integrating game theory [47] and policy iteration [48]. Game theory has been

shown to be suitable for analyzing the performance of multiagent systems [49], in which human–robot interaction is deemed as a two-agent game. In game theory, a variety of interactive behaviors can be described by different combinations of individual objective/cost functions and different optimization criteria. Given a game with known objective/cost functions for linear systems, a conventional method that solves a coupled Riccati equation can be used to obtain the optimal control [50]. However, the human's objective is generally unknown to the robot in a typical human–robot interaction scenario. Therefore, in this research we proposed using inverse differential game theory to learn human-robot cooperative objective functions, which, in our understanding, no one has tried to formulate such problem before.

2.3 Wearable Electrophysiological Sensing for Human–Smart Environment Interaction

Wearable technology will revolutionize our lives in the years to come. Wearable electronic devices that can be comfortably and conformably attached to human body have attracted great research and industrial interests in recent years [51]–[55]. The wearable electronic devices possess a crucial promote in the recent development of the "Internet of Things," taking advantages of Internet infrastructures to build a connection for the users with electronic devices and surrounding machines for wellness and personalized healthcare [56]–[60]. With the fast development of electronic technologies, the population using smart sensors were dramatically increased, which involve smart electronics, smart watches, and smartphones for the application in monitoring personal health conditions and environmental changes everywhere in real time with the wireless communication [51], [61].

The current trend is to augment ordinary body-worn objects—e.g., watches, glasses, bracelets, and clothing—with advanced information and communication technologies (ICT) such as sensors, electronics, software, connectivity and power sources. These wearable devices can monitor and assist the user in the management of his/her daily life with applications that may range from activity tracking, sport and wellness, mobile games, environmental monitoring, up to eHealth.

Electrophysiological sensors, which are able to continuously monitor human physiological signals, have significant effect on diagnosing, managing, preventing and postoperatively treating cardiovascular diseases, such as electrocardiogram (ECG), electromyography (EMG), as well as electroencephalography (EEG) [62]. Enormous interest in homecare has arisen because hospital-centered care costs too much and long-term recording is helpful, which can be achieved by developing wear-able devices and wireless communications. In order to meet the need for wearable devices with long-period monitoring, much attention has been focused on nano materials which serve as components of flexible/stretchable conductors and are hence considered as desirable materials for wearable electrophysiological sensing [63]. Imani et al. recently introduced a wearable equipment with which the chemical and electrophysiological form factor of one same epidermal patch can be measured at the same time [64]. Through the wearable sensor that monitors the epidermal on human body in a real-life fitness environment, it can be demonstrated that the electrocardiogram sensing is in accordance with current wearable devices and measuring lactate through constant-potential amperometry at the same time has no adverse effect on it.

Kuzum et al. have reported a neural electrode technology with great transparency and sensitivity on the basis of graphene, which is able to make the electrophysiological recording and the optical imaging occurring on flexible polyimide (Kapton) substrates at the same time.

2.4 Emotion Sensing using Physiological Signals

Long time ago, psychologist Paul Ekman, a pioneer in the study of emotions, defined six basic emotions: anger, disgust, fear, joy, sadness and surprise [65]. In the meantime, several other researchers adopted lists of basic emotions more or less similar to Ekman's list. Emotion regulation is an important component of the affective computing. This topic was introduced by Rosalind Picard [66]. With J. Healey, she constructed the term “Affective Wearable” describing a wearable system equipped with sensors and tools, that enable recognition of wearer’s affective patterns [67]. Affective patterns include expressions of emotion such as a glad smile, an irate gesture, a strained voice or a change in autonomic nervous system (ANS) activity such as heart rate or increasing skin conductivity.

In recent years, research in the field of automated recognition of emotional states has intensified. Most of researchers are trying to recognize emotion using physiological signals. Some of them are using only GSR [68], while others are combining more signals: GSR, BVP, EMG, skin temperature and respiration in [69], BVP, EMG, GSR, skin temperature in [70], and ECG and GSR in [71].

Different researches use measured signals to get different information: emotions were detected in [68, 71, 72, 73], the state of health in [74], activity level in [75], and different information for the analysis of biking performance in [76].

In [72] researchers focused on emotions, and used signals to recognize emotions such as happiness, surprise, disgust, grief, anger and fear. They used video for eliciting emotional state: 6 video segments for 6 emotions. Each video segment lasted about 5 minutes, after which there was video (also about 5 minutes long) for calm recovery. To acquire signal for emotion detection they used only GSR.

In [70] researchers tried recognizing emotional states like sad, dislike, joy, stress, normal, no-idea. Based on this they classified emotional states as positive or negative. They used the international affective picture system (IAPS) images for eliciting emotions. Each image was displayed for 5 seconds. After participants have seen all images, they used a questionnaire to choose the exact emotional state. To detect the emotional state of the participant, researchers used eHealth platform connected to a Raspberry Pi computer.

Researchers in [69] have focused on recognizing 6 emotional states: amusement, contentment, fear, neutral, disgust and sadness. For each emotion, ten images were presented during 50 seconds. IAPS was used as an image source. We used similar method to elicit emotion in our work.

In [77] researchers used EMG and GSR signals as the source of information. Emotion detection was used to address affective gaming by adding real time emotion detection to a game scenario. They used arousal and valence scales. Arousal scale was divided into three groups: normal, high and very high. Valence scale was divided into two groups: positive and negative. In our research, we used similar division. Bayesian network was used for user's emotional state detection. Five emotional states could be detected: fear, frustrated, relaxed, joyful, and excited.

In [78] researchers used EEG, GSR, EMG, BVP, electrooculogram EOG and skin temperature as signals. In this very interesting paper, the most important thing was that

researchers created affective databases for the emotion recognition. Their databases included speech, visual, or audio- visual data. Emotional labels included neutral, anxiety, amusement, sadness, joy, disgust, anger, surprise and fear. In our work, we also use database, that includes pictures used to elicit participant's emotion, which are randomly picked and presented. Furthermore, we use database to synchronize the data from participants and from sensor system, by giving timestamps of every phase of data acquisition.

Another research that is related to our work is [79]. It is based on measuring EEG, ECG, GSR and facial activity Since emotions were elicited using multiple means (audio, video) and expressed by humans in number of ways (facial expressions, speech and physiological responses), database was needed to acquire, organize and synchronize all data. Researchers used a multimodal database for implicit personality and affect recognition (ASCERTAIN database) for easier and better understanding of the relation between emotional attributes and personality traits. Multimodality is important part of this paper, thus for us it was a very important work.

3.0 Biomimic Cooperative Learning and Adaptive Control Framework by Using Co-Adaptive Optimal Control and Differential Game Theory

Human–Robot Interaction is an important research field due to the urgent need of robotics in unstructured environments and ad hoc human inaccessible tasks. In general, humans and robots have complementary advantages: the former excel in reasoning and problem solving, while the latter are good in execution with a guaranteed performance. The combination of these advantages in a common task is found to be useful and is necessary in many applications, such as teleoperation [37], co-assembly [38], and co-transportation [39]. To develop a natural and efficient human–robot interaction strategy is nontrivial. On the one hand, analysis of interactive behaviors of two agents is difficult, which can be very complex in different tasks and in different phases within a task. Abundant research effort has been made to address this issue, in the fields of multiagent systems and distributed intelligence [40]. Most of the works in this direction focus on robots themselves, instead of considering both humans and robots. On the other hand, human-in-the-loop robotic applications introduce inevitable problems of uncertainties and unobservable states, not to mention the consideration of ergonomics and human factors [41]. Many solutions have also been proposed to cope with these problems in the literature, including intention recognition based on different cues, e.g., haptic and visual cues [35], [42]. While how to address these two issues individually is still an open problem, a general framework is required to take both of them into account simultaneously. Therefore, adaptive frameworks/models for human–robot interaction have been proposed in recent studies [39], [43], [44], beyond a simple yet robust passive leader–follower model [45]. These studies point out that the robot should play an adaptive role to lead a task or to follow based on the human's intention or a specific

circumstance, where the role is usually relevant to the balance of contributions of the human and the robot in a task [46].

Therefore, our goal is to develop a general framework (model) to describe the interactive motion behavior for a robot in physical contact with a human user, with which these two agents can optimally react to each other by learning each other's control. To address the issues of simultaneous co-adaptation, learning and control, we model the robot's and human's task objectives through respective cost functions in a **Co-Adaptive Optimal Control** and **Nonzero-Sum Differential Game** framework, which enables us to specify the desired control strategy, and predict the mutual joint behavior. In Co-adaptive Optimal Control, the human and the robot are treated as two separated optimal controllers, coordinatively controlling a dynamical system in a parallel structure. The feedback gain of each controller can be computed iteratively by solving its respective Riccati equation, and taking its counterpart's feedback gain and the dynamical system as a whole new system to be controlled in every computation cycle. In contrast, in Nonzero-Sum Differential Game, the human and robot is deemed as a cooperative two-agent game, where a variety of interactive behaviors can be described by different combinations of individual objective/cost functions and different optimization criteria. Given a game with known objective/ cost functions for linear systems, we can retrieve the consensus feedback gain of each controller by solving the coupled Riccati equation, similar to the solution obtained in the optimal control [50].

In this chapter, we will detailly describe the backgrounds and the reasoning of our proposed Human-Robot cooperative interaction model. Also, we will introduce how we can learn the human's and the robot's control behaviors by using **Inverse Optimal Control** and **Inverse Differential Game** in each of our proposed model. The elaborated theoretical derivations will be

given, and the experimental evaluation will be performed to demonstrate the feasibility of our distributed cooperative control strategy, which is comparable to the centralized optimal control with the best optimal control policy.

3.1 Physical Interaction Improves the Motor Performance in Human

Joint action is a fundamental aspect of human life, as we collaborate or interact with peers in most actions. Many common tasks rely on the motor interaction of two humans, such as sawing, dancing, physical rehabilitation, fighting, mating, carrying a table, etc. (see some examples in Fig. 3.1). In addition, knowing how humans control motor interaction with a partner may aid in the design of efficient human–robot interaction (HRI) strategies. Furthermore, a robot adapting its role and action the same way a human partner does may be more intuitive to a human operator, thus requiring less effort during use.

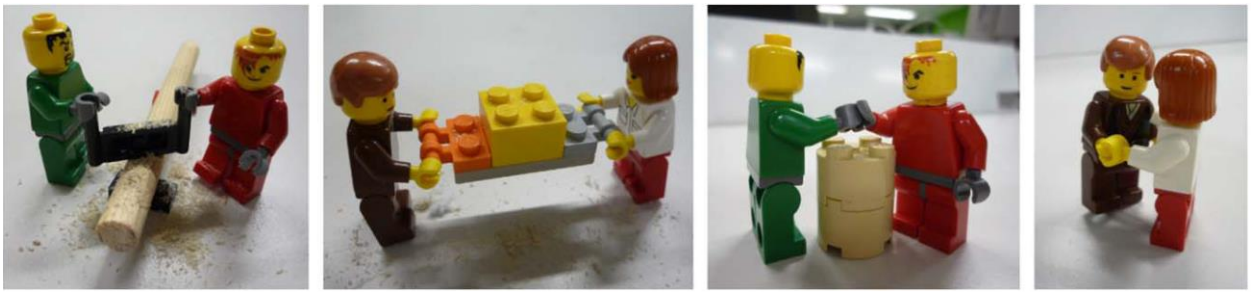

Figure 3.1. Different tasks requiring interaction between two agents (here represented with Lego parts and characters). From left to right: sawing, lifting a heavy load together, agonistic arm wrestling task and interactive dancing task.

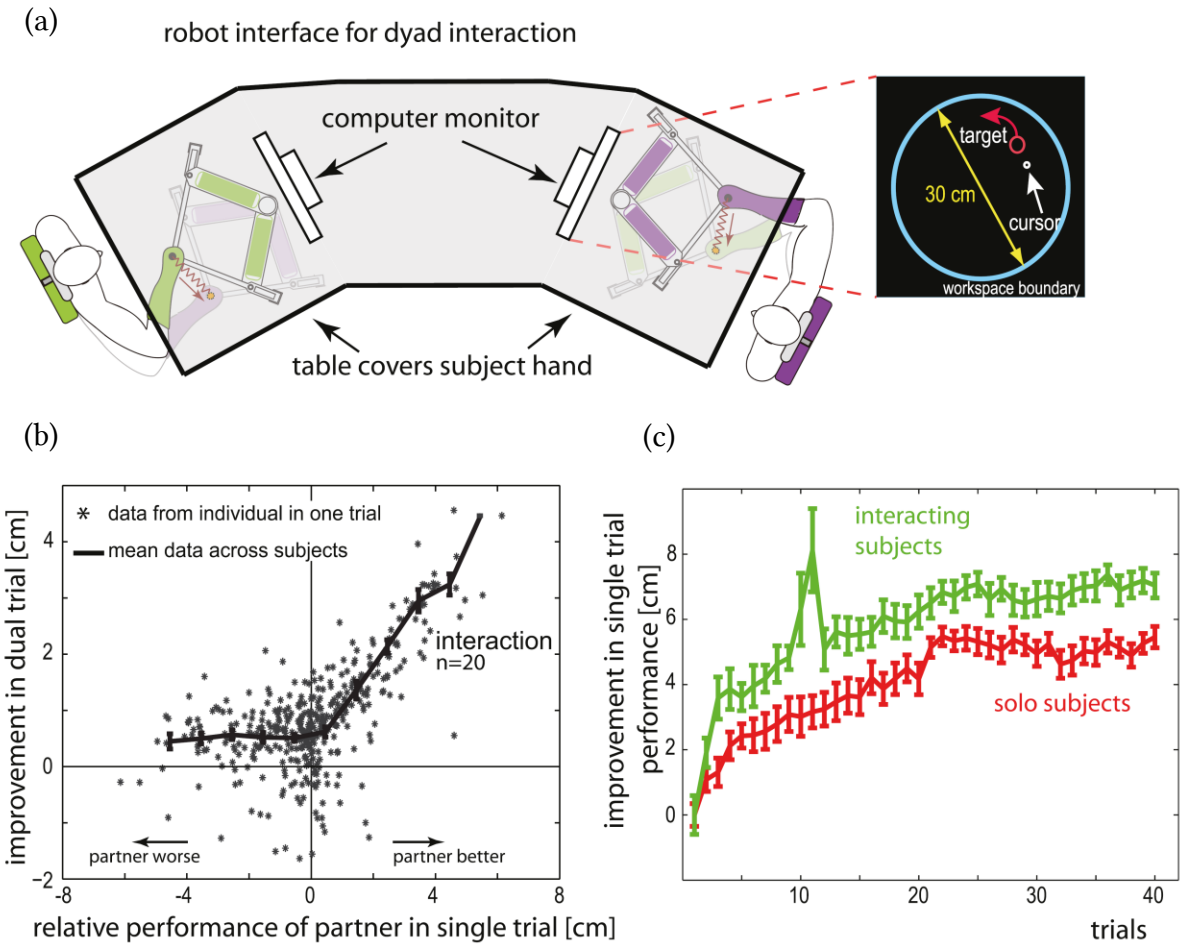

Figure 3.2. Physical interactions improve motor performance in humans (Adapted from [9]). (a) Setup: The figure shows a cartoon of the setup used for the experiment. Subjects worked in dyads, each holding a handle of the robot interface. They tracked a moving red target on their respective monitor with a cursor (white dot) representing their hand position. They had no visual information of their arm which was covered by the table. The target movement was the same for both subjects in the dyad. In the dual trials, their hands were connected by a virtual elastic band (represented in brown) such that each subject was pulled towards the hand position of the partner. The subjects could see their partner but could not see the partner's hand or monitor. (b) Improvement during interaction: The improvement in task performance in each subject for each dual trial was plotted against the relative performance of their partner. The dual trial improvement was measured by the change in tracking error by a subject during a single trial compared to his individual tracking error in the immmediatly preceding dual trial. It is observed that when connected to a better performing partner (+ abcissa), an individual's performance improved. Interestingly, the individual

performance improved even when connected to a partner with inferior performance in the task (- abcissa). (c) Learning during interaction: The improvement in task performace (relative to the first trial) across the single trials of the interacting subjects (green trace) in the visuomotor learning sessions was compared to improvement of task performance by solo subjects (red trace) who never interacted with a partner. Note that the trace combines single trials across subjects such that each data point and error bar represents single trials made by ten of the (total of 20) subjects. Intermittent interaction enabled significatly higher motor learning in individuals.

It is very inspiring to observe on how human-human interaction can improve each other's performance. And therefore, it can motivate us in designing comparable interactive robot systems to help human achieve a common goal. The research study by Ganesh et al. (2014) [9] investigated the motor responses and the consequent adaptations that govern physical interactions between humans. They used a dual-robot system in which pairs of individuals are physically connected during a motor coordination task without conscious knowledge of the connection (Fig. 3.2). Interestingly, they observed that physical interactions are consistently beneficial to the interacting individuals and enable them to improve their motor performance both during and after interactive practice. They also showed that these benefits are present only in physical interaction with an active partner and cannot be explained by multisensory integration of the visual and haptic sensory information in an individual [80].

3.2 Taxonomy of Human-Robot Interaction Types in Game Theory

The observation from natural Human-Human interaction motivates us to design comparative robotic systems to help human perform interactive tasks. It is critically important to understand how humans interact with each other in tasks requiring motor coordination, so it can

help us create robots that react as humans do during interactions, as well as enable efficient human-robot dyads that provide the best of the human and the robot joint performance. As a result, having a taxonomy of interaction types and strategies would be extremely helpful.

It has been shown in neuroscience studies that humans interact with the environment by minimizing error, *e*, and effort, *u*, [81], [82], which can be modelled as the minimization of the cost function:

$$V_i(t) = Q_i e_i^2(t) + R_i u_i^2(t), \quad i = 1, 2. \tag{3.1}$$

Furthermore, when interacting with novel dynamics, humans adapt force, mechanical impedance and trajectory to minimize such a cost function [83]–[85]. Similar cost functions will be used to model the interaction of two agents.

Game theory [86], which describes and analyzes situations where interactive decisions take place, appears as a natural framework to consider the motor interaction in a human-human, human-robot or robot-robot dyad. Game theory comprises a set of analytical tools to predict the outcome of complex interactions among decision makers, obeying to a strategy based on perceived or measured results. “Two-player games”, such as the motor interactions considered in this dissertation, play a fundamental role in analysis.

Models that address the interaction among individual decision makers are called “Games” and the rational decision makers are referred to as “Agents”. Interaction between the agents is represented by the influence that each agent has on the resulting outcome through a cost function representing its objectives. Steady-state conditions in which each player is assumed to know the equilibrium strategies of the other players, and no player has anything to gain by changing only his own strategy unilaterally, known as Nash equilibria, can be identified [87], [88]. The interaction tasks being analyzed in this dissertation can be seen as “Differential

Games" [29], also called utility-based games, where the evolution of the partners' state variables is governed by differential equations. The problem of finding an optimal strategy in a differential game is closely related to optimal control. Each interaction behavior will arise from the combination of the minimization of the individual cost functions:

$$V_i(Q_{ii}, Q_{ji}, e_i, e_j, R_{ii}, R_{ji}, u_i, u_j), \quad i \neq j, \quad i = 1, 2. \tag{3.2}$$

The behaviors adopted to perform interactive tasks can be classified in three main categories: **Cooperation**, **Collaboration** and **Competition**. Competition will be mainly observed during the antagonistic tasks as a non-cooperative game, whereas various kinds of cooperation and collaboration will mainly occur during agonistic tasks and will be treated as a cooperative game (the partners are able to form binding commitments). These categories and the associated cost functions are described below. Note that the associated cost functions suggest a utility-based game theoretic approach, in which the behavior of the agents depends on the utilities being chosen.

Competition vs. collaboration: In a competition, both agents focus on their own action and effort, and if necessary impede the other's performance in this purpose:

$$V_i(t) = Q_{ii} e_i^2(t) + R_{ii} u_i^2(t) - \left(Q_{ji} e_j^2(t) + R_{ji} u_j^2(t)\right), \quad i \neq j, \quad i = 1, 2. \tag{3.3}$$

In this scheme the two agents may have different goals, such as reaching different targets at the same time with the same object, or the same goal, such as when two children attempt to grasp the same cookie. In contrast, in a collaboration both agents jointly try to develop a consensual solution to solve a problem [89], and, as in cooperative games, no agent has incentive to leave the coalition formed and receive a smaller utility. A collaboration is also modelled as a

symmetric behavior (i.e., the cost function's structure does not change under the permutation 1↔2), but this time with positive influence on the partner.

$$V_i(t) = Q_{ii}e_i^2(t) + R_{ii}u_i^2(t) + \left(Q_{ji}e_j^2(t) + R_{ji}u_j^2(t)\right), \quad i \neq j, \quad i = 1,2. \tag{3.4}$$

Each agent minimizes its and the partner's error and metabolic cost (i.e., energy, force, etc.).

Cooperation vs. collaboration: In a collaboration, there is no a priori roles distribution, but a spontaneous roles distribution depending on the interaction history. Any physical interaction with negotiations and discussions to accommodate others while considering their perspective, belong to this category. In this case, activity is synchronized and coordinated in order to build and maintain a shared conception of a problem [90].

In contrast, a cooperation occurs when different roles are ascribed to the agents prior to the beginning of a task and this distribution is not questioned until its completion. While in collaboration the agents work on an even basis, cooperation has an uneven distribution of subtasks or roles during the task [89]. Cooperating agents work towards the same end and need each other to complete the task, but are not equal. In fact, cooperation is characterized by an asymmetric behavior, in the sense of asymmetry in the cost functions as tested from the permutation 1↔2.

Master-slave vs. education: The most typical asymmetric relationship of a cooperation is the master-slave scheme. This behavior is characterized by the following cost functions:

$$\begin{aligned} V_1(t) &= Q_{21}e_2^2(t) + R_{21}u_2^2(t), \quad \text{slave,} \\ V_2(t) &= Q_{22}e_2^2(t) + R_{22}u_2^2(t), \quad \text{master.} \end{aligned} \tag{3.5}$$

The master is only considering himself, while the slave considers only (his perception of) the master needs. The above cost functions illustrate the danger of this relation, where the slave does not consider its own effort expense and may eventually lose all its energy.

We want now to examine the teacher-student relationship. This relation is critical to human society and education, and also to developing service robots, virtual reality-based training systems, and robot-assisted physical rehabilitation, etc. One may a-priori think that the master-slave scheme applies here as well, with the teacher as master and the student as slave. However, efficient learning schemes suppose that the student is building his own capacities while the teacher is assisting this process. Therefore, the master-slave interaction behavior is not appropriate for education. However, an altered version of an assistance can be considered for the relationship between a teacher and his student. A good teacher will try to maximize the student's independence. Therefore, the teacher can minimize his own effort in order to challenge the student, let him perform according to his capabilities and eventually increase them. In the education behavior, the cost functions V1 of the teacher and V2 of the student are thus defined as:

$$\begin{aligned} V_1(t) &= R_{11}u_1^2(t) + Q_{21}e_2^2(t), \quad \text{teacher,} \\ V_2(t) &= Q_{22}e_2^2(t) + R_{22}u_2^2(t), \quad \text{student.} \end{aligned} \tag{3.6}$$

This definition describes the main quality of a good teacher as the capability to maximize student involvement and action. Even if the teacher is an expert in the task (good at minimizing goal error) or wants to help the student, he should not care too much about the task achievement (i.e., adopt the slave role), but let the student try and improve his or her performance.

Mutual assistance: Finally, the anecdotical mutual assistance or reciprocal altruism [91] can also be represented in our taxonomy, using cost function:

$$V_i(t) = Q_{ji}e_j^2(t) + R_{ji}u_j^2(t), \quad i \neq j, \quad i, j = 1, 2. \tag{3.7}$$

This ideal interaction behavior occurs in particular contexts such as the iterative prisoner dilemma and associated strategies such as tit-for-tat [92], where the interaction strategy is selected by considering long term benefits.

3.3 Co-Adaptive Optimal Control

Here, we are going to introduce our first prosed hypothesis that the human-robot cooperation is achieved in a dual optimal control paradigm, similar to the cooperative differential game [93], where each controller is trying to minimize its own and the counterpart's cost functions [94]. To evaluate these hypothesises, we developed a human-robot Co-Adaptive Optimal Control and Cooperative Differential Game strategy to realize this interactive behavior. It composes two optimal controllers constantly learning and interacting with each other (Fig. 3.3 and Fig. 2.2). Under this control structure, pHRI is just like two persons symbiotically living together, finding each other's intention, and adapting, conforming to each other's behaviour all the times. The difference between Co-Adaptive Optimal Control and Cooperative Differential Game is in their cost function structures. The previous one only considers its own cost, minimizing its own state trajectory and its own control input. And the counterpart controller will be treated as part of the controlled system with changing dynamics to be learned. On the other hand, the cooperative differential game approach considers both controllers' control input as part of each other's cost function, and jointly minimize them all together. In this Subtask, we will mathematically formulate each control framework, and evaluate and discuss their feasibilities in the subsequent subtasks.

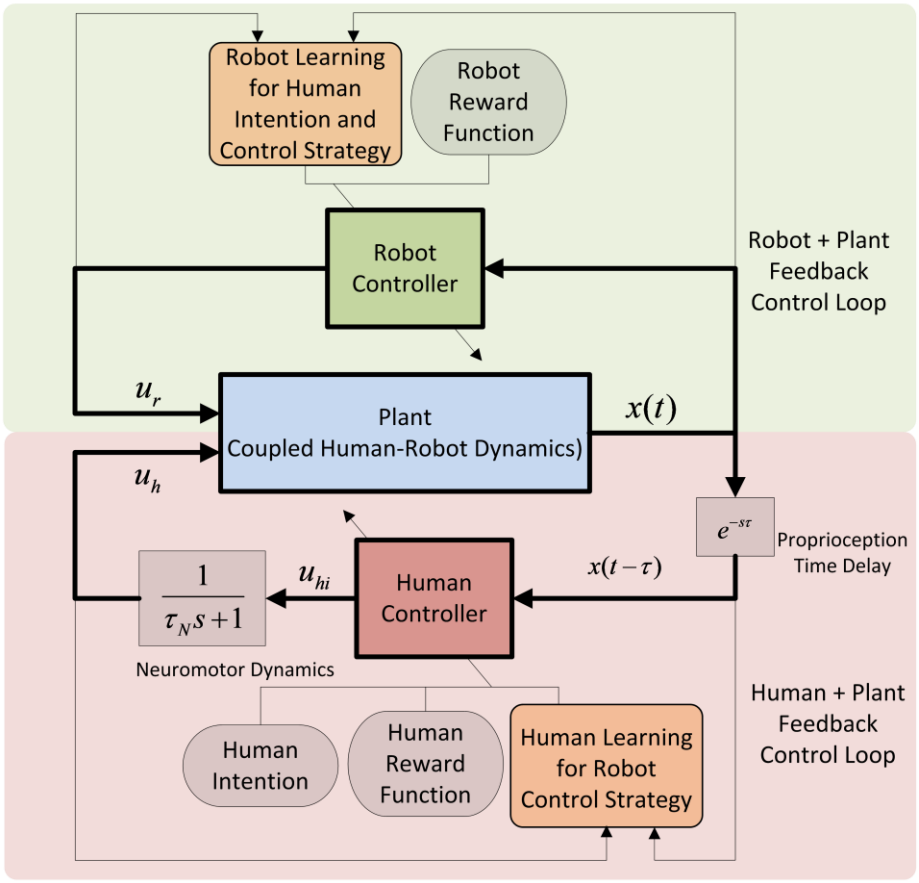

Figure 3.3. Co-Adaptive Control framework for pHRI. $x(t)$**: system output state;** $x(t-\tau)$**: human perceived state;** u_h**: human actual motor output;** u_{hi}**: human intended motor output;** u_r**: robot motor output.**

Since exoskeletons closely work with human operators, it is beneficial for the robot to build an intuitive human-friendly physical interaction strategy, similar to our human being. As a consequence, the wearer can easily discover and predict the exoskeleton's behavior, and adequately collaborate with it seamlessly and safely. In this section, we introduce how we model the physical human-robot interaction (pHRI) behavior like human and human performing interactive tasks.

3.3.1 Optimal Physical Human-Robot Interaction (pHRI) Behavior

Optimal feedback control as a theory of human motor coordination has been studied for over thirty years [1]-[5]. We can actually transfer this human-like skill onto the robot and mathematically formulate its co-adaptive behavior. We model either the human or robot having optimal control strategy with quadratic cost function as:

$$\begin{aligned} &\left(u^{*}, x^{*}\right)=\arg\min_{u,x}\left\{\sum_{t=1}^{T_f}\left(x_t-x^{goal}\right)^{T} Q\left(x_t-x^{goal}\right)+u_t{}^{T} R u_t\right\}, \\ &s.t. \quad x_{t+1}=f\left(x_t, u_t, K_t\right), \end{aligned} \tag{3.8}$$

where $x_{t+1}=f\left(x_t, u_t, K_t\right)$ is the controlled plant with changing dynamics under the feedback gain K_t from its counterpart controller (i.e., human's counterpart is robot, and vice versa). Notably, the weight matrices, $\{Q, R\}$, in the cost of each optimal controller can be interpreted as the human or the robot's control strategies. They reflect how human or robot controls the system. The term x^{goal} denotes each controller's intended goal position.

During the interactive activities, we only consider the cooperative case, i.e., human and robot have the same goal. And after learning human's intention x^{goal} and control strategy $\{Q, R\}$, the robot will use its own control strategy to cooperate with the human. Here, the way how robot cooperates with the human is to treat the human as part of its controlled plant and try to stabilize the entire system. In the meanwhile, the human is doing the same thing, trying to adapt his/her own control strategy to stabilize the new system controlled by the robot. This mutual stabilization behavior results in iterative adaptations of the feedback gain K_t. Under the assumption that the human movement is Piecewise Linear [95], we can actually divide the entire pHRI process into many short segments and approximate the cooperation as linear control

systems in each computation interval. And with the Equilibrium Point hypothesis [96], human and robot are jointly stabilizing the linearized system on their intended common goal. Therefore, we can simplify and approximate both human and robot as two Linear Quadratic Regulator (LQR) controllers interacting with an LTI system.

Consider a coupled discrete-time LTI system:

$$x_{t+1} = Ax_t + B_h u_{ht} + B_r u_{rt}\,, \tag{3.9}$$

where u_{ht} and u_{rt} are the control input from human and robot respectively at the time instance *t*. By solving the discrete time Algebraic Riccati Equation (ARE), we can find each control input as

$$u_{ht}(k) = -K_h(k)x_t\,, \tag{3.10}$$

$$u_{rt}(k) = -K_r(k)x_t\,, \tag{3.11}$$

where $K_h(k)$ and $K_r(k)$ are the optimal state feedback gains of human and robot respectively, and *k = 1, 2, 3, ...* is the gain update iteration number.

Substituting (3.10) and (3.11) into the original LTI system (3.9), we can get two updated feedback control systems:

(a) w.r.t. human, the controlled plant is

$$x_{t+1}(k+1) = \left(A - B_r K_r(k)\right)x_t + B_h u_{ht}(k+1)\,. \tag{3.12}$$

(b) w.r.t. robot, the controlled plant is

$$x_{t+1}(k+1) = \left(A - B_h K_h(k)\right)x_t + B_r u_{rt}(k+1)\,. \tag{3.13}$$

From (3.12), we can generate new $u_{ht}(k+1) = -K_h(k+1)x_t$ by solving ARE again, and so does (3.13). Based on the same idea, we can substitute above new $u_{ht}(k+1)$ and $u_{rt}(k+1)$ into

(3.9) one more time to get new updated version of feedback control systems (3.12) and (3.13), where $k \to k+1$.

As the iterations goes on, from the numerical solution of the above equations, we found that the mutual update of the feedback gain K_h and K_r will eventually reach to a stable consensus behavior, i.e., as $k \to \infty$, the entire LTI system will become:

$$x_{t+1} = \left(A - B_h \bar{K}_h - B_r \bar{K}_r \right) x_t \,, \tag{3.14}$$

where $\{\bar{K}_h, \bar{K}_r\}$ is the consensus feedback gain of human and robot. The eigenvalues of the entire system will converge to a constant negative value. Fig. 3.4 illustrates the trace of eigenvalues of the overall human-robot co-adaptation behavior.

This result gives us a very important information that mutual coordination between human and robot will reach to a consensus stable behavior, just like human-human interaction. We will use this characteristic to build our co-adaptive controller in **Section 3.3.2**, and the prediction of human-robot consensus behavior in **Section 3.5**.

3.3.2 Co-Adaptive Optimal Stabilization Simulation

In order to model the human-robot interaction behaviors described in **Section 3.3.1**, we build up the Human- Robot Co-adaptive Control framework, which consists of two adaptive controllers in parallel with the system plant, i.e., coupled human-robot dynamics. Fig. 3.3 illustrates our control structure. Human, robot controller, along with exoskeleton mechanism, form two interacting feedback control loops (i.e., human- exoskeleton feedback control loop and robot-exoskeleton feedback control loop), and each controller will take the other feedback control loop as a part of its controlled plant. The objective of two controllers is to cooperatively

stabilize the system. Any unilateral change of one feedback gain will result in a corresponding gain adjustment of its counterpart controller.

Note that in this structure, since human is already an existing controller there, we are not actually building the human controller. However, we do have a virtual human controller model built in the robot "brain." We let the robot learn this model. And based on the interaction between the virtual human controller and robot controller, we can predict the future consensus behaviors and generate optimal cooperative command from the robot.

To build the simulation platform introduced later in **Section 3.6** to verify our idea, we assume all the kinematic information can be acquired by robot. For example, robot has joint encoders, which can measure all the joint angles and angular velocities (denoted by system state x_t). It also has torque and force sensors to measure joint torque u_{rt} and contact forces exerted from the human (transferred into joint space as u_{ht}). Robot can use this information to learn the coupled human-robot dynamics (by system identification), along with the human intention x^{goal} and control strategy $\{Q, R\}$ (by inverse optimal control method, introduced in **Section 3.3.3**). All these learning results can be utilized to reconstruct the virtual human controller model and predict the consensus cooperative behavior. Thereafter, robot will use its own optimal control strategy $\{Q, R\}$ to generate optimal cooperative gain $\bar{K}_r$ to stabilize the system. Recall that human is doing the similar to learn, predict and stabilize the system at the same time. Therefore, we will have two controllers constantly adapting to each other's behavior.

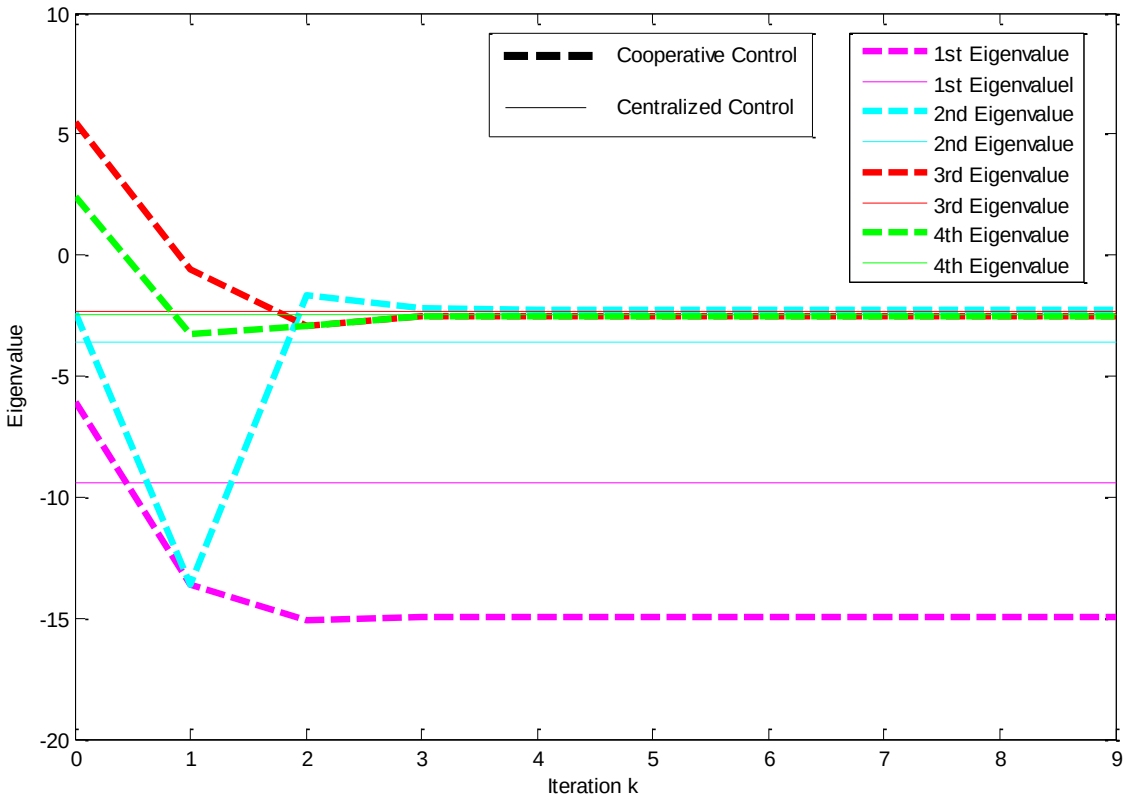

Figure 3.4. Stability examination of simulated human-robot cooperative balance of double-inverted pendulum. The real parts of all the eigenvalues go to negative and are very close to the centralized optimal control strategy, i.e., robot is responsible for controlling both joints.

3.3.3 Inverse Optimal Control to Estimate Human Control Strategy

The key component of the proposed adaptive learning algorithm is to let robot learn human's control strategy, $\{Q, R\}$, and intention, x^{goal}. Human is an intrinsic optimal controller [97] and can learn robot's intention and control strategy. In order to let robot estimate human

intention and control strategy, we use inverse optimal control method by giving actual measurement, (u_t, x_t), and use optimization methods to find out:

$$\left(Q^*, R^*, x^{goal}\right) = \arg\min_{Q,R,x^{goal}} \left\{ \sum_{t=1}^{T_f} \left(x_t - x^{goal}\right)^T Q \left(x_t - x^{goal}\right) + u_t{}^T R u_t \right\}, \tag{3.15}$$

where $Q > 0, R > 0$.

There are different ways to solve this optimization problem. One is the gradient descent method. Gradient descent has the advantage of simplicity. However, it suffers from the slow convergence and local minimum. For real-time implementation to estimate large amount of parameters, it is not suitable. Here, since we assume the system is linear and the optimal controller has convex quadratic cost functions, we can formulate the problem as a convex optimization problem subject to linear matrix inequality (LMI) constraints [98], [99].

Assuming we can identify all the system state matrices, for human to control the robot-plant-coupled system, we can write the discrete time LTI robot-controlled plant as:

$$e_{t+1} = \left(A - B_r K_r\right) e_t + B_h u_{ht}, \tag{3.16}$$

where $e_t = x_t - x_g$, x_g is the human goal state.

The objective here is: Given the estimation of K_h, we need to determine the cost parameters Q_h, R_h and x_g, such that $Q_h > 0, R_h > 0$, and K_h satisfies:

$$K_h = (B_h{}^T P B_h + R_h)^{-1} B_h{}^T P (A - B_r K_r), \tag{3.17}$$

where P is the unique positive semi-definite solution to the discrete time Algebraic Riccati Equation (ARE):

$$\begin{aligned} &\left(A - B_r K_r\right)^T P \left(A - B_r K_r\right) - P \\ &- \left(\left(A - B_r K_r\right)^T P B_h\right)\left(B_h{}^T P B_h + R_h\right)^{-1} B_h{}^T P \left(A - B_r K_r\right) + Q_h = 0. \end{aligned} \tag{3.18}$$

To solve the above problem, we further formulate it as a convex optimization problem subject to LMI:

$$(Q_h, R_h, P, \alpha) = \arg \min_{Q_h, R_h, P, \alpha} \alpha^2, \tag{3.19}$$

$$P \geq 0\,, \tag{3.20}$$

$$(A - B_r K_r)^T P (A - B_r K_r) - P - (A - B_r K_r)^T P B_h K_h + Q_h = 0\,, \tag{3.21}$$

$$B_h{}^T P \left(A - B_r K_r\right) - \left(B_h{}^T P B_h + R_h\right) K_h = 0\,, \tag{3.22}$$

$$I \leq \begin{bmatrix} Q_h & 0 \\ 0 & R_h \end{bmatrix} \leq \alpha I\,, \tag{3.23}$$

where α is the condition number to ensure the numerical stability [100], [101] and also help us obtain the unique solution to this problem [101].

3.4 Nonzero-Sum Cooperative Differential Game

3.4.1 Differential Game Physical Human-Robot Interaction (pHRI) Behavior

Consider we have a LTI system with 2 players:

$$\dot{x} = Ax + B_1 u_1 + B_2 u_2\,, \tag{3.24}$$

where $x = x_1 = x_2 \in R^n$ is the coupled system states, and $u_1, u_2 \in R^m$ are the control vectors of each player. Assume that the entire system is under the **closed-loop optimal control** with **infinite horizon** and **free-final states**.

Each player has cost function $J_1(x,u_1,u_2),\ J_2(x,u_1,u_2) \in R$, defined as:

$$J_1 = \frac{1}{2}\int_{t_0}^{\infty} (x^T Q_1 x + u_1^T R_{11} u_1 + u_2^T R_{12} u_2)\ dt\ , \tag{3.25}$$

$$J_2 = \frac{1}{2}\int_{t_0}^{\infty} (x^T Q_2 x + u_1^T R_{21} u_1 + u_2^T R_{22} u_2)\ dt\ , \tag{3.26}$$

where $Q_i \in R^{n\times n},\ R_{ij} \in R^{m\times m},\ i, j = 1,2$ and $Q_i,\ R_{ij} > 0$

Based on Pontryagin's minimum principle [102], we define the Hamiltonian of Player 1 and Player 2, $H_1(x,u_1,u_2), H_2(x,u_1,u_2) \in R$ as:

$$H_1 = \frac{1}{2}(x^T Q_1 x + u_1^T R_{11} u_1 + u_2^T R_{12} u_2) + \lambda_1^T (Ax + B_1 u_1 + B_2 u_2)\ , \tag{3.27}$$

$$H_2 = \frac{1}{2}(x^T Q_2 x + u_1^T R_{21} u_1 + u_2^T R_{22} u_2) + \lambda_2^T (Ax + B_1 u_1 + B_2 u_2)\ . \tag{3.28}$$

To obtain the optimal solution, let's start with Player 1.

Costate Equation of Player 1:

$$-\dot{\lambda}_1 = \frac{\partial H_1}{\partial x} = Q_1 x + A^T \lambda_1\ . \tag{3.29}$$

Stationary Condition of Player 1:

$$0 = \frac{\partial H_1}{\partial u_1} = R_{11} u_1 + B_1^T \lambda_1 \quad \longrightarrow \quad u_1 = -R_{11}^{-1} B_1^T \lambda_1\ . \tag{3.30}$$

Substitute (3.30) into (3.28), and take the costate dynamics (3.29) as an additional constraint, the Player 2's Hamiltonian (3.28) becomes:

$$H_2 = \frac{1}{2}(x^T Q_2 x + \lambda_1^T B_1 R_{11}^{-T} R_{21} R_{11}^{-1} B_1^T \lambda_1 + u_2^T R_{22} u_2) + \lambda_2^T (Ax - B_1 R_{11}^{-1} B_1^T \lambda_1 + B_2 u_2) + \psi^T (-Q_1 x - A^T \lambda_1)\ . \tag{3.31}$$

Similarly, the optimal solution of Player 2 can be derived as follows:

Costate Equation of Player 2:

$$-\dot{\lambda}_2 = \frac{\partial H_2}{\partial x} = Q_2 x + A^T \lambda_2 - Q_1 \psi\ , \tag{3.32}$$

$$-\dot{\psi} = \frac{\partial H_2}{\partial \lambda_1} = B_1 R_{11}^{-T} R_{21} R_{11}^{-1} B_1^T \lambda_1 - B_1 R_{11}^{-1} B_1^T \lambda_2 - A\psi \,. \tag{3.33}$$

Stationary Condition of Player 2:

$$0 = \frac{\partial H_2}{\partial u_2} = R_{22} u_2 + B_2^T \lambda_2 \quad \longrightarrow \quad u_2 = -R_{22}^{-1} B_2^T \lambda_2 \,. \tag{3.34}$$

Using sweep method (Bryson and Ho 1975) [103], we assume that $x(t),\ \lambda_1(t),\ \lambda_2(t),\ \psi$ satisfies the following linear relation for all $t \in [t_0, \infty]$.

$$\begin{aligned} \lambda_1(t) &= S_1(t)x(t) \,, \\ \lambda_2(t) &= S_2(t)x(t) \,, \\ \psi(t) &= S_3(t)x(t) \,, \end{aligned} \tag{3.35}$$

where $S_1(t),\ S_2(t),\ S_3(t) \in R^{n \times n}$ are positive definite matrices.

Then, we can differentiate (3.35) and obtain:

$$\begin{aligned} \dot{\lambda}_1(t) &= \dot{S}_1(t)x(t) + S_1(t)\dot{x}(t) \\ &= \dot{S}_1(t)x(t) + S_1(t)(Ax - B_1 R_{11}^{-1} B_1^T \lambda_1 - B_2 R_{22}^{-1} B_2^T \lambda_2) \,, \\ \dot{\lambda}_2(t) &= \dot{S}_2(t)x(t) + S_2(t)\dot{x}(t) \\ &= \dot{S}_2(t)x(t) + S_2(t)(Ax - B_1 R_{11}^{-1} B_1^T \lambda_1 - B_2 R_{22}^{-1} B_2^T \lambda_2) \,, \\ \dot{\psi}(t) &= \dot{S}_3(t)x(t) + S_3(t)\dot{x}(t) \\ &= \dot{S}_3(t)x(t) + S_3(t)(Ax - B_1 R_{11}^{-1} B_1^T \lambda_1 - B_2 R_{22}^{-1} B_2^T \lambda_2) \,. \end{aligned} \tag{3.36}$$

Now, let's substitute (3.29), (3.32), (3.33), and (3.35) into (3.36) again. We can obtain:

$$\begin{aligned} &-Q_1 x - A^T \lambda_1 = \dot{S}_1 x + S_1(Ax - B_1 R_{11}^{-1} B_1^T S_1 x - B_2 R_{22}^{-1} B_2^T S_2 x) \\ &\qquad\qquad \downarrow \\ &-\dot{S}_1 x = (Q_1 - A^T S_1 + S_1(A - B_1 R_{11}^{-1} B_1^T S_1 - B_2 R_{22}^{-1} B_2^T S_2))x \,, \\ &-Q_2 x - A^T \lambda_2 + Q_1 \psi = \dot{S}_2 x + S_2(Ax - B_1 R_{11}^{-1} B_1^T \lambda_1 - B_2 R_{22}^{-1} B_2^T \lambda_2) \\ &\qquad\qquad \downarrow \\ &-\dot{S}_2 x = (Q_2 + A^T S_2 - Q_1 S_3 + S_2(A - B_1 R_{11}^{-1} B_1^T S_1 - B_2 R_{22}^{-1} B_2^T S_2))x \,, \end{aligned} \tag{3.37}$$

$$-B_1R_{11}^{-T}R_{21}R_{11}^{-1}B_1^T\lambda_1+B_1R_{11}^{-1}B_1^T\lambda_2+A\psi=\dot{S}_3x+S_3(Ax-B_1R_{11}^{-1}B_1^T\lambda_1-B_2R_{22}^{-1}B_2^T\lambda_2)$$

$$\downarrow$$

$$-\dot{S}_3x=(B_1R_{11}^{-T}R_{21}R_{11}^{-1}B_1^TS_1-B_1R_{11}^{-1}B_1^TS_2-AS_3+S_3(A-B_1R_{11}^{-1}B_1^TS_1-B_2R_{22}^{-1}B_2^TS_2))x\ .$$

Since the above equations hold true for all state trajectories given any $x(t_0)$, we can cancel all x . Rearrange them as:

$$\dot{S}_1+Q_1-A^TS_1+S_1(A-B_1R_{11}^{-1}B_1^TS_1-B_2R_{22}^{-1}B_2^TS_2)=0\ , \tag{3.38}$$

$$\dot{S}_2+Q_2+A^TS_2-Q_1S_3+S_2(A-B_1R_{11}^{-1}B_1^TS_1-B_2R_{22}^{-1}B_2^TS_2)=0\ , \tag{3.39}$$

$$\dot{S}_3+B_1R_{11}^{-T}R_{21}R_{11}^{-1}B_1^TS_1-B_1R_{11}^{-1}B_1^TS_2-AS_3+S_3(A-B_1R_{11}^{-1}B_1^TS_1-B_2R_{22}^{-1}B_2^TS_2)=0\ . \tag{3.40}$$

Assume Player 1 and Player 2 will eventually achieve a consensus behavior, i.e., feedback gains converge to a constant value.

$$\begin{aligned}K_1(\infty)&=R_{11}^{-1}B_1^TS_1(\infty)=const.\ ,\\ K_2(\infty)&=R_{22}^{-1}B_2^TS_2(\infty)=const.\ ,\\ \dot{S}_1(\infty)&=\dot{S}_2(\infty)=0\ .\end{aligned} \tag{3.41}$$

Set $\dot{S}_1=\dot{S}_2=0$ in (3.38), (3.39), (3.40). We can obtain the following Algebraic Riccati Equations (ARE):

$$Q_1-A^TS_1+S_1(A-B_1R_{11}^{-1}B_1^TS_1-B_2R_{22}^{-1}B_2^TS_2)=0\ , \tag{3.42}$$

$$Q_2+A^TS_2-Q_1S_3+S_2(A-B_1R_{11}^{-1}B_1^TS_1-B_2R_{22}^{-1}B_2^TS_2)=0\ , \tag{3.43}$$

$$B_1R_{11}^{-T}R_{21}R_{11}^{-1}B_1^TS_1-B_1R_{11}^{-1}B_1^TS_2-AS_3+S_3(A-B_1R_{11}^{-1}B_1^TS_1-B_2R_{22}^{-1}B_2^TS_2)=0\ . \tag{3.44}$$

If we can solve all the AREs at the same time, we can obtain the following consensus feedback gain:

$$K_1 = R_{11}^{-1} B_1^T S_1 ,$$
$$K_2 = R_{22}^{-1} B_2^T S_2 . \tag{3.45}$$

3.4.2 Learning Multi-Objective Cost Function

The key component of the Inverse Differential Game is to let robot learn human's cooperative strategy $(Q_h^*, R_{hh}^*, R_{hr}^*)$ and use its own strategy (Q_r, R_r, R_{rh}) to generate optimal cooperative control (u_r, x_r) to work with the human.

To more easily formulate the problem, we set human as Player 1 and robot as Player 2. Here, the objective is: Given the estimation of human control gain K_1, we need to determine the cost parameters $(Q_1^*, R_{11}^*, R_{12}^*)$, which satisfies

$$\left(Q_1^*, R_{11}^*, R_{12}^*\right) = \arg\min_{Q_1, R_{11}, R_{12}} \int_{t_0}^{\infty} \begin{pmatrix} \left(x(t) - x^{goal}\right)^T Q_1 \left(x(t) - x^{goal}\right) + \cdots \\ \cdots\ u_1(t)^T R_{11} u_1(t) + u_2(t)^T R_{12} u_2(t) \end{pmatrix} dt . \tag{3.46}$$

Since the simplified system is linear and the optimal controller has convex quadratic cost function, we can formulate the problem as a Convex Optimization problem subject to Linear Matrix Inequality (LMI) [98], [99] constraints:

$$(Q_1^*, R_{11}^*, R_{12}^*, S_1^*, S_2^*, S_3^*, \alpha^*) = \arg \min_{Q_1, R_{11}, R_{12}, S_1, S_2, S_3, \alpha} \alpha^2 , \tag{3.47}$$

$$Q_1 - A^T S_1 + S_1 (A - B_1 R_{11}^{-1} B_1^T S_1 - B_2 R_{22}^{-1} B_2^T S_2) = 0 , \tag{3.48}$$

$$Q_2 + A^T S_2 - Q_1 S_3 + S_2 (A - B_1 R_{11}^{-1} B_1^T S_1 - B_2 R_{22}^{-1} B_2^T S_2) = 0 , \tag{3.49}$$

$$B_1 R_{11}^{-T} R_{21} R_{11}^{-1} B_1^T S_1 - B_1 R_{11}^{-1} B_1^T S_2 - A S_3 + S_3 (A - B_1 R_{11}^{-1} B_1^T S_1 - B_2 R_{22}^{-1} B_2^T S_2) = 0 , \tag{3.50}$$

$$S_1 > 0, \quad S_2 > 0, \quad S_3 > 0 \ , \tag{3.51}$$

$$K_1 - R_{11}^{-1} B_1^T S_1 = 0 \ , \tag{3.52}$$

$$I \le \begin{bmatrix} Q_1 & 0 & 0 \\ 0 & R_{11} & 0 \\ 0 & 0 & R_{12} \end{bmatrix} \le \alpha I \ . \tag{3.53}$$

3.5 Biomimic Cerebellum Learning and Neuromuscular Control Model as Human-like Cooperation Control Strategy

For human beings, fast, smooth, and coordinated movements cannot be achieved by basic feedback control alone because delays associated with feedback loops are long (about 200 ms for visual feedback and 100 ms for somatosensory feedback) and feedback gains are low. In addition, feedback controllers such as the commonly used PID (proportional, integral, and derivative) controllers do not incorporate predictive dynamic or kinematic knowledge of controlled objects or environments. From observing the fact that humans can manipulate a vast number of tools smoothly, and exhibit an almost infinite number of behaviors in different environments. We can conclude that the internal models in the brain must exist, and it is acquired through motor learning in order to accommodate the changes that occur with the growth of controlled objects such as hands, legs, and torso, as well as the unpredictable variability of the external world.

Fig. 3.5 (a) shows the concept of cerebellar feedback-error-learning model (CBFELM) (Kawato, 1999 [6]). When a nonzero difference is present between the desired trajectory and the

realized trajectory of the movement, the difference signal is transmitted to Purkinje cells in the cerebellum and controls both motion output and initiation time. The cerebellum structures feedforward control and learning of inverse model for voluntary movement. We call this the learning of internal dynamic models which can predict the future behavior. However, this structure only describes the unilateral motor control of body movement, it does not considered the bilateral interactions between the human and his/her counterpart and figure out how to generate coordinated movement in the brain.

We hypothesize that there must be a mechanism in the cerebellum that can learn and predict the coordinated human-human cooperative behavior, similar to the Kawato model, and generate feedforward control to work with the spinal-muscular reflex feedbacks to have a smooth interaction. As a consequence, we propose that our developed two learning and control frameworks – Co-adaptive Optimal Control and Cooperative Differential Game can exactly fit into this category, and be utilized to realize the biomimic cerebellum learning and neuromuscular control model as a human-like cooperative control strategy. Fig. 3.5 (b) & (c) shows how we can incorporate our co-learning and adaptive control model into the feedforward and feedback control structure. We will evaluate the feasibility of this hypothesis and conduct a series of experiments.

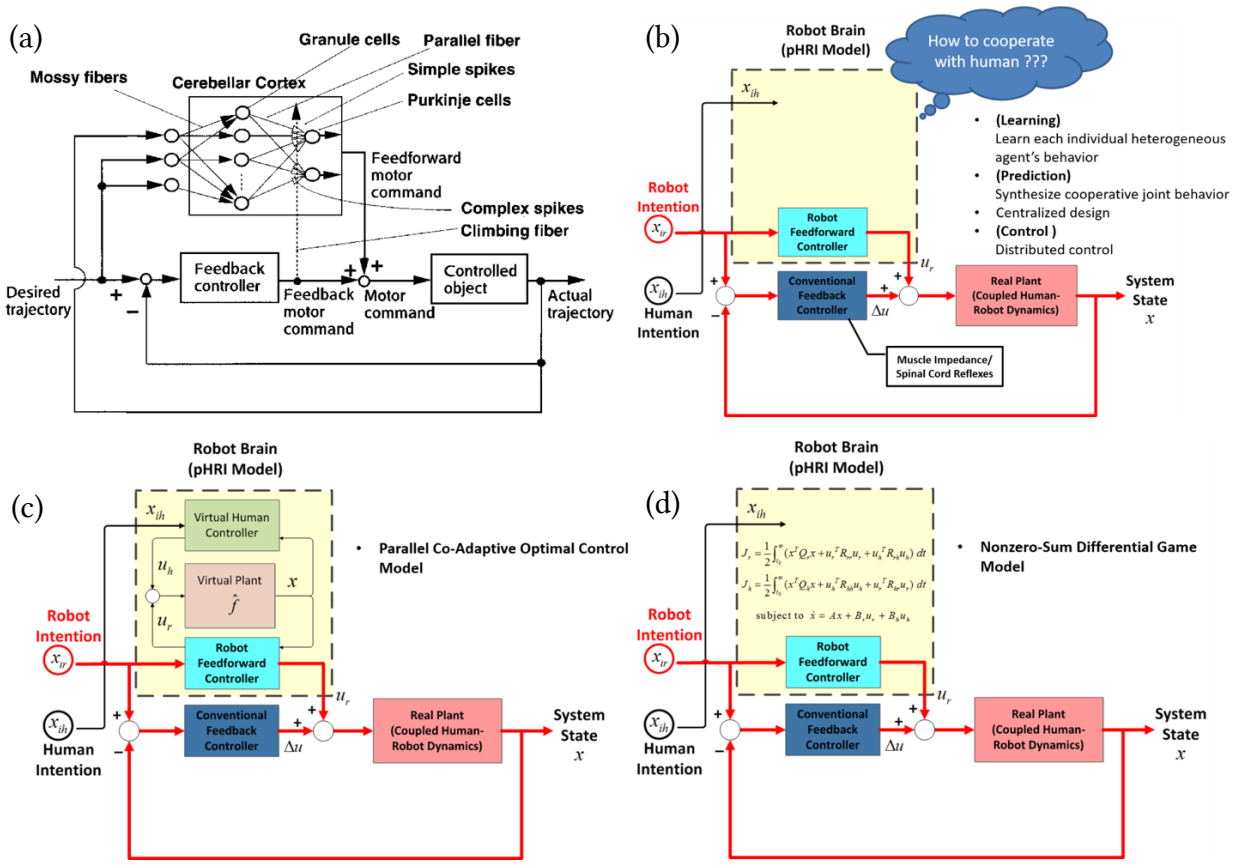

Figure 3.5. The biomimic cerebellum-like cooperative learning, and feedforward and feedback control model. (a) The cerebellar feedback-error-learning model (CBFELM) (Kawato, 1999) [6]. The "controlled object" is a physical entity that needs to be controlled by the CNS, such as the eyes, hands, legs, or torso. The feedback-error learning learns the inverse dynamics of the controlled object and send the predictive feedforward motor command. (b) The similar thing happens in human-robot cooperation, the robot brain (cerebellum) will figure out how to work with the human and send predictive consensus motor command. (c) The hypothesis of the Co-Adaptive Optimal Control as the co-learning and predictive feedforward control paradigm. (d) The hypothesis of the Nonzero-Sum Differential Game theory as the co-learning and predictive feedforward paradigm. Both (c) and (d) are simulating the cerebellum function of learning the cooperation task dynamics.

3.6 Exoskeleton Simulation to Verify the Theoretical Framework with Human Subject Experiment

To verify the feasibility of our Human-Robot Co-Adaptive Optimal Control and Cooperative Differential Game, we will use MATLAB Simulink to establish a virtual reality environment to simulate human-robot cooperative balancing task (Fig. 3.6). Human, as an intrinsic adaptive optimal controller, will use force feedback joystick as input to control the robot. Meanwhile, the robot, as another adaptive optimal controller, will response to the human input. The goal of the experiment of cooperative balancing task is to build a virtual double-inverted pendulum, which represents a simplified exoskeleton platform, and human and robot are cooperatively maintaining the virtual double-inverted pendulum at the upright balance position.

In this simplified platform, human can use force and on-screen visual (i.e., position) feedback to learn the robot control behavior. Also, the embedded torque sensors and encoders in joystick can let robot learn human's control behavior.

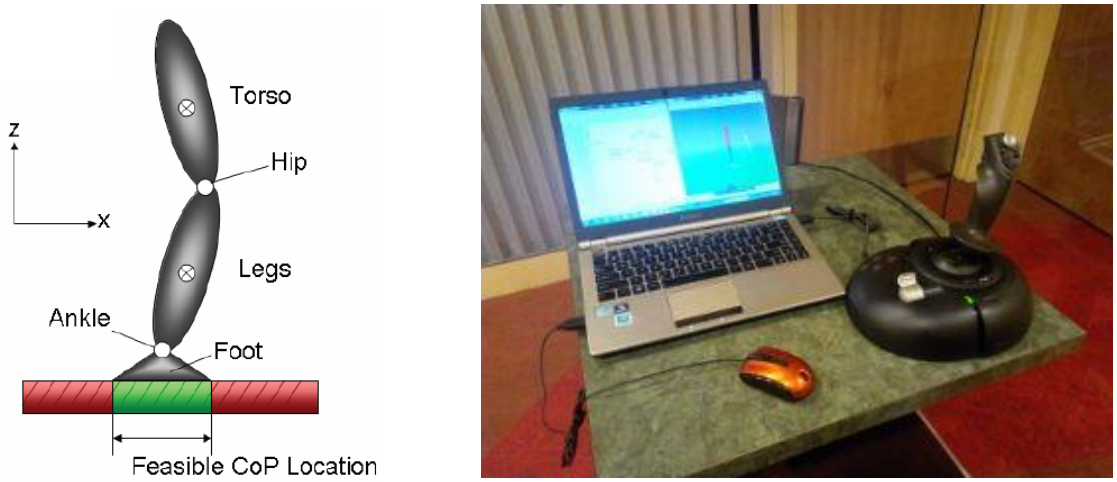

Figure 3.6. Matlab Simulink platform of double-inverted pendulum. Human can cooperate with the robot by using joystick to control the hip joint, while robot will be responsible for controlling the ankle joint.

The nonlinear dynamics of the double-inverted pendulum has been linearized at the upright balance position. The model of double-inverted pendulum is an underactuated system, meaning that even though each controller is responsible for different joints, they can still influence the other joint, since the entire system is controllable.

During the first experiment, we temporarily do not include human behavioral learning component inside. In doing so, we want to verify the performance of human and robot controller individually, and compare them with the centralized controller (i.e., robot controls both hip and ankle joints at the same time). This way can give us a general idea on how well we can improve the performance if we add the human-robot cooperative control strategies later. Here, the robot optimal control cost parameters are $Q = I_{4x4}$, $R = I_{1x1}$, and the centralized control strategy is $Q = I_{4x4}$, $R = I_{2x2}$. Human just control the hip joint with joystick using his or her own control strategy. The correspondent trajectories are plotted in Fig. 3.8. From Fig. 3.8, we can observe the worse performance at all joints by the human hip controller (green line). Human spends longer time for the states to converge to zero (Fig. 3.8 (a) and 3.8 (b)), and applies a lot of control effort (Fig. 3.8 (c)), compared to the other control methods (robot ankle controller (red line) and centralized controller (blue line)).

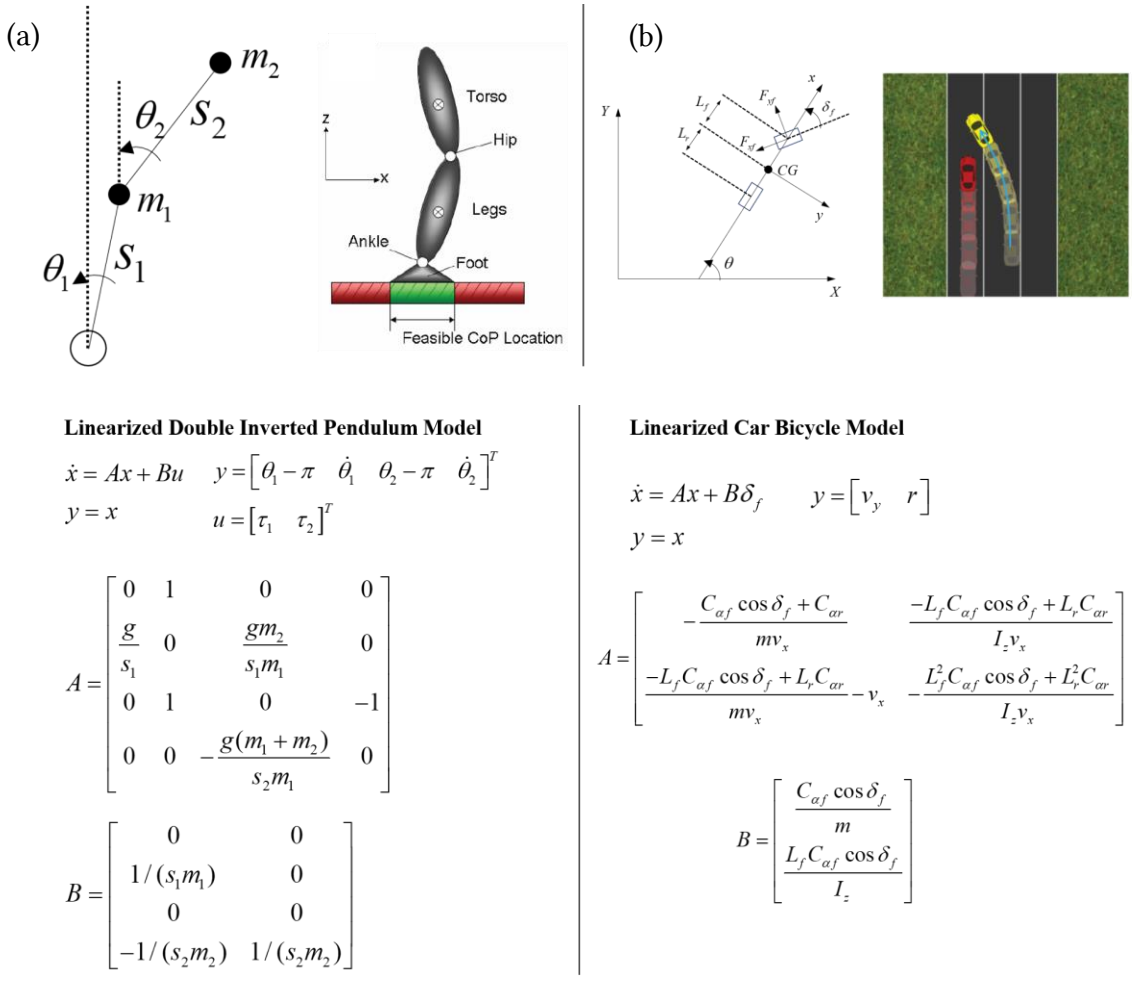

Figure 3.7. Human-Robot cooperation tasks with the linearized model. (a) Human and robot are cooperatively maintaining the double-inverted pendulum at the upright position. Human is controlling the hip joint, while the robot is responsible for the ankle joint (Hip-Ankle balancing strategy) to simulate that humana and robot are cooperaive balancing on an exoskeleton device. (b) Human-Robot cooperative driving scenario with linearized model. This model is often simplified by projecting the front and the rear wheels on two virtual wheels located at the middle of the car. It is called the bicycle model. Human and robot will consider their mutual cost function to figure out the optimal cooperation strategies to merge in a single lane.

(a)

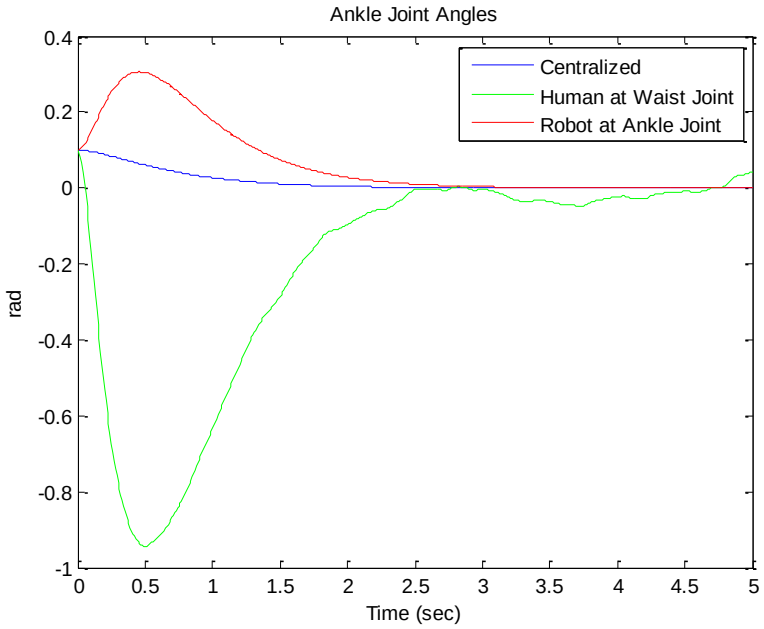
Ankle Joint Angles
Centralized
Human at Waist Joint
Robot at Ankle Joint
rad
Time (sec)
0.4
0.2
0
-0.2
-0.4
-0.6
-0.8
-1
0
0.5
1
1.5
2
2.5
3
3.5
4
4.5
5

(b)

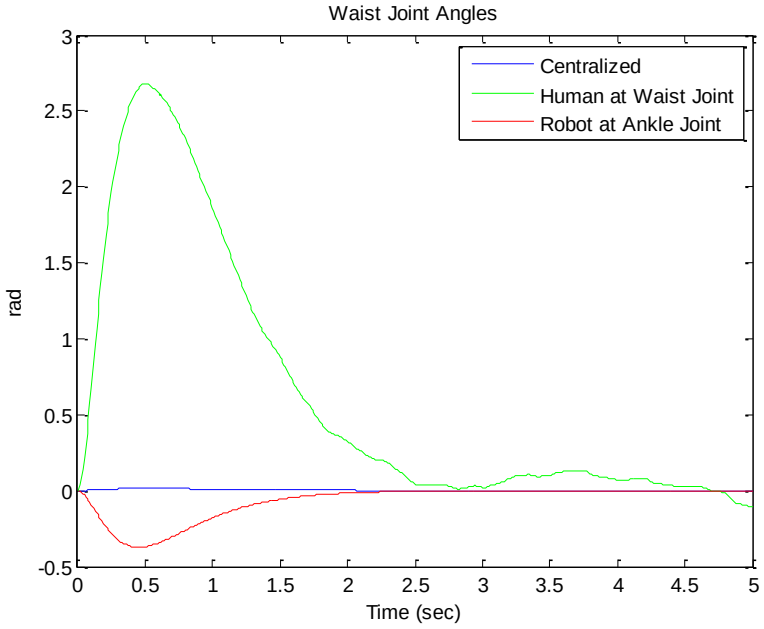
Waist Joint Angles
Centralized
Human at Waist Joint
Robot at Ankle Joint
rad
Time (sec)
3
2.5
2
1.5
1
0.5
0
-0.5
0
0.5
1
1.5
2
2.5
3
3.5
4
4.5
5

(c)

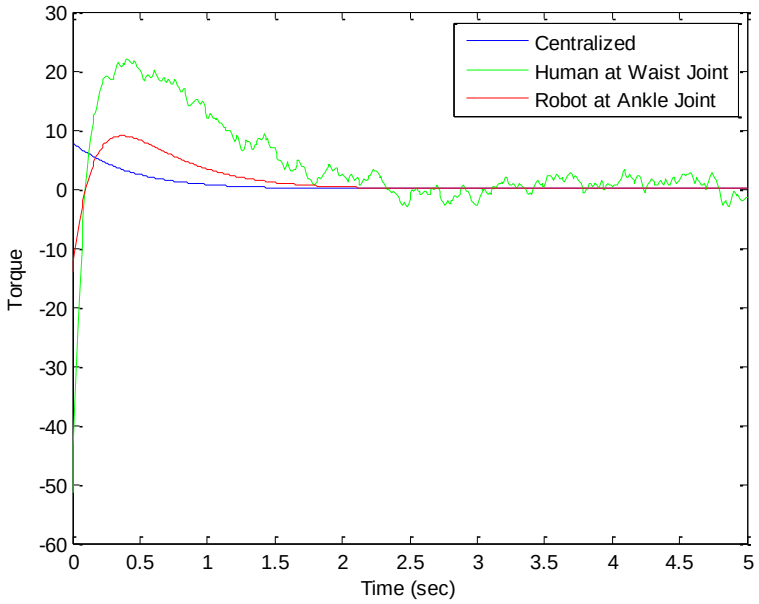

Figure 3.8. Performance comparison between each individual controller (i.e., human control the hip joint and robot control the ankle joint separately) and the centralized control strategy (i.e., robot control both joints at the same time). (a) Ankle joint trajectory. (b) Waist joint trajectory. (c) Overall torque output from both joints.

In the second experiment, we verified the performance of our proposed human-robot co-adaptive optimal control framework. Since both human and robot are going to maintain the double-inverted pendulum at upright position, we already know that their intended goals are the zero joint angles, so we do not need to estimate human intentions during our experiment. Before we implement our cooperative control strategy, we let the human practice several times to try to cooperate with the robot. It is for the purpose to ensure that human can use his or her subconscious reflective response to cooperate with the robot. This can also make sure that human will use the same control strategy, {Q, R}, to cooperate with the robot in the later experiment. Therefore, our predictive control algorithm can be correctly applied.

To solve the convex optimization problem stated in (12)-(16), we used CVX, a package for specifying and solving convex programs [104], [105]. Thereafter, we can use the learned human control strategy {Q, R}, to reconstruct a virtual human control model in the robots' brain. Robot will figure out how to cooperate with the human and accordingly generate consensus control gain to balance the pendulum with the human. Fig. 3.9 illustrates the system trajectory under our cooperative control framework.

Here, we use least square method to estimate the human feedback gain K_h from the recorded joystick torques and the on-screen system states (double-inverted pendulum joint angles):

$$k_h = \begin{bmatrix} 29 & 23.5 & 11 & 7.6 \end{bmatrix}. \tag{3.54}$$

The learned human control strategy after convex optimization is:

$$Q_h = \begin{bmatrix} 19.7817 & 9.2819 & 1.4567 & 8.5022 \\ 9.2819 & 7.2829 & -5.8330 & 3.4732 \\ 1.4567 & -5.8330 & 26.4347 & 3.4747 \\ 8.5022 & 3.4732 & 3.4747 & 5.1618 \end{bmatrix}, \quad R_h = 1. \tag{3.55}$$

Fig. 3.9 shows that the cooperative control strategy under our proposed framework is very similar to the centralized control. Fig. 3.9 (a) seems to have a large discrepancy, but it has a small unit scale on the y-axis. The overall performance has been improved compared to the previously mentioned methods, where we used each single controller to control all the joints.

(a)

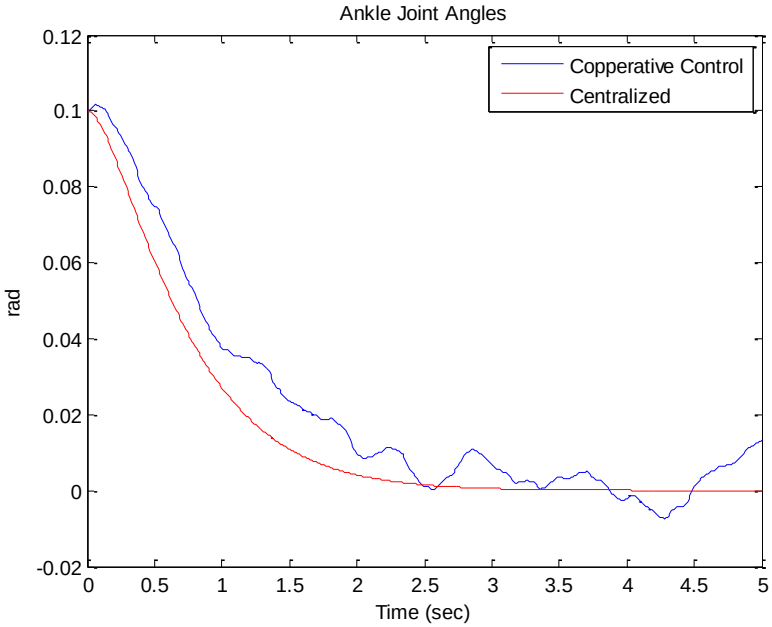
Ankle Joint Angles
Copperative Control
Centralized
rad
Time (sec)
0.12
0.1
0.08
0.06
0.04
0.02
0
-0.02
0
0.5
1
1.5
2
2.5
3
3.5
4
4.5
5

(b)

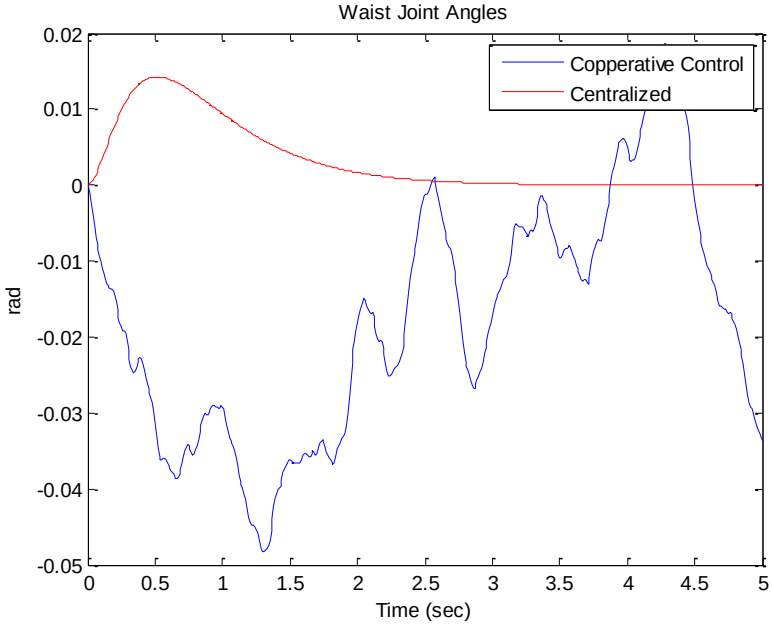
Waist Joint Angles
Copperative Control
Centralized
rad
Time (sec)
0.02
0.01
0
-0.01
-0.02
-0.03
-0.04
-0.05
0
0.5
1
1.5
2
2.5
3
3.5
4
4.5
5

(c)

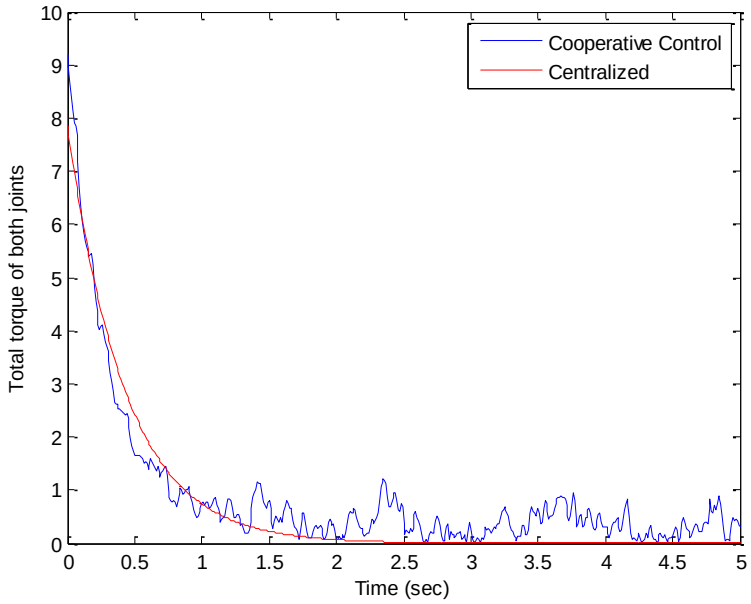

Figure 3.9. Performance comparison between the cooperative controller (i.e., human and robot control hip and ankle joints cooperatively) and the centralized control strategy (i.e., robot control both joints at the same time). (a) Ankle joint trajectory. (b) Waist joint trajectory. (c) Overall torque output from both joints.

4.0 Development of Human-Centered HMI System for Seamless Human-Machine Interaction

In the future, Human-Machine Interaction (HMI) should be enabled by a compact, human-centered and ergonomic wearable device that can merge human and machine altogether seamlessly by constantly identifying each other's intentions. To meet this end, we have developed an ergonomic and light-weight wearable device that can identify human's facial/eye, body gestures with deep physiological signal learning technology. Since human's intentions are usually coupled with eye movements and facial expressions, through proper design of interactions using these gestures, we can allow people interact with the robots or smart IoT devices naturally and intuitively. With the help of computer vision and Human-Robot cooperative AI, we can let people use very simple and straightforward interaction strategies to send high-level commands to operate telepresence robot and control smart IoT objects remotely, totally "Hands-Free". People can wear a VR head-mounted display and see through the robot's eyes (the remote camera attached on the robot) and interact with the surrounding smart devices by simple facial gestures or eye movements. It is tremendous beneficial for the astronaut to do multiple tasks at the same time. For example, they can use facial/eye gestures to control a third robotic arm to help manipulating the objects while their hands are busy at working on something else or operating other hand-held devices. They can also control a telepresence robot to navigate around the environment by intuitive facial/eye movements and let their hands to remote-control the other two robotic arms to do bimanual tasks simultaneously. It not only provides extra controllability in hyper-dimensional space for the normal people, for the people with motor

impairment, they can also use our device as an assistive tool to control their surroundings without using their hands at all.

4.1 Brain-Computer Interface Combining Eye Saccade Two-Electrode EEG Signals and Voice Cues to Help People with Motor Disabilities

Recent advancement of AI (Artificial Intelligence), Big Data, IoTs (Internet of Things), Robotics, and AR/VR (Augmented Reality/Virtual Reality) technologies outline a promising near- future of our societies. The news about such rapidly growing technologies can be seen from almost everywhere, such as TV programs, reports/magazines, internet search results and/or other everyday public medias. While people highly praise the development of these technologies, however, we should not forget that such technologies have to center around the human beings, to serve the necessary human's needs. Without human at the center of the intelligence, these promising technologies will lose their meanings, and will not be as impactful as they are supposed to be. To address this issue, a human-centered interaction interface that seamlessly connects human with those beneficial technologies and therefore deliver intuitive messages to the surrounding smart environment is imperatively needed.

However, such developments often neglect the needs for the immense population of the communities with people who have movement or motor disabilities, such as the lost/damage-of-limbs, spinal cord injury, cerebral palsy, multiple sclerosis (or ALS) disease [106]. Because of the lacking of feasible control interface for these people (Current assistive devices usually use head tracking control, sip-and-puff system, camera-based eye tracker, and wheel-mounted joysticks, etc., where users still need to apply a lot of body/lung strength and/or extensive fine

motor control to operate the device. In the meanwhile, these technologies are usually attached to a wheelchair, which is not portable and confines the use to times when the users are seated. The people with speech problems are also not able to use voice assistant), the disabled communities are often segregated from the potential application of such Smart Home technologies to benefit their daily life.

To address this issue, an easy and simple control interface is imperatively needed. For this demand, Brain-Computer Interfaces (BCIs) have been developed for a long time, which provide an alternative approach to solve the above problems.

Electroencephalography (EEG) is a non-invasive technique for measuring the electrical potentials produced by the brain, and has been used in various Brain-Computer Interfaces (BCIs). BCIs offer a direct communication pathway between wired brain signals and an external device, such as a prosthetic arm or a robotic manipulator, which allows them to be incredibly useful in the field of assistive technology [107] - [109]. Fig. 4.1 illustrates some state-of-the art technologies of EEG-based BCIs and their applications. Despite the advantages of BCIs, many critical issues face the development of a BCI. First of all, EEG signal classification methods have low accuracy, because brain waves consist of signals that originate from various parts of the body, so the imagined movement is often lost in this mixture of various signals [110]. Furthermore, the training process for the user to operate a BCI is often tedious, since most brain wave classifiers are non-adaptive. Therefore, human users must learn to adapt his/her brain waves to match the classification method of the machine, a process that is both challenging and time-consuming [111], [112]. Finally, the numbers of identified mental states while operating a BCI is currently very limited. For instance, the current off-the-shelf BCIs, such as Neurosky Mindwave [113] and Emotiv EPOC [114], can only identify two mental states – “focus” and

"relaxation", and are not suitable to generate multiple commands to control complicated maneuvers. Designing a seamless human-machine interface that is easy to use, portable, has high fidelity, and can generate as many commands as possible to communicate various devices would definitely be beneficial.

Figure 4.1. Non-invasive EEG and its state-of–the-art applications. (a) 2014 World Cup kick off by a paraplegic man with the help of a full body robotic EEG-signal-controlled exoskeleton (Developed by Duke university) [115]. (b) BCI-based humanoid robot control system [116]. (c) Graz-BCI Game Controller controlling World of Warcraft (Blizzard Inc.) just using EEG [117]. (d) Puzzlebox Orbit, a brain-controlled helicopter with the help of NeuroSky MindWave EEG headset [118].

There have been many research efforts attempting to address the aforementioned problems. Subha et al. [119] detailed the effect of environmental and physical factors on EEG

signals. As a result, more sophisticated methods of variability analysis are required to differentiate between physiological signals and signals caused by environmental disturbances. Co-adaptive learning algorithms can alleviate the tedious human-learning problem, since the machine can adaptively optimize its learning structure to conform to the human-learning performance in order to maximize the classification efficiency/accuracy of the BCI [120]. However, this co-learning behavior often encounters conflicts. Although the human user can naturally adapt to the demands of the machine, it is difficult for the machine to predict how the human user will change his/her brain waveform, since human brain waves are affected by many different physiological activities, and are not very stable. Another method to reduce the human-learning effort is to extract existing EEG signals that correlate to specific body movements. Since these control signals are innately developed, capturing these signals to operate an external device eliminates the human-learning effort. In this research, we focused on neurophysiological signals associated with eye saccade movement, which can provide an ideal source of EEG data to generate useful commands.

4.1.1 Approaches

Presently, signals from eye saccades are largely viewed as artifacts in EEG data [121], however recently, Meyberg et al. [122] discovered that eye saccades are actually followed by "cognitively-modulated brain potentials" that can be used to communicate with and to control a BCI. However, few researchers have explored the possibility of using eye saccade EEG data for such purposes. Therefore, we hypothesized that EEG signals associated with saccade movement can be used as a trigger to communicate with a BCI. We design a machine-learning algorithm that can identify neural activities and separate EEG signals associated with eye movement, and

use these signals to operate a human-machine interface. Because raw EEG data contains a mixture of signals that originate from different physiological and environmental movements, specifically extracting saccade signals presented a challenge. In order to solve this problem, we proposed to use Independent Component Analysis (ICA) [123] to separate the different kinds of signals. Furthermore, we used K-Nearest Neighbors (KNN) [124], [125] and Support Vector Machine (SVM) [124], [126] algorithms in order to classify EEG signals associated with saccade movement as different categories. Once these meaningful signals were extracted from the raw data and classified, we used them for control purposes. The developed strategy can be further implemented on any external platform, such as a robotic wheelchairs (in our experiment) or wearable devices.

Since one of our research aims is to create a portable, universal human-machine interface to control any possible external device, we want generate as many commands as possible. For this reason, we propose to combine additional earbuds to provide periodical or voice-mailbox-typed voice cues to inform the user on when to make adequate eye saccadic movements. Thereafter, we can select the correspondent functions from the voice menus and consequently trigger the commands. Under this approach, even if we have limited number of identified mental (saccadic) states, through properly designing the contents, as well as unlimitedly expanding the options of voice menu, we can easily generate lots of commands to operate the external devices. We will verify this idea by generating commands to drive a robotic wheelchair to navigate around the environment.

Also, based on our placement of the two electrodes on top of the left and the right ears, it is very sensitive to the eye related movements. We can get a very high-quality eye saccade-related EEG signals. The selection of only two electrodes can guarantee a simple design, and

they can be seamlessly integrated into the existing off-the-shelf sporttyped earbuds. As a result, we can have a very compact and portable design that can be easily hooked up on any user's ear and be carried around. We expect that this technology will have a tremendous impact on human-machine interaction and can be a universal controller to control lots of different appliances in the future. Fig. 4.2 shows the general design concept and the strategy of our approaches.

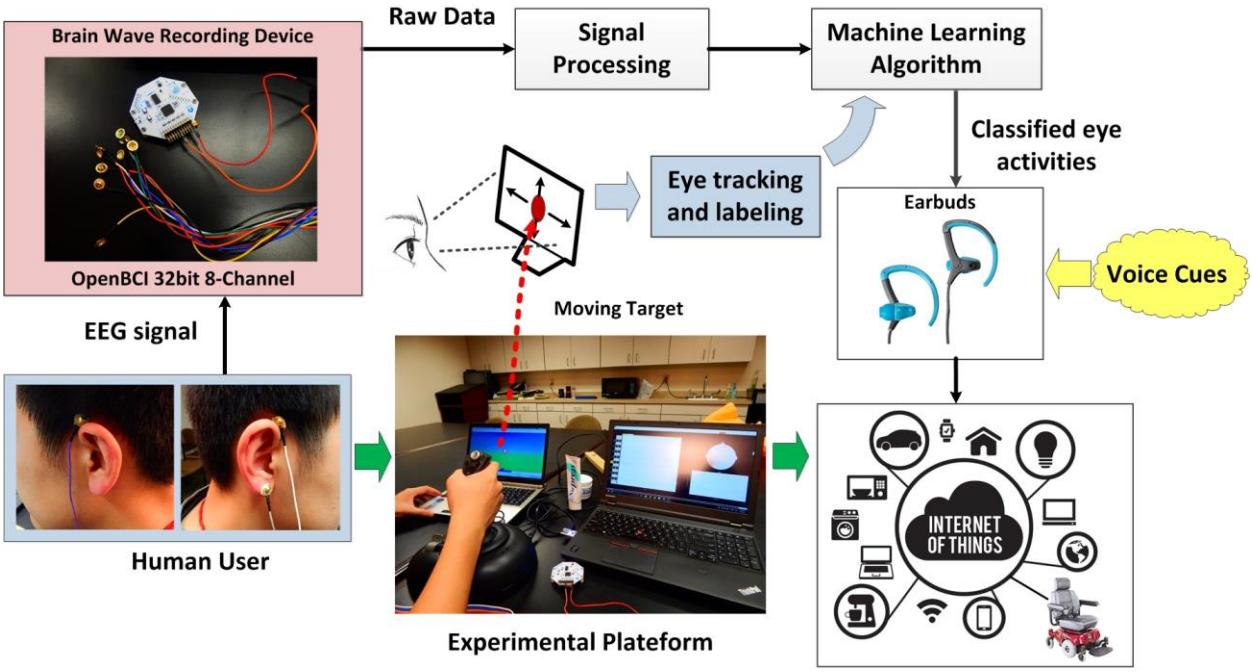

Figure 4.2. Experimental platform and the general architecture of the proposed eye-tracking enhanced BCI to control wheelchair and internet of things.

4.1.2 Methods

4.1.2.1 Experimental Procedure

Thirteen participants (3 females, 10 males) with a mean age of 28 (standard deviation (SD): 8.9) were seated in a chair and instructed to watch a computer screen located at eye level. All subjects reported normal or corrected vision, however we asked all participants to remove

eyeglasses to eliminate foreign contact with EEG electrodes. Subjects participated in a real-time simulation, followed by a wheelchair navigation experiment. We designed the real-time simulation to record EEG saccade data for learning and classification purposes (as shown in Fig. 4.2). In this study, the classification accuracy was calculated based on the categorization of the real-time data by our learning algorithm, while the control performance was evaluated based on the performance of the wheelchair experiment. The computer simulation consisted of a large red ball that is moved by a joystick. In our experiment, thirteen participants were asked to complete two tasks. The first task was to follow a red ball moving left and right on the computer screen controlled by the joystick with solely eye movement. The joystick was used for the purpose of labeling the correct eye movement as the ground truth. Here, we move the joystick roughly every one second. The second task required the participant to blink every time the red ball reached the top of the screen, which occurred every two seconds. All tasks lasted for 90 seconds.

EEG signals were acquired during the real-time simulation using an OpenBCI 32-bit, 8-channel board [127] at a sampling frequency of 250 hertz (samples/s). It provided a simple method for data collection, along with USB noise elimination when wireless communicated between the recording computer and the testing electrodes. Two EEG electrodes were attached to the upper area behind the left and right ears, close to the eyes. This position allowed us to capture EEG signal without the obstruction of hair. Also, because we used only two electrodes, the participant felt minimal discomfort. A third electrode was attached to the right earlobe as a reference signal. Assigning electrodes to such locations allowed us to detect groups of neuronal activity that is associated with eye saccade movement. Based on our testing results, we confirmed that this location can guarantee the best quality of the eye-activity-related EEG signals.

4.1.2.2 Classification Algorithms

After recording the EEG signals from the right and left ears, we applied a band-pass-filter (BPF) from 1 to 45 Hertz, as EEG signals are limited to that range and anything higher would be electric power line or other environmental noise. Additional cleaning was required to remove the DC offset, which was caused by the power supply and can be removed by subtracting the mean value from each waveform. Then, the mixture of raw EEG signals was decomposed through Independent Component Analysis (ICA). Independent Component Analysis splits the artifacts from the EEG signals into independent components based on the characteristics of the data, without dependence on the reference channels. The ICA algorithm decomposes the multi-channel EEG data into temporal independent and spatial fixed components, and has been proved computationally efficient [128]. Fig. 4.3 describes the general concept of ICA algorithm utilized in our study. Previously, ICA has been used to remove artifacts, such as eye saccades and other physiological activities, from EEG signal. However, in this study, we proposed that eye saccades are not merely artifacts, but has many interesting features that can be learned by a proper machine-learning algorithm and can serve as an indicator of human intention.

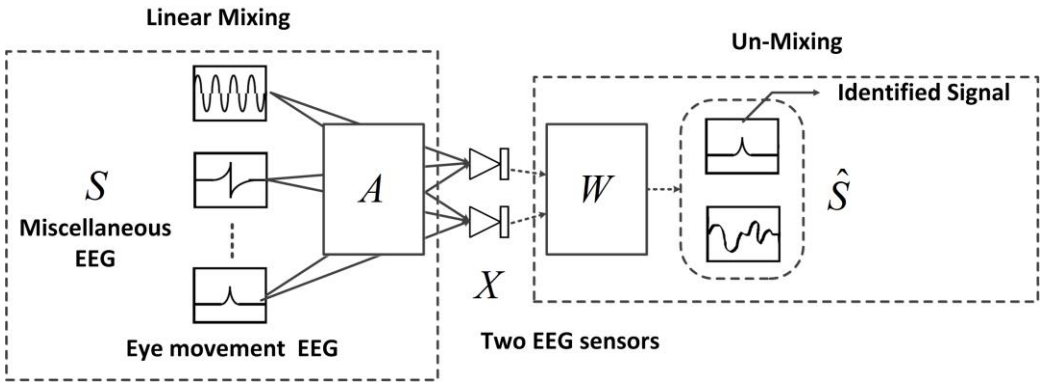

Figure 4.3. The ICA algorithm we have used to separate the independent eye movement component.

Suppose we have a mixture of raw data expressed as vector $X \in R^2$, has dimension 2 because we only have two electrodes to collect EEG data. We also have n miscellaneous EEG source signals $S = [s_1, s_2, ..., s_n]^T$ to be separated from the raw data. The linear transformation between *X* and *S* can be expressed as *X* = *AS*. The objective here is to find $W = A^+$, where *W* is the pseudoinverse of *A*. Thereafter, we can separate the source using $\hat{S} = WX$. Here, if all the source signals are non-Gaussian and independent, we can use the gradient descent learning rule and maximum likelihood estimation to maximize the joint probability distribution (4.1) to find *W* [128].

$$p(X) = \prod_{i=1}^{n} p_s(w_i^T X)|W| \ . \tag{4.1}$$

The raw captured data and the resulting signal after BPF and ICA are plotted in Fig. 4.4 and Fig. 4.5. We can observe a pretty clear and much cleaner signal compared to the raw data. After then, according to the previously described experimental procedure, we had used joystick controlled red ball to record the eye saccade occurrence. It gives us clues on when to label the onset of eye movement as the ground-truth training data. In order to double check the correctness of the labeling, we also determined the saccade-related components by observing all the time series data after ICA, and marked the data points that had the most obvious responses during the saccade onset and offset time roughly every one second as the eye saccade-related signals. After labeling the saccade movements and blink patterns with their respective EEG signals, we can notice from Fig. 4.5 that each eye movement has unique waveform patterns and can be suitably used as training datasets to train our classifiers.

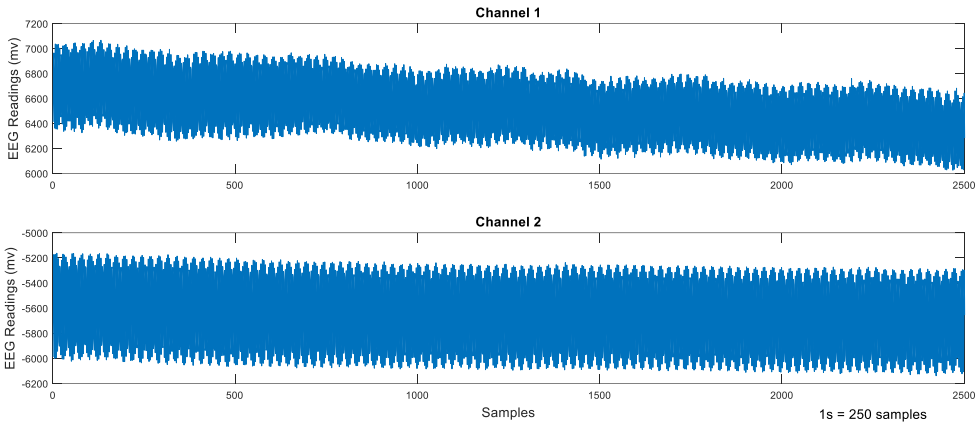

Figure 4.4. Captured raw channel data from the right and left electrodes.

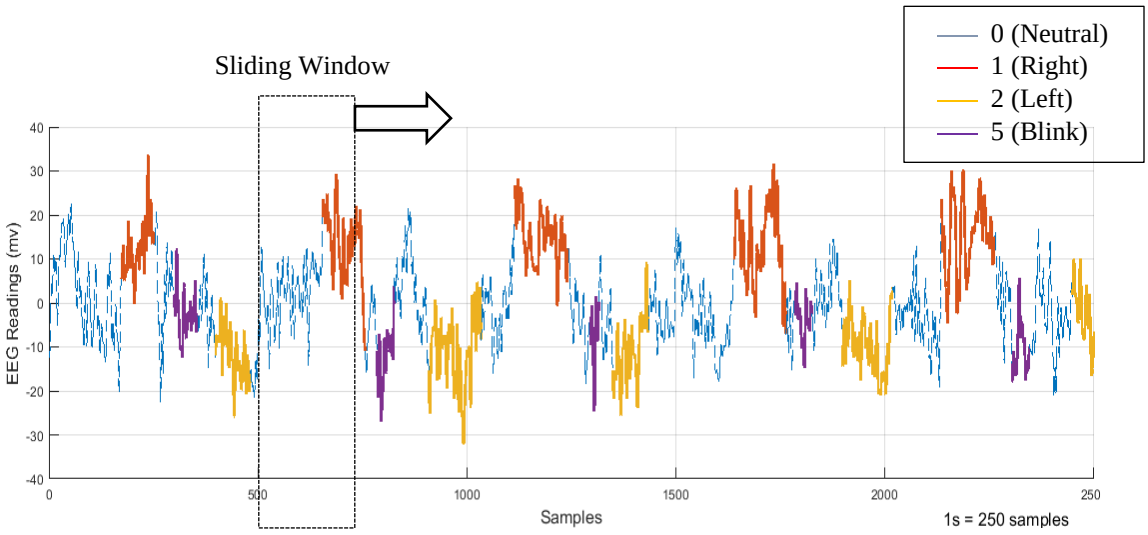

Figure 4.5. The extracted signal after the application of band-pass filter and ICA. The ground truth labels of the signals that correspond to various eye motion directions and the blinks are indicated in the legend.

After the ICA and the manual labeling, the data points were extracted and stacked up into the interested EEG features by Sliding Window method [129]. We then used Multiclass Support Vector Machine (MSVM) and K-Nearest Neighbor (KNN) to classify the EEG features into 3 classes: left, right and blink. The Support Vector Machine (SVM) [126] classifier is widely used by most BCI applications. It finds the hyperplane that maximizes the margin between the plane itself and the nearest data points for each class. K-Nearest Neighbor (KNN) [125] assigns the

feature vector to the class based on its nearest neighbors, and predicts the test dataset's membership based on the k-closest training examples in the feature space. The extracted feature space data points by the Sliding Windows method were manually labeled into the respective 3 categories as previously mentioned, and were used to train and test the aforementioned two learning algorithms.

4.1.2.3 Eye Controlled Wheelchair Maneuvers

To demonstrate the efficacy of the proposed classification algorithm, we created a customized application system for this project, where the participant can control a wheelchair navigating around the environment through eye movement (left, and right), and blink. Using EEGLAB and the open source software Lab Streaming Layer [130], we were able to live stream the raw EEG data from the electrodes using a data capturing device (OpenBCI 32-bit 8-channel board), to MATLAB to complete the previously mentioned signal processing and offline machine-learning procedure. After we trained the classifier model using offline learning, we used the model as well as the live-streamed data to complete the real-time signal classification. We were able to generate eye movement related commands from the recorded EEG signals and use these commands to select the directional maneuvers from the predefined voice menu with the use of earbuds. Fig. 4.6 illustrates our overall offline training and online classification architecture to access voice menus in real-time. Fig. 4.7 and Fig. 4.8 show the results.

4.1.3 Experimental Results

After completing the experimental procedure, we noticed significant responses from the machine-learning algorithm for eye movement in the left-right directions. Since from a

biological point of view, humans mostly live in a horizontal space, our brains largely process horizontal neural information rather than that from a vertical space. We noticed nearly perfect classification results for eye movement in the horizontal directions and eye blinks. Table 4.1 shows the classification performance of the KNN algorithm, while Table 4.2 demonstrates that of the SVM algorithm. From the results generated from 13 participants using the applied learning algorithms, the average signal classification accuracy was around 97%, as detailed in the box plots of Fig. 4.8. The precision and specificity of the aforementioned activities using the KNN algorithm reached percentages near and above 90%. These results demonstrate the efficacy of our proposed approach to combine ICA and the classification learning algorithm to differentiate between the various classes of eye movement.

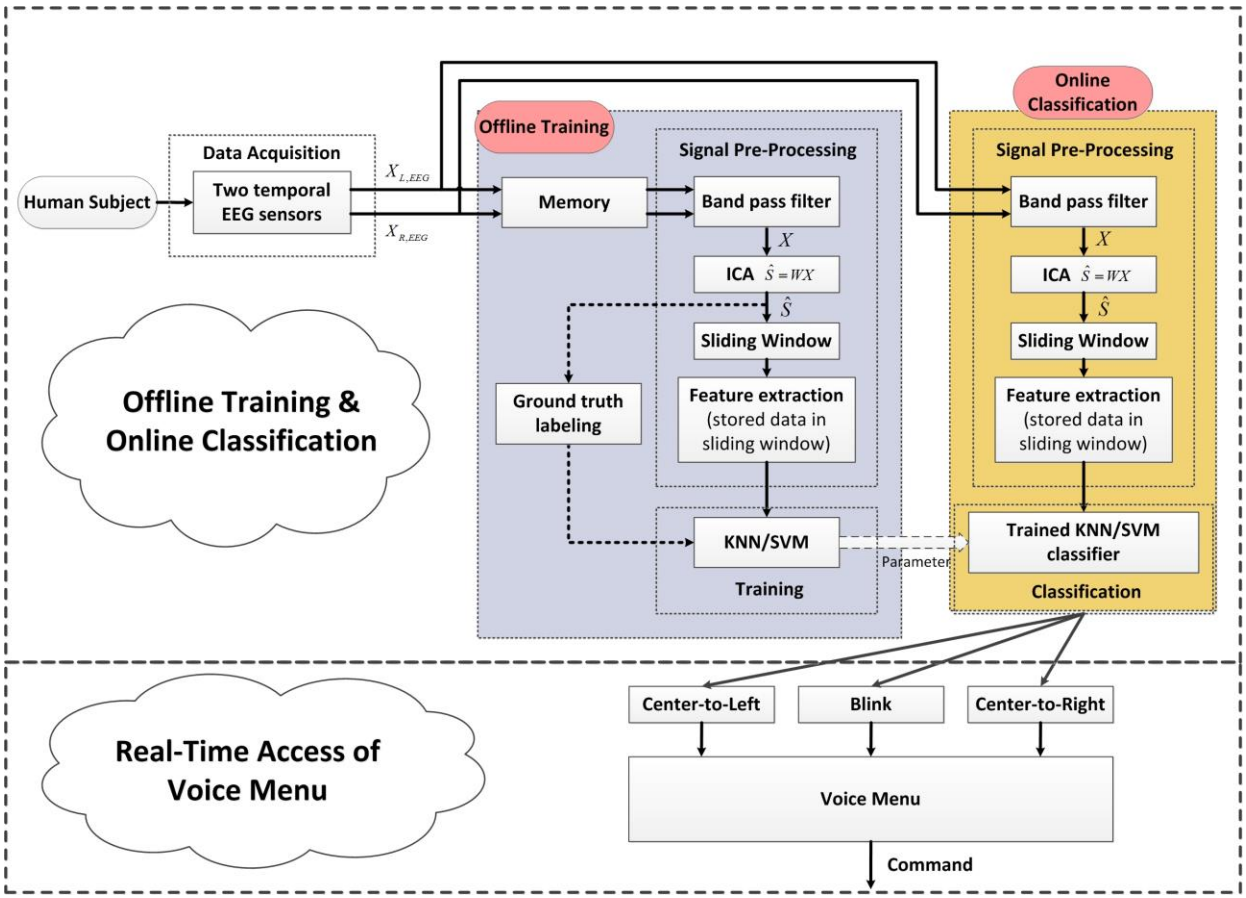

Figure 4.6. Overall offline training and online classification architecture to access voice menu in real-time.

Table 4.1. Classification performance of KNN

	Class 0: Neutral		Class 1: Right		Class 2: Left		Class 5: Blink	
	AVG	SD	AVG	SD	AVG	SD	AVG	SD
Accuracy	0.9841	0.0092	0.9743	0.0132	0.9686	0.0207	0.9713	0.0242
Sensitivity	0.9882	0.0119	0.6950	0.1427	0.6771	0.1659	0.7818	0.1181
Specificity	0.8512	0.1362	0.9897	0.0120	0.9910	0.0073	0.9930	0.0047
Precision	0.9903	0.0069	0.9281	0.0380	0.9057	0.0457	0.8239	0.1150

Table 4.2. Classification performance of SVM

	Class 0: Neutral		Class 1: Right		Class 2: Left		Class 5: Blink	
	AVG	SD	AVG	SD	AVG	SD	AVG	SD
Accuracy	0.9666	0.0113	0.9621	0.0122	0.9650	0.0108	0.9766	0.0104
Sensitivity	0.9910	0.0102	0.5218	0.2855	0.4914	0.3709	0.3189	0.2338
Specificity	0.5739	0.3956	0.9919	0.0072	0.9866	0.0149	0.9988	0.0016
Precision	0.9729	0.0171	0.9099	0.0477	0.9429	0.0580	0.9248	0.0709

The performance of the SVM algorithm is slightly lower than that of the KNN algorithm, especially in the sensitivity category, which has lower average values and a larger standard deviation. The reason may be due to the overly precise learning model that caused over-fitting of the training dataset. The SVM algorithm we used had a nonlinear Gaussian kernel, with a scale of 2.5. The algorithm easily included all of the noisy data points into the boundaries separated by its hyperplane, which then caused a correct testing dataset to be non-observable. Another major reason that could have affected the performance of the SVM algorithm was the manual labeling and selection of the length of the Sliding Window. The manual labeling may have failed to correlate a correct dataset with its respective category. Also, the manual selection of the length of

the sliding window may not have included all of the interested features of the dataset into the container vector. It also had the possibility to over-include the unnecessary data points into the feature space, or include an insufficient amount of data to represent the whole feature.

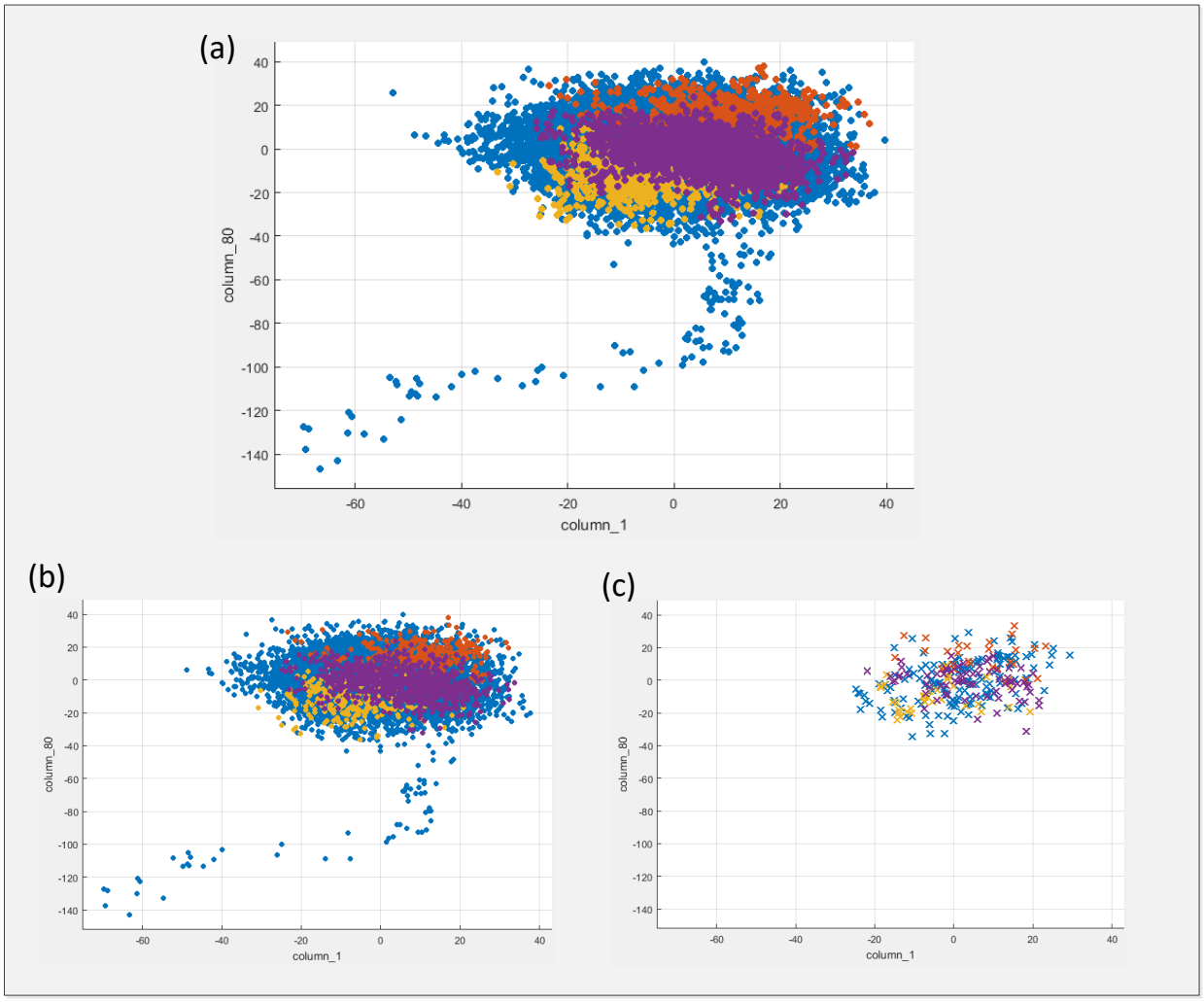

Figure 4.7. Scattered plot of the dataset (shrunk in 2-D space). Here we picked the first and the 80th elements as an illustrative 2D scattered plot for the purpose of easier visualization, instead of the hyper-dimensional (100-D) space scattered plot) trained with KNN. (a) The training dataset. (b) The testing dataset with correct predictions. (c) The testing dataset with incorrect predictions.

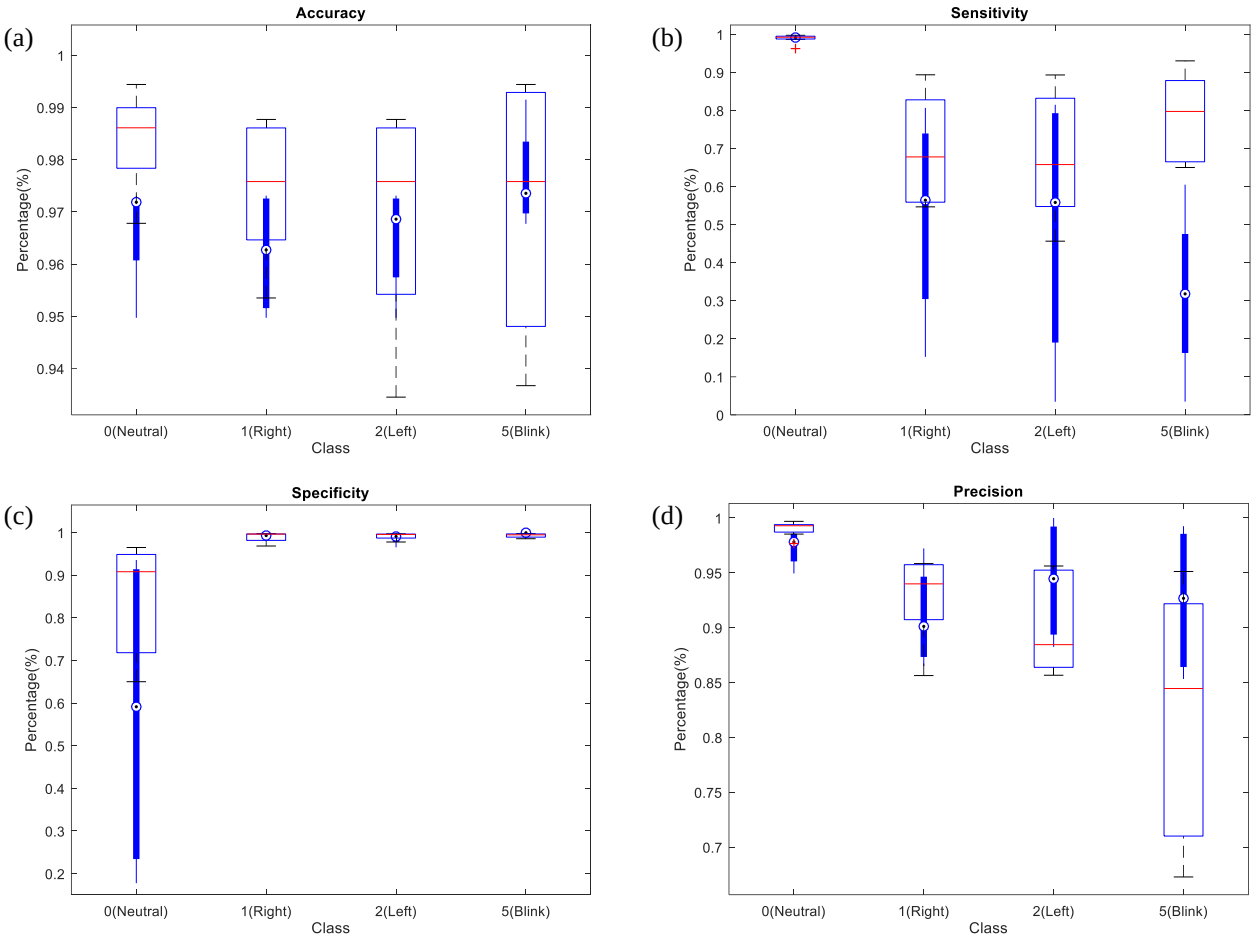

Figure 4.8. Performance box plots. The bolded, outlined box represents the performance of the KNN algorithm, while the thinner, solid blue box represents the performance of the SVM algorithm. The central mark (red line for KNN, small blue circle for SVM) in each class corresponds to its median, the edges of the box are the 25th and 75th percentiles, and the whiskers represent the most extreme data points. The sub-figures are the (a) Accuracy, (b) Sensitivity, (c) Specificity, and (d) Precision, for each class.

The proposed method of using eye saccade EEG signals as probes of human intention and the combination of earbuds to generate infinite number of commands to interact with an external device is a new approach in human-machine interaction. Through this work, we can help both

handicapped and able-bodied users use their eye movements as a means of controlling wheelchairs, smart home applications (internet of things), wearable devices, and computers. We aimed to contribute our development, as illustrated in Fig. 4.9, to be the next generation universal controller of everything. The impact of this product is foreseeable remarkable.

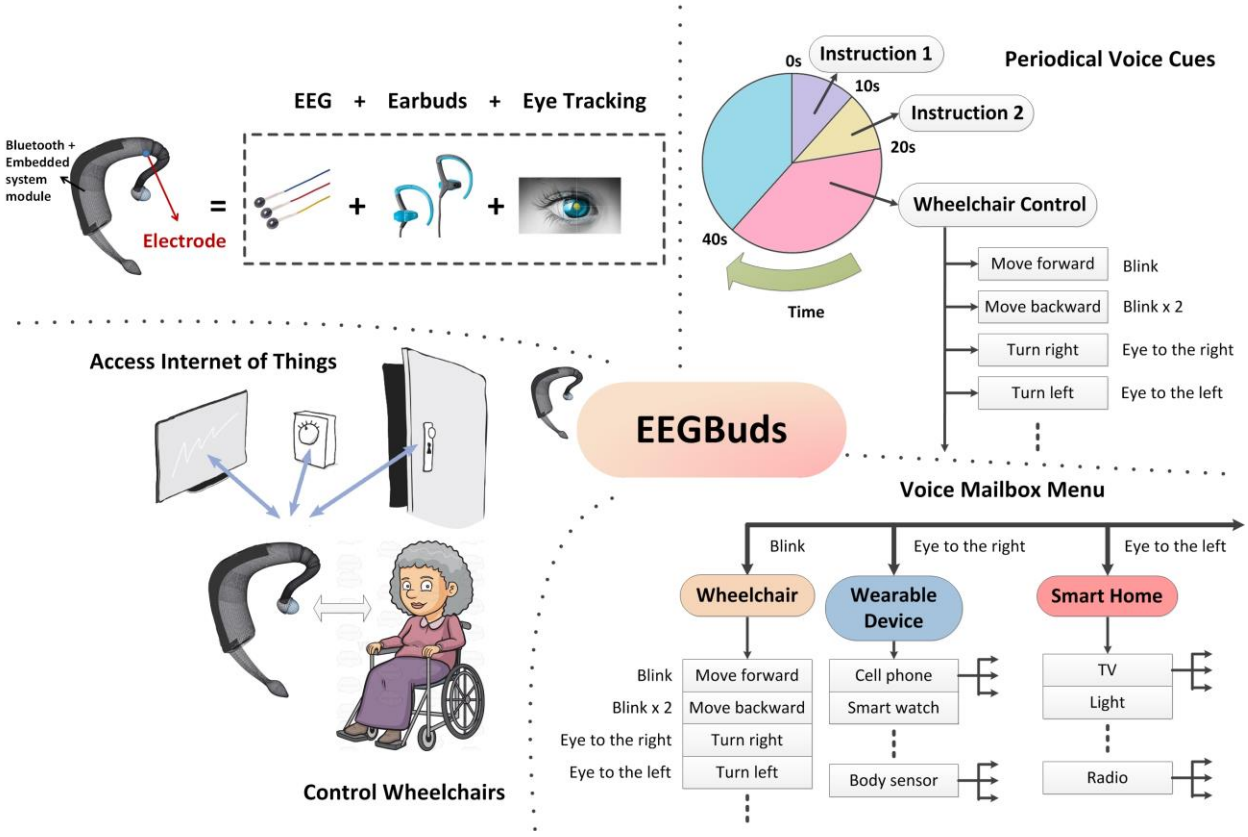

Figure 4.9. Our schematic "EEGBuds" design and its application on rehabilitation and Internet of Thing applications. The beautiful and compact design makes it easily acceptable to the general public. Combining EEG with just two electrodes and the current off-the-shelf earbuds makes it cheap and affordable to everyone. Especially, earbuds can generate voice cues, along with the reliable eye movement EEG commands, we can build an user friendly interface, which can have infinite application possibility, such as rehabilitation and IoT.

4.2 Co-Adaptive HMI Decoder Design

Although the previous step of using traditional machine learning algorithms (i.e., ICA, SVM, an KNN) can get very high accuracy (AVG. 95%), when doing the online classification, it still needs tedious human training to maintain the signal quality as good as it was in the offline training. If the signal patterns drift away, the pretrained classifier will not be feasible anymore. Having our eye movement and facial expression activities as examples, the users must move their facial gestures in a specific timing sequence, similar to what they did during the offline training. If they slightly change the tempo of that activity, the existing classifiers cannot identify the new waveforms, even though they are doing the same activity, such as "Move eyes to the right" or "Blink twice", as before.

This situation reminds us the problem of BCI illiteracy, which means that some people cannot control their brainwaves or physiological signal patterns, so the machine decoder cannot interpret the signals and identify the activities. To solve this problem, we will introduce a new HMI decoder design using our proposed co-adaptive learning and control framework in a cascade system.

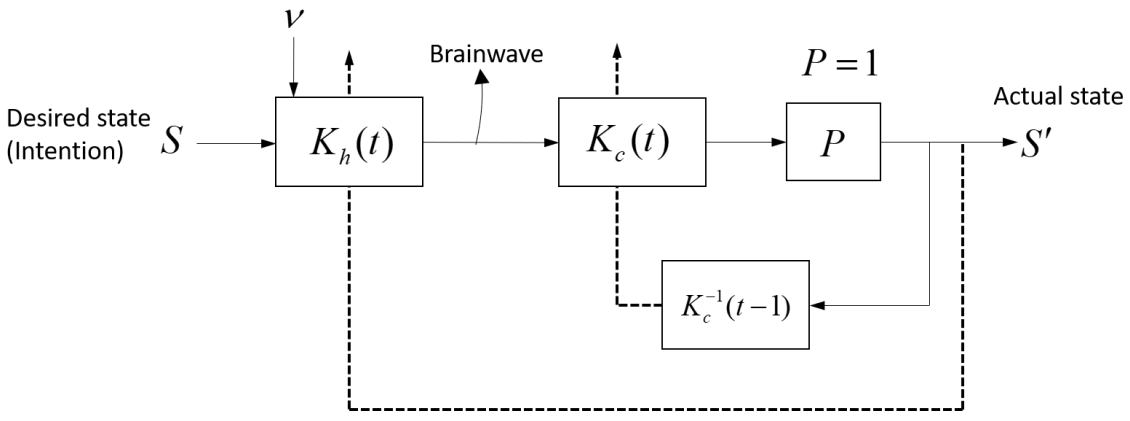

Figure 4.10. Co-adaptive HMI decoder structure.

Fig. 4.10 illustrates the entire structure of our co-adaptive decoder design. *S* is the desired state (human intentions generated from the brain, or desired physiological activity induced by muscle movements). S' is the actual states. $K_h(t)$ and $K_c(t)$ represent the human encoder and machine decoders respectively (Human brain can directly translate the desired intention into the correspondent brainwave waveforms, we call it human encoder).

ν is the drifting noises that effect the signal qualities. And *P* is the controlled plant. Here, we treat *P* = 1, since we simply want to read out the output of the decoder, and we don't have any dynamic system to be controlled at here. The following descriptions show the mathematical formulation of the entire problem.

We can rearrange the parameters in $K_h(t)$ as:

$$K_h(t) = R_h \varphi_h(t) , \tag{4.2}$$

where $\varphi_h(t)$ is the column vector of the rearranged parameters in matrix $K_h(t)$, and R_h is the rearrange matrix.

Similarly, we can rearrange the parameter in $K_c(t)$ as:

$$K_c(t) = R_c \varphi_c(t) . \tag{4.3}$$

Now, we assume we can measure or estimate the changing dynamics of the human encoder, so we can obtain the encoder dynamics as:

$$\varphi_h(t) = A_h \varphi_h(t-1) + B_h u_h(t-1) + \nu . \tag{4.4}$$

A_h and B_h are the system dynamic matrices, and ν is the human control input (i.e., human knows how to change his/her waveforms). Here, we inject the noise to simulate the constantly drifting signal quality that causes the changes of the encoder parameters.

Similarly, we can also write down the dynamics of the machine decoder we are going to design:

$$\varphi_c(t) = A_c\varphi_c(t-1) + B_c u_c(t-1) \ . \tag{4.5}$$

Recall that the purpose of the decoder is to minimize the difference between the desire states and the actual states, i.e., $\min(S' - S)$. We can further formulate this case as the infinite horizon optimal control problem as:

$$\begin{aligned}
&\min \sum_{t=0}^{\infty} \left\| S' - S \right\|_2^2 \ , \\
\rightarrow \quad &\min \sum_{t=0}^{\infty} \left\| (K_c K_h - 1) S \right\|_2^2 = \sum_{t=0}^{\infty} \left\| (R_c\varphi_c(t) R_h\varphi_h(t) - 1) S \right\|_2^2 \\
\rightarrow \quad &= \min \sum_{t=0}^{\infty} (R_c\varphi_c(t) R_h\varphi_h(t) - 1)^T (R_c\varphi_c(t) R_h\varphi_h(t) - 1) \\
\rightarrow \quad &= \min \sum_{t=0}^{\infty} (R_c\varphi_c(t) R_h\varphi_h(t) - 1)^T (R_c\varphi_c(t) R_h\varphi_h(t) - 1) \\
&\text{subject to:} \quad \varphi_h(t) = A_h\varphi_h(t-1) + B_h u_h(t-1) + \nu \ , \\
&\qquad\qquad\quad \varphi_c(t) = A_c\varphi_c(t-1) + B_c u_c(t-1) \ , \\
&\qquad\qquad\quad \varphi_h(0) = \varphi_{h0} \ , \\
&\qquad\qquad\quad \varphi_c(0) = \varphi_{c0} \ .
\end{aligned} \tag{4.6}$$

The problem is reduced to how to find convex transformation R_h , R_c , and design suitable machine decoder dynamic equation, A_c , B_c , so we can use convex optimization under linear equality to find optimal update law, u_c , of the machine decoder.

4.3 Design and Implementation of Intelligent, Ergonomic Wearable Device for Smart Environment Interaction

Recently, Elon Musk has announced the breakthrough advancement of Brain-Computer Interface (BCI) of his Neuralink company, where they have developed microelectrodes arrays and bio-compatible ultra-fine polymer threads which can be inserted into brain tissue with as many as 3,072 electrodes, with micron precisions. In the meanwhile, Facebook Reality Labs' sponsored research project in University of California San Francisco has also built a BCI that accurately decodes dialogue (words and phrases both heard and spoken by the person) from brain signals recorded by implanting high-density ECoG (electrocorticography) electrodes on the surface of the cerebral cortex, in real time. These two big advancements outline a promising future of the direct brain-machine communication, and the dawning of a new era of commercial-grade BCI devices, which is already on the edge ready to hit the vast consumer market, and can potentially benefit every one of us. However, even though both of the companies' devices can read high precision, high bandwidth, real-time brain information, they are pretty invasive. The people have to receive medical surgeries in order to implant the electric circuitries inside the brain.

On the other hand, the constant persuasion of non-invasive approaches is still keeping their momentums, for which so many research labs, startup companies are developing EEG (electroencephalogram) measurement system in either medication, healthcare or consumer applications. The non-invasive EEG electrodes have the advantage that they can easily be integrated into any VR/AR glasses or standalone headset with various form factors to suit different customers/patients' needs. But the low-fidelity, low S/N ratio (average the activity of

thousands of neurons and cannot record signals deep in the brain) is just as what it is the drawbacks of the EEG-wearable devices.

In this dissertation, we want to demonstrate the possibility of high accuracy, low latency brain actionable command generation capability, by using a simple, ergonomic wearable device that identify motion artifacts of the non-invasive EEG signals. We will showcase how we can use an earbud-like device, with two electrodes attached on our brain's temple positions, to detect motion artifacts and generate interaction commands to interact with the environment, the people surrounding you, or communicate with your loved ones remotely.

4.3.1 Approaches and Methods

Our dissertation is on the mission to showcase the next generation Neuro-wear (i.e., wearable device that detect neural signals) for the futuristic human-computer interface. The innovations we demonstrate include the following three important factors, which could help us migrate our Neuro-wear into consumer market smoothly and make it acceptable by the general mass majority: **(a) Human-centered wearable form factor design:** We will showcase our developed wearable device design, with form factors, including materials (bio-compatible with the human body), appearance (sleek, compact, fashionable design, just like decorative accessories attached to the human body), lightweight (people will feel it as a part of their body without external burdens), delicate artworks (breaking the traditional bulky electronic circuits into small pieces and make it soft and flexible, so it can hide inside the fabric materials and be bent around the human body to reduce the overall size). **(b) High-accuracy EEG-physiological signal identification:** Our innovative Deep Learning architecture could potentially identify and reconstruct the original high-fidelity EEG signals, representing the body movement artifact (i.e.,

eye movement, facial expressions, hand gestures, limb movements, emotions, imaginations of the beloved friends), from lossy, sparse, noisy, and inaccurate EEG data. **(c) Engaging Human-smart environment interaction experience design:** In the future, BCI or Neuro-wear devices enable a futuristic interaction methodology that never exists before. Compared to traditional body gesture control or voice command (like Alexa or Google home), which is more perceivable, our team had extensively co-designed various interaction modalities with the end-user groups using non-traditional customer behavior studies and futuristic user experience exploratory design. Therefore we have designed series BCI interaction methodologies, with smooth, non-tiring and engaging user experiences. For instance, you can look at the light bulb and blink your eyes twice to turn it on, smile to open the door, rotate your wrist “Clockwise” or ”Counter Clockwise” to turn on/off the microwave remotely, scratch your skin for “5” seconds to tune up the volume of the radio, think about your loved ones for a couple of seconds, and he/she will detect your intention and receive vibrotactile feedback from our developed wearable robotic wristband (In the meanwhile, your friends can interact with you by thinking about you, or stroke his/her hands for 5 seconds to generate touch-stimulated emotion, and trigger interactive command remotely). We will show case all these possibilities during our demonstration. **(d) Simple ear/headset device to capture all the above-mentioned body gestures/emotions:** Very interestingly, since our brain is the central controller for all our body movements, it turns out we can decode all these control signals directly from our brain. So we don’t have to use extra sensors attached on other parts of our body, like hands, arm or legs to detect motion signals This way dramatically increases the comfortability and improves the mobility of our daily life by just using a simple earbud-like wearable device.

4.3.1.1 Ergonomic, Customizable, and User-friendly Product Development

In our design, we have developed our own noninvasive, self-adhesive, miniaturized, Electrooculography/Electromyography (EOG/EMG) dry electrode sensors, and micro-scale Bluetooth Low Energy (BLE) communication modules (Fig. 4.11, the 3rd generation). The collected signals by electrodes can be clock-synchronized and transmitted to the cellphone App via Bluetooth communications, and then sent to the cloud server for training our Machine Learning classifiers to identify different end-user's physiological signals. In addition, by placing sensors at different locations in their favorite ways, we introduce a human-centered customizable Body Sensor Network array, so people can pick their preferred numbers/locations of the sensors for training and identification purposes. Even more, the users can integrate our sensors into their existing earbuds or headsets and wear it comfortably for long hours for different control applications.

Figure 4.11. Our developed ergonomic, human-centered wearable device provides flexible hardware and software solutions. Users can customize their own design to place sensors at different locations to measure different physiological signals. We also provide software Apps with built-in Machine Learning libraries on the cloud, such that users can pick different eye/facial gestures and compose their own control commands to interact with different applications.

4.3.1.2 Machine Learning Algorithms to Identify Various Eye and Facial Expressions

To verify our Machine Learning algorithm, in our experiment, 23 participants (8 females, 15 males) with a mean age of 30 (standard deviation (SD): 8.7) were recruited to collect raw signals of eye and facial activities. The electrodes were placed on both sides of the face at locations near the ears (as shown in Fig. 4.11). Since the locations have enough distance far away from the eyes, it is un- obtrusive and will not affect the user's natural face-to-face interactions. The raw physiological signals were denoised through 1~50 Hz signal conditioning bandpass filter, and the eye movement and facial expression related components were extracted from the compound of all the body-related physiological signals, using Independent Component Analysis (ICA). Then, the extracted signal's time-series electric potentials will be collected by "Sliding Window", and then used as learning features to train the DNN classifiers, as indicated in Fig. 4.13., and then to identify the correspondent eye/facial activities. The classification accuracy of our approach could achieve average above 95%. At the end, these classified eye movements and facial expressions would be utilized to design an intuitive and engaging multimodal interaction method to interact with the surrounding environment.

4.3.1.3 Easy-to-Use Software Apps, Labeling Tools and API/SDK for End-Users to Integrate with Their Existing Solutions

To satisfy a variety of applications and the preference of different end-users, we have developed an easy-to-use UI App software, and the affiliated API/SDK for flexible programing and customizable design. The App can be installed in either cellphone or computer to collect the miniaturized body sensor network data via Bluetooth. They can assign different number of sensors and its locations through our user-friendly App and carry out data annotations through our gaming-like calibration environment, so they will not feel tiring when doing the repetitive

annotation procedures to learn their favorite facial/body gesture signals. After the first-time labelling, the system will automatically track the performance of the signals and do the automatic calibration by itself. For the general purpose applications, we already have built-in functions to control the cellphone, screen cursors, etc. For the customizable applications, we also provide API packages (C++/Python), so they can embedded our distributed sensing and control strategies using physiological activities into their own product solutions. Fig. 4.14 illustrates the schematic implementations of using our device.

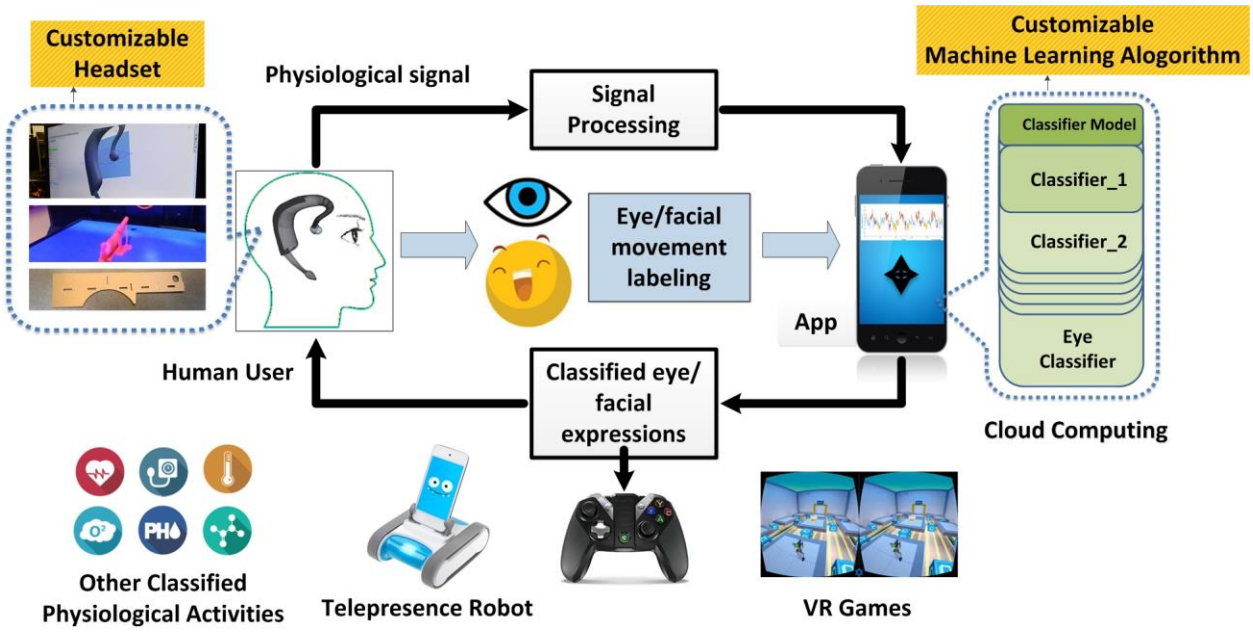

Figure 4.12. EXGbuds hardware and software concept design. Users can customize their own ergonomic design to place sensors at different locations to measure different physiological signals. EXGbuds App also provides built-in Machine Learning libraries that users can pick different Machine Learning classifiers to identify each specific physiological activity.

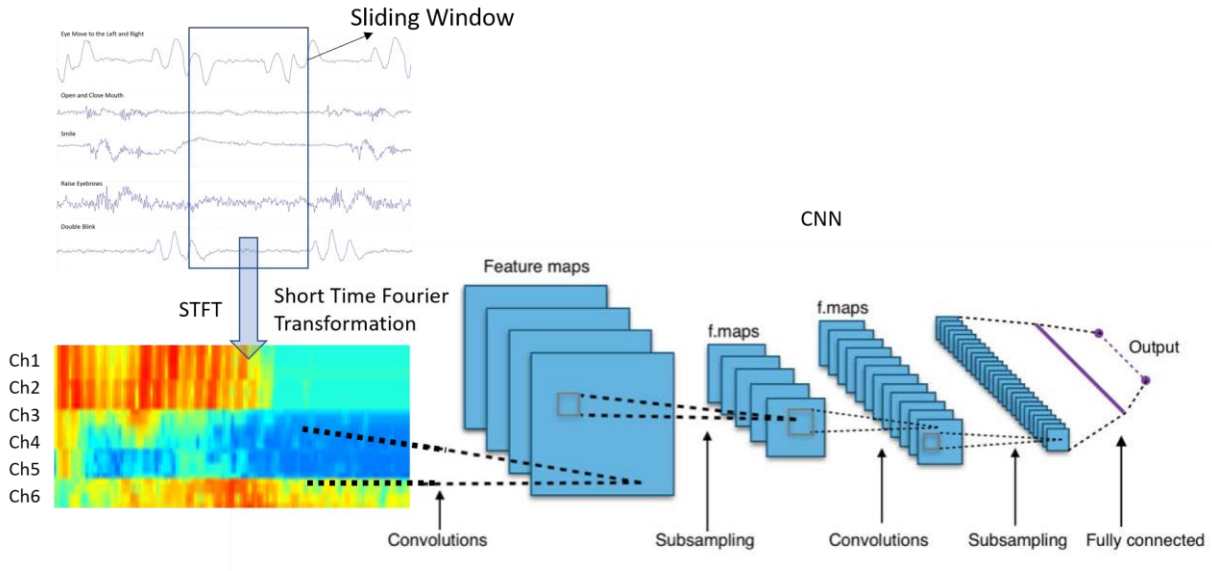

Figure 4.13. The developed Machine Learning algorithm using Short Time Fourier Transformation (STFT) and Convolution Neural Network (CNN). The collected physiological signals of different channels (totally 6 channels) within short period of time (collected by Sliding Window) will be transformed into their corresponding power spectrums, and further sent into CNN Deep Learning architecture to train the user's specific physiological gesture model. Users can arbitrarily train their favorite eye/facial gestures to generate actionable commands to control different smart home applications.

Table 4.3. Classification performance of STFT-CNN architecture

	Neutral		Eye move to the left		Eye move to the right		Double Blink	
	AVG	SD	AVG	SD	AVG	SD	AVG	SD
Accuracy	0.9841	0.0092	0.9743	0.0132	0.9686	0.0207	0.9713	0.0242
Sensitivity	0.9882	0.0119	0.6950	0.1427	0.6771	0.1659	0.7818	0.1181
Specificity	0.8512	0.1362	0.9897	0.0120	0.9910	0.0073	0.9930	0.0047
Precision	0.9903	0.0069	0.9281	0.0380	0.9057	0.0457	0.8239	0.1150

	Open and close the mouth		Smile		Raise the eyebrows	
	AVG	SD	AVG	SD	AVG	SD
Accuracy	0.9628	0.0138	0.9586	0.0144	0.9798	0.0283
Sensitivity	0.9782	0.0212	0.7829	0.1549	0.8771	0.1813
Specificity	0.7821	0.1632	0.9798	0.0312	0.8570	0.0237
Precision	0.9888	0.0024	0.9345	0.0598	0.8863	0.145

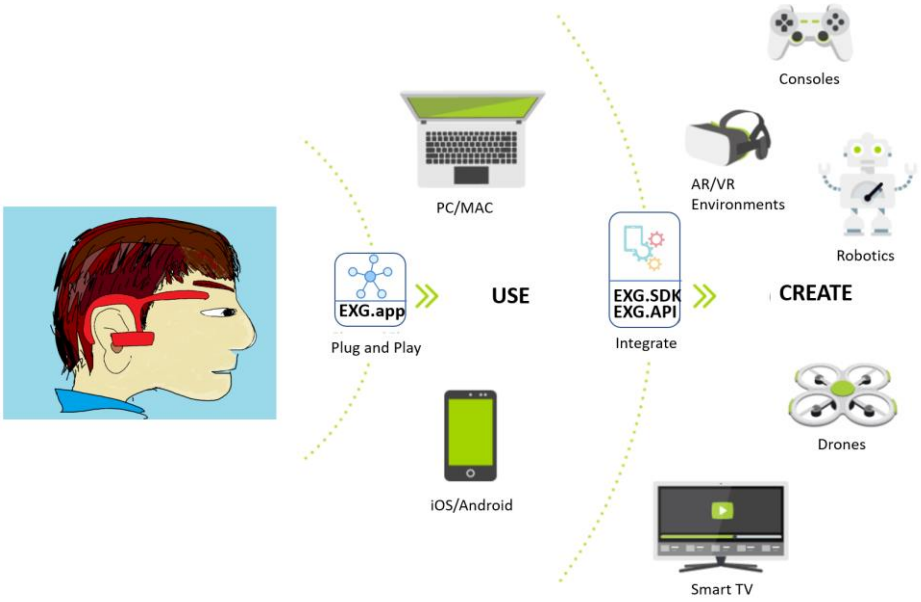

Figure 4.14. Schematic illustration of using our software App and API/SDK packages for customizable design and flexible integration of different applications.

4.3.2 Experimental Evaluation

Through the Design Thinking approach, we have come up with several intuitive and engaging interaction strategies to interact with smart home environment, games and telepresence robots.

4.3.2.1 Smart Home/IoT Interaction

We will combine our Neuro-wear device with the assistance of 3D localization and mapping to operate the Smart Home IoT devices. Here, we use external cameras for 3D human position localization. The human body center locations will be captured by computer vision, and the human face heading directions will be calculated by the embedded IMUs (accelerometer and

gyroscope) information. Since all the smart home devices' locations are fixed and pre- registered in the environment map, after we calculated the human position and face heading angle, we will know where the user is looking at, and which device he/she is going to operate. This information will be sent to cellphone/computer and integrate other facial/eye movements and hand gestures as an integrated multimodal control. For instance, when you look at the lamp, you can "Blink your eyes" to turn on the light; when you look at the TV, you can "Move your eyes to the right, and back to the center" to select TV channels; and "Smile" to turn on the radios, etc. At the same time, we can use voice command to switch on and off the Neuro-wear interface functionality. This kind of multimodal interaction strategy would give user a very straightforward and engaging experience.

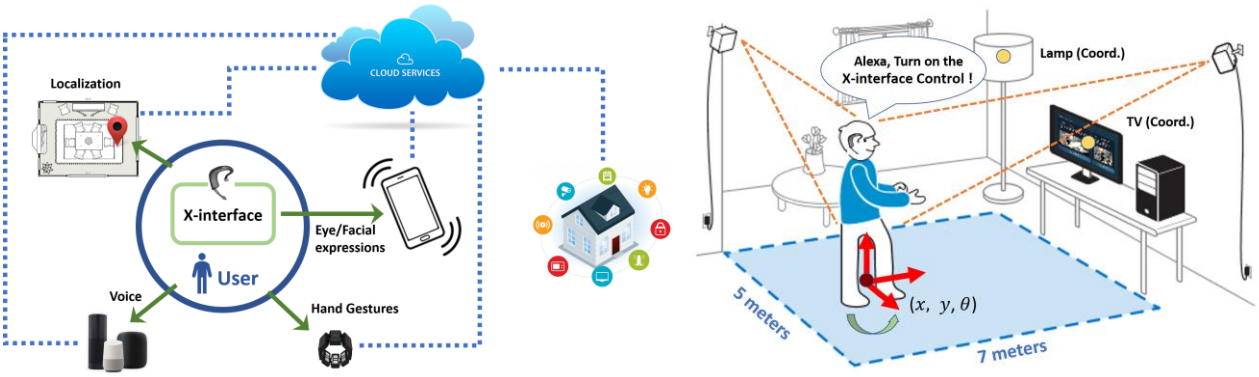

Figure 4.15. System architecture of human-smart home IoT control. We use cloud services to integrate all the eye/facial expressions, hand gestures, voice commands and indoor localizations to do the selective operations to each specific smart home (IoT) device.

4.3.2.2 Telepresence Robot and Game Control

(1) Telepresence Robot Control Using VR Headset under First-Person's View (FPV): We have built our prototyped telepresence robot as shown in Fig. 4.16, where users can attach their cell phone at the front of the robot and use the built-in camera to look around the

environment. The real-time image will be transmitted to the Virtual Reality (VR) headset and seen by the wearer. In this setup, users can use our device to control any camera-mounted robot (e.g., endoscopic camera, drone, or any robotic manipulator) in the first-person's view to directly control the robot using eye movements and facial expressions. For instance, users can use: left, right, such eye movements to steer the robot rotate in the Yaw-axis, and use "open the eyes wider (raise the eyebrows)" or "Blink the eye twice", such facial gestures to move the robot forward or backward along the depth direction. In such way, the people with disability can teleoperate the robot to explore the remote environment, or even interact with their family far away. **(2) 2D gaming control:** The users can also use eye movements and facial expressions to play 2D games such as Super Mario Bros in an interesting and engaging way (Fig. 4.17), where he/she can move his/her eyes (left and right) to control the Mario moving in the left and right directions, with "smile" to run, "raise the eyebrows" to jump, and "open and close the mouth" to spit the fire balls, etc. **(3) First-person's view 3D VR gaming control:** Users can easily use their eyes and facial expressions to play the first-person's view VR game in an immersive way, just like the previously mentioned control of telepresence robot. Fig. 4.19 shows the user using our strategy to play the video game – Doom. The player can use his directional "left" and "right" eye movement to navigate in the virtual environment (with "raise the eye brows" to move forward and "smile" to move backward). The player can also fire the gun to shoot the enemies by "open and close his mouth".

Figure 4.16. Concept of telepresence robot control by using physilogical gestures. (Left) Fist-person's view control of a telepresence robot. The person can use hand-eye coordination to grasp a cup of water; (Right) First Person's View control of VR telepresence drone. The user can see through the drone's camera and simply use eye movement and facial gestures to navigate around.

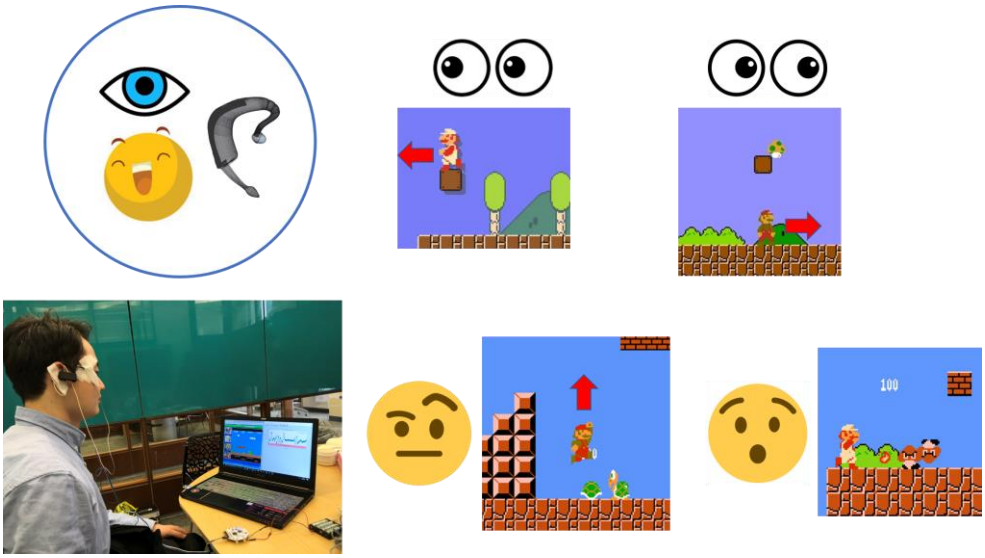

Figure 4.17. Control of 2D game using physiological gestures. Super Mario Bros control using eye movements and facial expressions.

Figure 4.18. People with dsability use eye movements and facial expressions to play Tetris game.

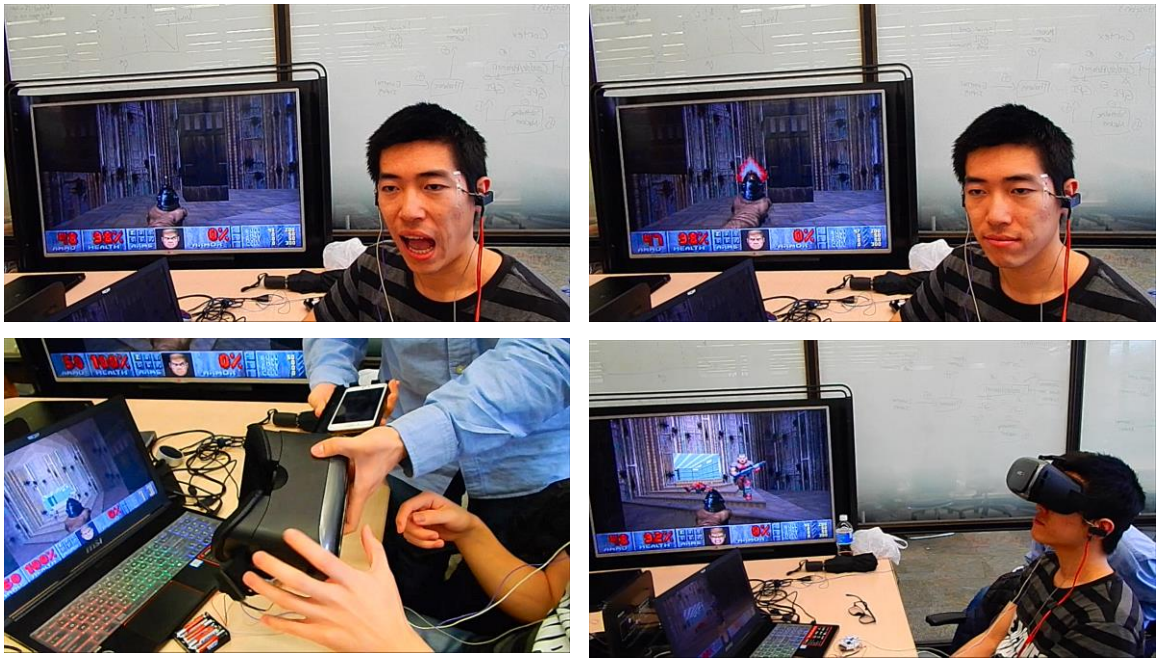

Figure 4.19. Control of 3D game for engaging and emersive experience. (Upper-left & right) Illustration of the strategy of firing a gun by open and close the mouth. (Lower-left) Our device can easily integrate with the off-the-shelve, phone-insertion-type VR headset to increase the controllability and functionality. (Lower-right) User can wear our X-interface device and VR headset seamlessly to control the VR game without conflict.

4.3.2.3 Control of Telepresence Drone to Interact with Smart Home Objects

We have set up a very engaging and intuitive interaction method to control the telepresence drone by using eye movements and facial expressions, and come up with the strategies to interact with the smart home objects with the assistance of computer vision object recognition algorithms. We use the commercially available DJI Spark Drone in the demonstration. The real-time image captured from the drone's camera will be transmitted to the Virtual Reality (VR) headset and seen by the wearer, and use the previously mentioned methods to navigate around the environment by facial/eye gestures.

At the same time, the smart home objects in the remote environment will be recognized by our computer vision Deep Learning algorithm, modified using Transfer Learning to suit our own needs of the used smart home device. When people see through the robot's eyes (the remote camera attached on the drone) with VR headset, the smart home object will be automatically identified, and the menu of the correspondent control methods will be displayed alongside the identified objects. In such way, people can easily steer the drone to target any smart home device he/she wants to control, and the system will understand which device will be selected and then people can use simple facial gestures to turn on/off the light, open/close the door, or switch the TV channels, etc., for instance.

The experimental videos can be found from the following links:

http://tinyurl.com/y826dkax (Telepresence Drone - Smart Home Interaction)

http://tinyurl.com/ybha7o6g (3D VR Game Play)

(a)

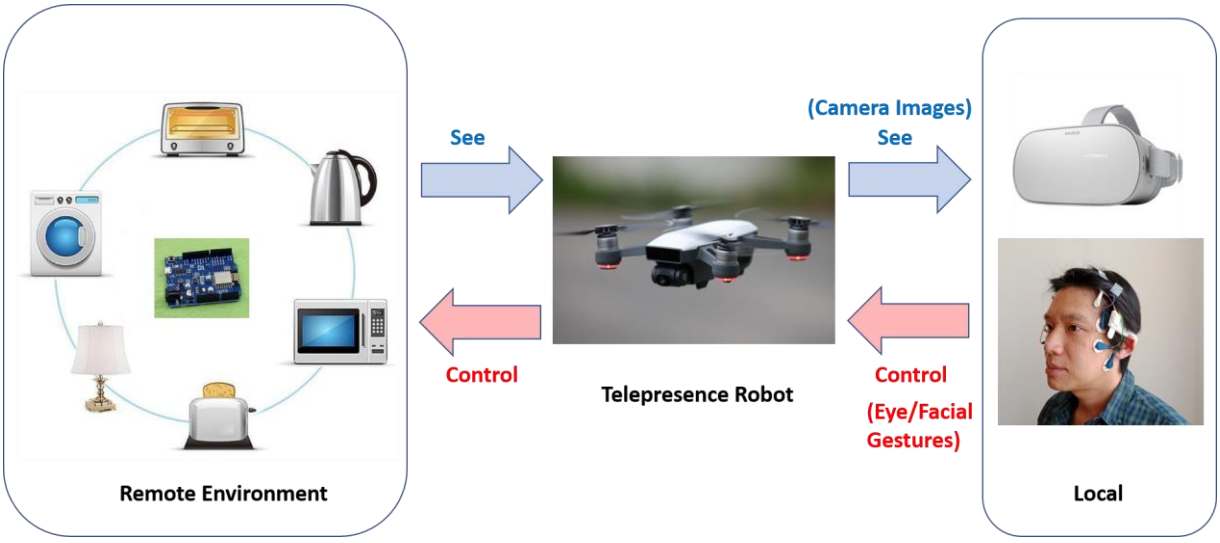

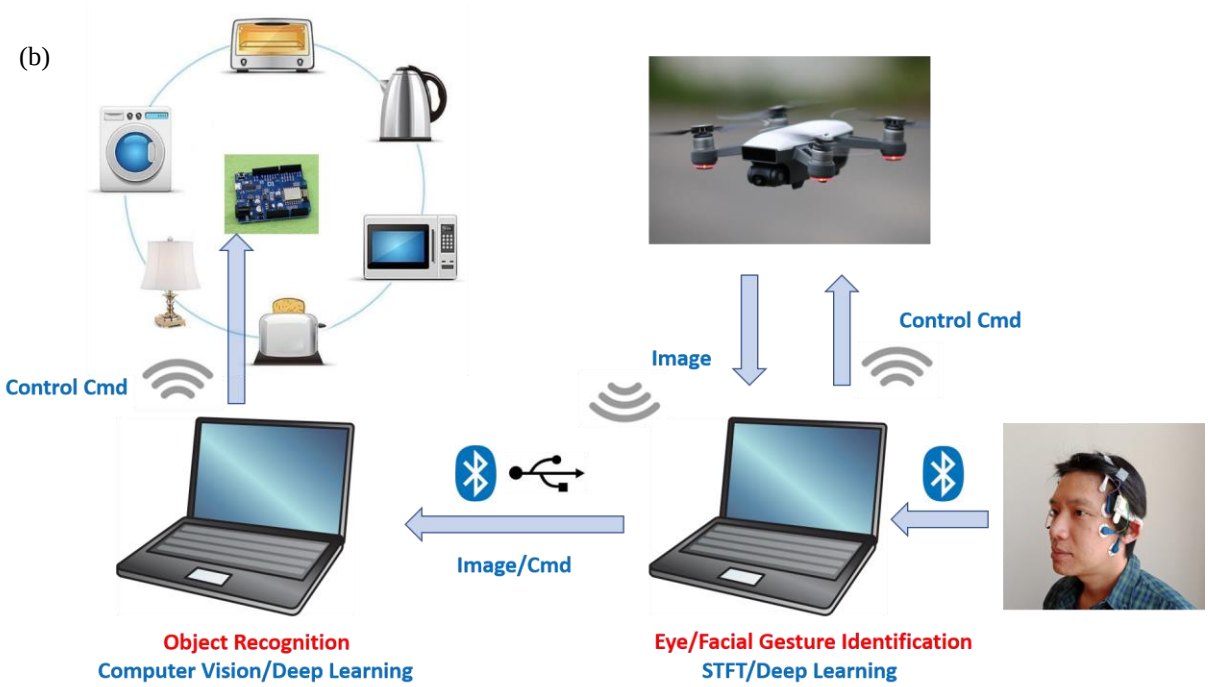

Figure 4.20. Strategy of telepresence drone control with computer vision-aided smart home objects interaction. (a) The concept that user can steer the drone with first-person's view seeing through the remote camera, and target each object recognized by the computer vision algorithm to switch on/off the facial gesture control authorities. (b) System architecture of the proposed strategy.

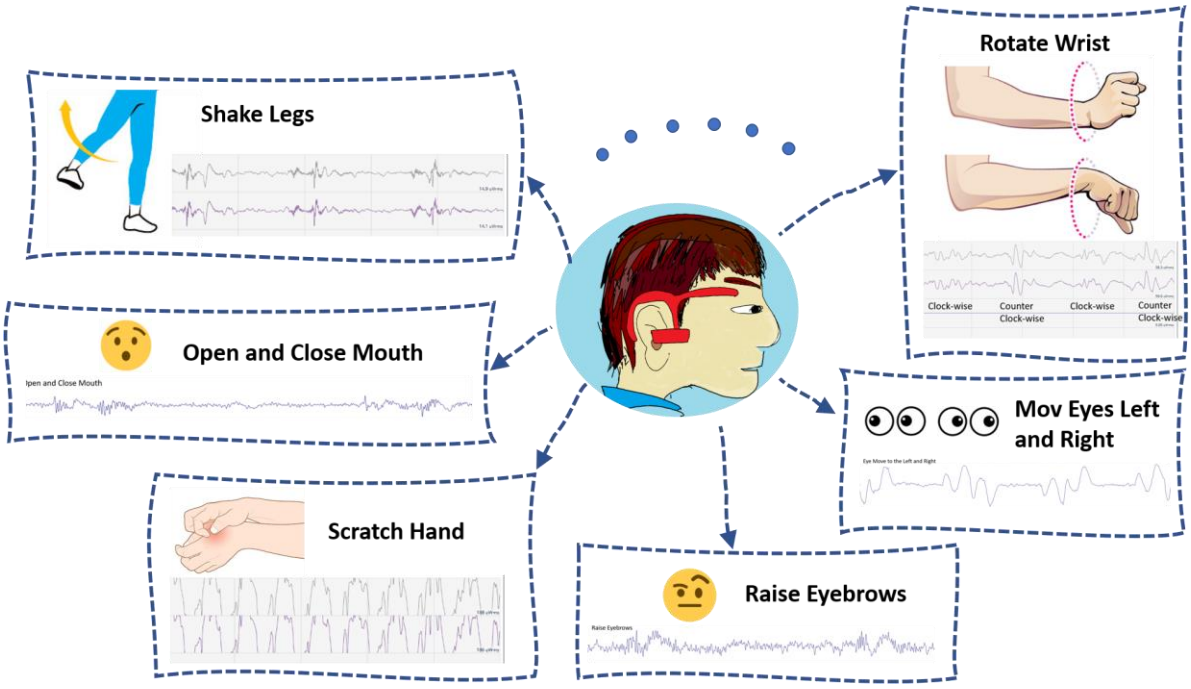

Figure 4.21. The possible ways of interaction.

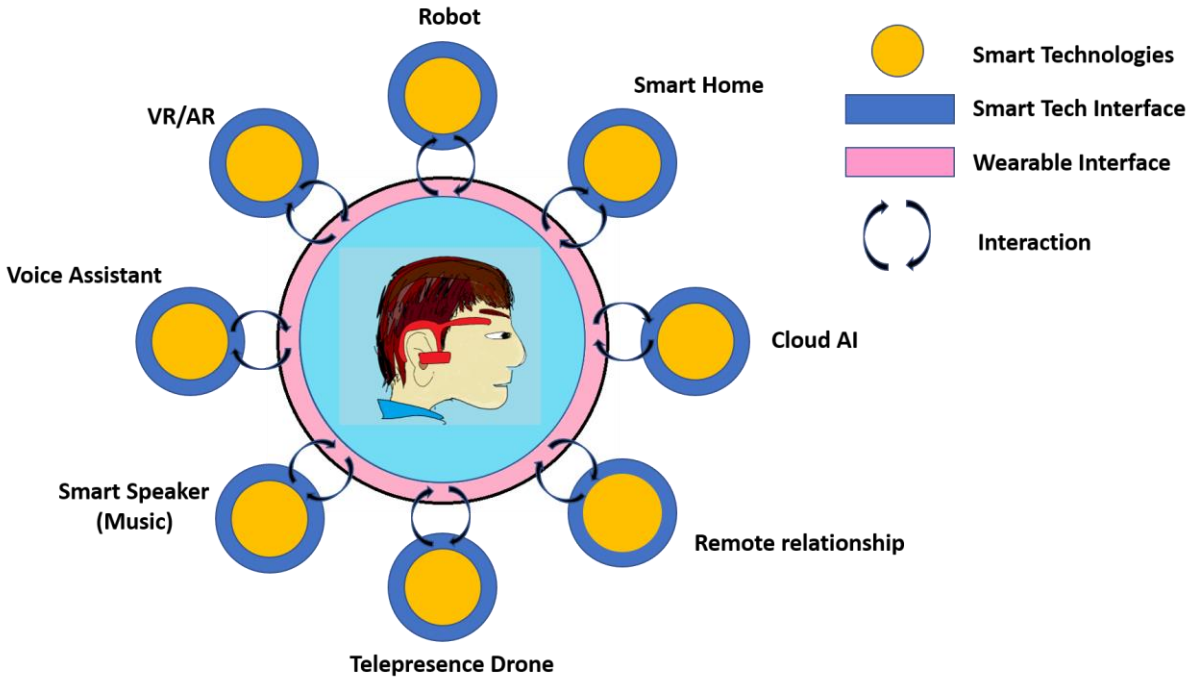

Figure 4.22. The possible applications of using our Neuro-wear interface in the daily life.

5.0 Conclusions and Future Works

The research works conducted in this dissertation have established the fundamental building block to answer the question on how human-human perform the interaction tasks, and how to computationally and mathematically model this co-learning and co-adaptive behavior, and apply it onto the human-robot interaction. We try to answer this question by using Co-Adaptive Optimal Control and Nonzero-Sum Differential Game theory to model the human motor coordination behavior in the brain-neuromuscular control level. Co-Adaptive Optimal Control and Nonzero-Sum Differential Game were both used to mimic cerebellum leaning and prediction function to figure out the consensus, stabilized joint actions for the human and robot, while Inverse Optimal Control and Inverse Differential Game is used to mimic leaning mechanism. The theoretical derivations and the experimental verifications on the simulated human-robot cooperative balancing task on exoskeleton device were provided, which demonstrate the feasibility of our proposed framework, with which it can achieve comparable performance as the centralized optimal control. At the same time, we also developed a compact, ergonomic and human-centered wearable earbud-like device to build a simple, intuitive human-machine interface. With the developed Deep Leaning EEG spectrogram decoder, we can identify eye movements, facial expressions, and body gesture signals with over 95% accuracy. It can potentially replace the cumbersome multi-channel EEG headset as a relatively portable solution for the general public. We also have demonstrated its feasibilities on smart home control, teleoperation, VR/AR gaming control, and to help people with disabilities perform normal daily tasks, with promising futuristic applications.

In the near future, a more rigorous effort will be put on the testing of Co-Adaptive Optimal Control and Differential Game framework in the real-world scenario. The non-linear, uncertain exoskeleton model will be taken into account. And also, the human and robot will not simply interact with each other, they will also interact with the environment. A good example is that the exoskeleton devices not only work and assist the human, they also react to the external environment by regulating its contact forces and impedance. In the future, the Human-Robot-Environment Interaction (HREI) research questions should be answered in order to develop the next generation symbiotic machines, as it matches the real scenario. The probabilistic model, multi-agent decentralized control, and reinforcement learning will be involved in developing more agile and robust solutions.

For the wearable interface, a softer, flexible, body skin compatible, and more invisible solution will be developed, to provide human more natural and seamless experiences. At the same time, the hardware should co-develop with the software (more advanced machine learning algorithms), as well as the end-users to maximize the functionalities and comfortabilities.

The ultimate goal is that with the use of smart interface, biosignal processing and biofeedback technologies, and advanced machine learning and control algorithms, the next generation intelligent symbiotic machines will enable humans to go beyond the existing cognitive and physical limitations, and achieve superior performance in motor generation and perceptual capabilities in the near future.

Appendix A Decoding Affective Emotions from EEG Brainwave Signals under Wearable Robot Affective Touch

Wearable robot that constantly monitors, adapts and reacts to human's need is a promising potential for technology to facilitate stress alleviation and contribute to mental health. Current means to help with mental health include counseling, drug medications, and relaxation techniques such as meditation or breathing exercises to improve mental status. The theory of human touch that causes the body to release hormone oxytocin to effectively alleviate anxiety shed light on a potential alternative to assist existing methods. Wearable robots that generate affective touch have the potential to improve social bonds and regulate emotion and cognitive functions. In this study, we used a wearable robotic tactile stimulation device, to mimic human affective touch. The touch-stimulated brain waves were captured from 4 EEG electrodes placed on the parietal, prefrontal and left and right temporal lobe regions of the brain. The novel Deep MS- CNN with emotion polling structure had been developed to extract Affective touch, Non-affective touch and Relaxation stimuli with over 95% accuracy, which allows the robot to grasp the current human affective status. This sensing and decoding structure is our first step towards developing a self-adaptive robot to adjust its touch stimulation patterns to help regulate affective status.

Appendix A.1 Wearable Robot to Regulate Mental States

Anxiety disorders led to a global total of 24.6 million YLD in 2015 and it is ranked as the sixth largest contributor to non-fatal health loss globally, according the World Health Organisation (WHO) [131]. Current therapies include psychological therapies including cognitive-behavioral therapy (CBT), medication [132] and applied relaxation. Other methods, like Yoga, meditation or breathing exercise can also boost emotion and improve your body and mind healthiness [133]. Yet a majority of people with anxiety access to treatment or efficient help, due to failure of recognition or lack of resources of health professionals [134]. The theory of human touch that causes the body to release hormone oxytocin to effectively alleviate anxiety shed light on a potential alternative to assist existing methods. Wearable robots that generate affective touch have the potential to improve social bonds and regulate emotion and cognitive functions.

In this research, we experiment with the approach of using wearable robot with tactile stimulations with the attempt to regulate human affective status. EEG (Electroencephalogram) recordings are used to interpret human emotions under Machine Learning algorithm. As such the robot can adaptively change its stimulation patterns according to the human emotion state readings in real time.

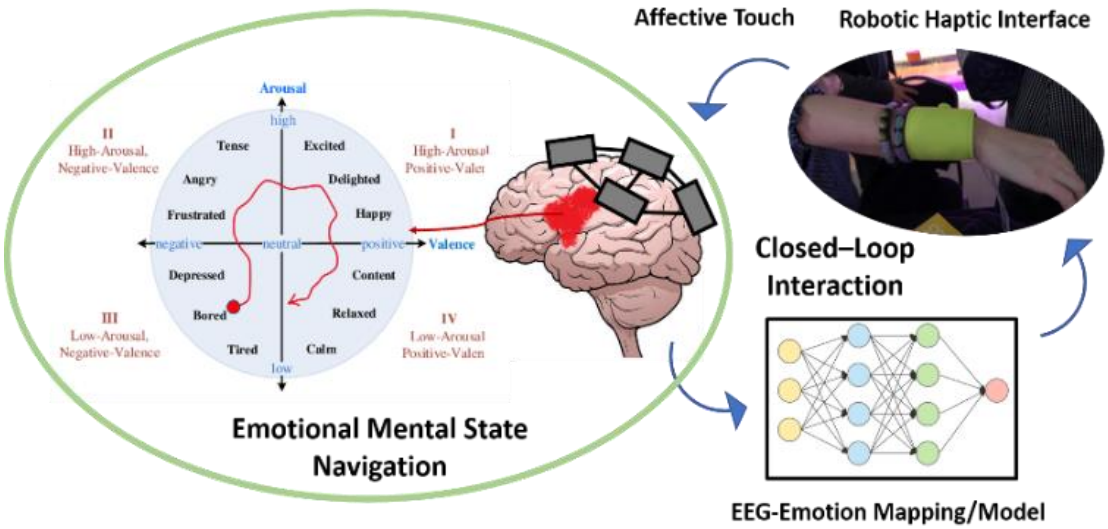

Appendix Figure A.1. Emotional mental states navigation. This picture shows the concept of using robotic haptic interface to generate synthesized affective touch to regulate human emotions. The human emotions are measured by EEG recordings, which can be further interpreted by deep learning neural networks. As a result, the robot can form a closed-loop system and change its stimulation patterns according to the current human emotion, so as to arbitrarily steer the human emotions in the emotional mental state space.

Appendix A.2 Methods and Related Works

Appendix A.2.1 Affective Touch Stimulations

Touch is the first of our senses to develop [135], setting the stage for one of the earliest maternal interactions [136], as well as being a necessary part of caregiving interactions [137], [138]. Human touch has commonly been suggested to evoke a sense of "proximity and establish the human connection" [139].

Traditionally, touch tactile research has predominantly focused on the sensory-discriminatory aspects of touch [140], mediated by fast-conducting, large diameter Aβ fibers

[141]. However, Olausson et al. [142], [143] argue that humans have a tactile system working in parallel with the sensory- discriminatory system. This system appears to be related to the social and affective aspects of touch, and parts of this signaling are thought to be mediated by a group of C-afferent fibers [9] (Appendix Fig. A.2).

C-tactile (CT) fibers are afferent, unmyelinated skin receptors that typically respond to stimuli similar to a light, stroking touch [144]. CT afferents exhibit an apparent velocity dependent firing frequency which also coincides with subjective pleasantness ratings in healthy humans [144], [145]. The preferred velocity seems to reside between 1 and 10 cm/sec, giving rise to an inverted "U", with lower CT-afferent firing and lower pleasantness ratings at slower and faster stroking velocities [144], [145]. The "Affective Touch", in particular, caress-like, slow velocity, gentle stroking touch, has recently been associated with the C Tactile (CT). And its well-studied positive affective value [146] has been shown to convey social support and intimacy with greater specificity than other types of social touch [147], [148].

Appendix A.2.2 Emotion Recognition with Machine Learning Using EEG Signals

Emotions are known as a group of affective states of human being arising as responses to stimuli from external environments or interpersonal events [146]. Different emotions possess critical influences on self-motivation generation and preferences of decision-making [147]. Representations of emotions include discrete scales in terms of angry, nervous, pleased, bored and so forth or using arousal-valence plane [148] – [150]. For the latter, 2-dimensional coordinates describe the nature of emotional experience via the core of the affections [151]. The arousal dimension is used to quantify different degrees from calm to excitement levels while the valence dimension indicates whether human feelings are positive (happy) or negative (sad) [152]

– [155]. Appendix Fig. A.3 shows a typical layout of the arousal-valence plane, where multiple discrete emotional states, e.g., neutral, cheerful, peaceful, depressing and angry, can be defined with different combinations of arousal and valence levels.

There are various methods to recognize emotions, such as using facial expression, speech, gesture, posture, etc., which has the advantage of easy data collections. On the other hand, using physiological signals, such as the electroencephalogram (EEG), body temperature (T), electrocardiogram (ECG), electromyogram (EMG), galvanic skin response (GSR), respiration (RSP), etc. These physiological sensors are more convenient to be embedded into wearable devices to make an integrated product.

Among all above physiological signals, EEG signals took advantages of time, spatial, frequency and asymmetric related characteristics, which can provide rich information for emotion identification then other sensing modalities. In recent years, a high number of neuropsychological studies have reported correlations between EEG signals and emotions. There are two main areas of the brain correlated with emotional activity: the amygdala (projection of anterior insula) (located close to the hippocampus, in the frontal portion of the temporal lobe); and the pre-frontal cortex (covers part of the frontal lobe). Although there is no consensus about a possible lateralization of the amygdala, its activation seems to be more related to negative emotions than positive ones [157].

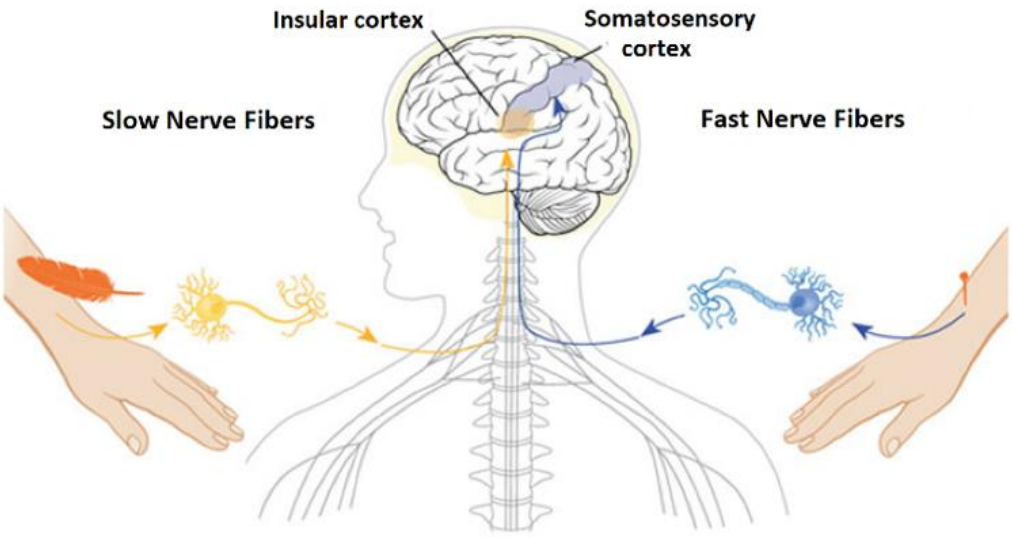

Appendix Figure A.2. The two touch nerve fiber systems. The slow nerve fibres are unmyelinated C-tactile afferents (CT), responding optimally to slow gentle touch and projecting to limbic systems (insular cortex) in the brain. The fast touch nerve fibres respond to a wide range of mechanical stimuli and project to primary somato-sensory cortex for rapid discrimination.

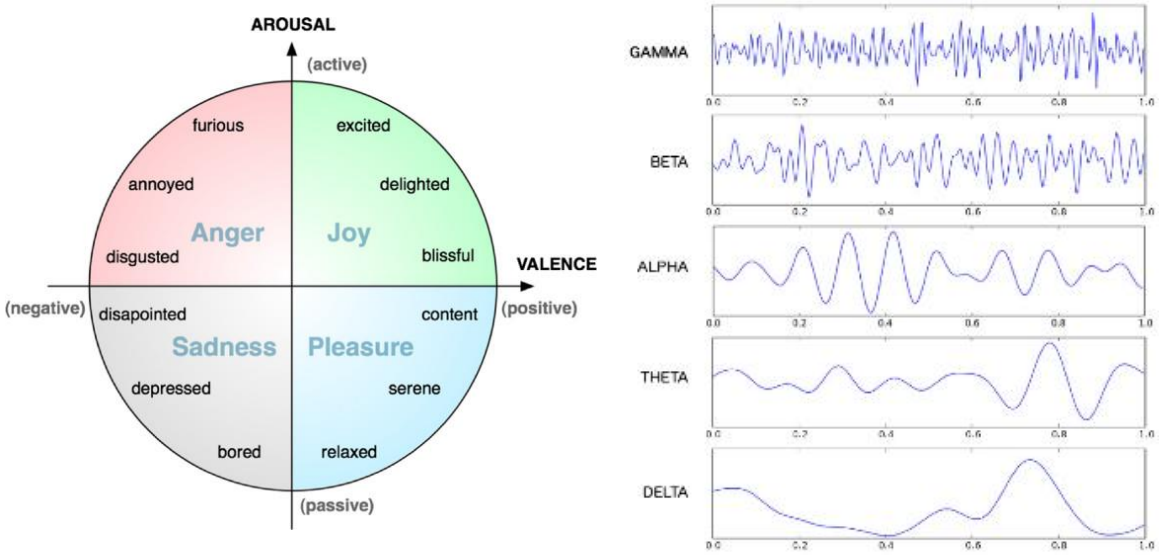

Appendix Figure A.3. Russell's valence-arousal model and EEG frequency bands. (Left) Interpretation of different emotions based on Russell's valence-arousal model [156]. (Right) EEG signal patterns in different frequency bands react to emotions.

To understand more about the emotion related brain activities, we can divide EEG frequency domain measurement into five frequency bands: delta (0.5–4 Hz), theta (4–8 Hz), alpha (8–13 Hz), beta (13–30 Hz), gamma (30–80 Hz), and mu rhythm (8–13 Hz). Alpha waves are typical of an alert but relaxed mental state and are evident in the parietal and occipital lobes. Beta waves are indicative of active thinking and concentration, found mainly in frontal and other areas of the brain. Changes in alpha power and asymmetry between the hemispheres of the brain are related to emotions. A relative right frontal activation is associated with withdrawal stimuli or negative emotions, such as fear or disgust. A relatively greater left frontal activation is associated with an approach stimuli or positive emotions, such as joy or happiness. Thus, the asymmetrical frontal EEG activity may reflect changes on the valence [157] – [160]. Beta bands are also related to valence [160]. Pre-frontal and parietal asymmetry in the alpha band and temporal asymmetry in gamma band are present for valence recognition, while pre-frontal asymmetry in alpha band and temporal asymmetry in the gamma band are observable for arousal recognition [161]. Changes in the gamma band are related with the happiness and sadness emotions, and so is the decrease in the alpha wave in different sides of the temporal lobe (left for sadness, and right for happiness) [162], [163].

Moreover, a recent work [164] demonstrated that, following a tactile stimulation caressing in the range of 2-4 cm/s, a suppression of μ-oscillations (8-12 Hz, the idling rhythm of sensorimotor regions) in electrodes over the contralateral somatosensory cortex occurs.

Appendix A.2.3 Soft Pneumatic Actuator as Affective Touch Stimuli

Interactive, pneumatically-driven actuators made from pliable materials and inspired by soft-robotic principles [165] are emerging as new kind of tactile stimuli. Several studies used this

type of actuators to investigate how such tactile sensations were perceived [165] – [167]. The pliable surface material, when deformed via pneumatic force enact tactile sensation through dynamic, seamless shape-changes against human skin. Such actuation affords a sensual quality resembling that of a human touch [165]. We refer such features as the "affective qualities" of the actuator. Such "affective qualities" lend soft pneumatic actuators comparable advantages to facilitate affective communication, than mechanical vibrators. Mechanical vibrators, although is currently the most widely used in wearable haptics design, have limitations in inducing pleasant sensations. For example one study showed that their high frequency movements can induce negative sensations after lengthy exposure [167].

In an effort to simulate human affective touch, AffectNode, a wearable, soft pneumatic actuators had been developed [168]. In a preliminary studies with AffectNode [168], 100% participants were able to identify a tactile pattern that they claim to give them pleasant feelings. AffectNodes2 (Appendix Fig. A.1) had since been designed, which contains an array of single actuators. The actuators could be actuated in a sequence with a velocity of 5-38cm/s and an applied force around 0.5N. We used AffectNodes2 in the current study.

Appendix A.3 Experimental Procedures

Appendix A.3.1 Experimental Protocol

We have recruited 7 participants aged 23~40 (5 males, 2 females) in our preliminary affective touch and EEG recording experiment. No participants reported physical limitations and any experience of mental or personality disorder that would affect the experimental outcomes.

Participants were comfortably seated, and the left forearm was horizontally placed on the supportive cushion. For all trials, participants wore earplugs in order to prevent auditory cues, and were restricted from watching the researcher with their eyes looking at different directions opposite to the positions where the touch experiment took place, to ensure that the tactile stimuli were not facilitated by visual input and eliminate any anticipatory effect resulted from knowing the type of stimuli treatment in advance.

In the experiment, we used robot tactile interface, where we can arbitrarily adjust the touch stimuli patterns in different speed and normal forces applied on the wearer's skin. The velocity and force profiles were preliminarily selected as 6 cm/s and 0.5N to simulate the affective touch (which is based on the previous literature studies that the 6 cm/s falls in the optimal speed of affective gentle touch, i.e., CT-Optimal touch), while 30 cm/s and 0.5 N are selected to generate the non-affective touch stimuli.

We executed 7 different sessions of stimulation protocols among each participant: **(Session 1) Relaxation:** The participant was simply doing nothing but with his/her arm resting on the supportive holder and stayed still to establish the baseline. The entire session lasted for 3 min. **(Session 2) Slow Brush Stroke:** The participants received stimulations from a cosmetic make-up brush (Natural hair brush, No 7, The Boots Company) with the stroke speed of 6 cm/s, normal force of 0.5N, according to the setups of affective, gentle touch criteria (CT-Optimal touch). The entire duration lasted for 2 min executed by the researcher (experimenter). There was 2s pause between each stroke. **(Session 3) Fast Brush Stroke:** The participants received stimulations from a paint brush with the stroke speed of 30 cm/s and normal force of 0.5 N. The entire session lasted for 2 min executed by the researcher. There was 1s pause between each stroke. **(Session 4) Slow Human Touch:** The researcher used one hand to apply a gentle touch

on the participant's forearm, again, with the speed of around 6 cm/s and normal force of 0.5N to generate CT-Optimal touch behavior with the duration of 2 min. There was 2s pause between each stroke. **(Session 5) Fast Human Touch:** The researcher used the hand to apply a very fast touch on the participant's forearm skin, with the speed of 30 cm/s, and force 0.6 N for totally 2 min. There was 1s pause between each stroke. Between each slow touch stimuli there was a 2s interval and 1s interval between fast touch stimuli. **(Session 6) Robot touch:** The wearable interface applied a force of 0.5N with a stimulation velocity of 6cm/s. Participants were also required to give feedbacks and ratings of emotion arousals and valence after each experiment session.

Appendix A.3.2 Data Collections and Analysis

For the whole experiments, brain signals were collected through the OpenBCI Cyton Biosensing Board (8-channels), with 250 Hz sampling rate and 24-bit resolution. The gold-plated (Au) cup electrodes were placed on the participant's head to measure EEG signals. To measure the most relevant emotion-related EEG signals, we put 4 electrodes on the scalp at standard positions T7, T8, CPz and Fpz (according to the International Standard 10-20 System) (Appendix Fig. A.4), which correspond to the left and right temporal lobe, central parietal lobe, and pre-frontal lobe regions. The specific emotional responses can be found in these regions accordingly as described in **Section - Appendix A.2**. There is also one GND electrode attached on the left earlobe to provide the reference signal. We only use totally 5 electrodes to reduce the burden of the participants and make the wearable platform as compact as possible.

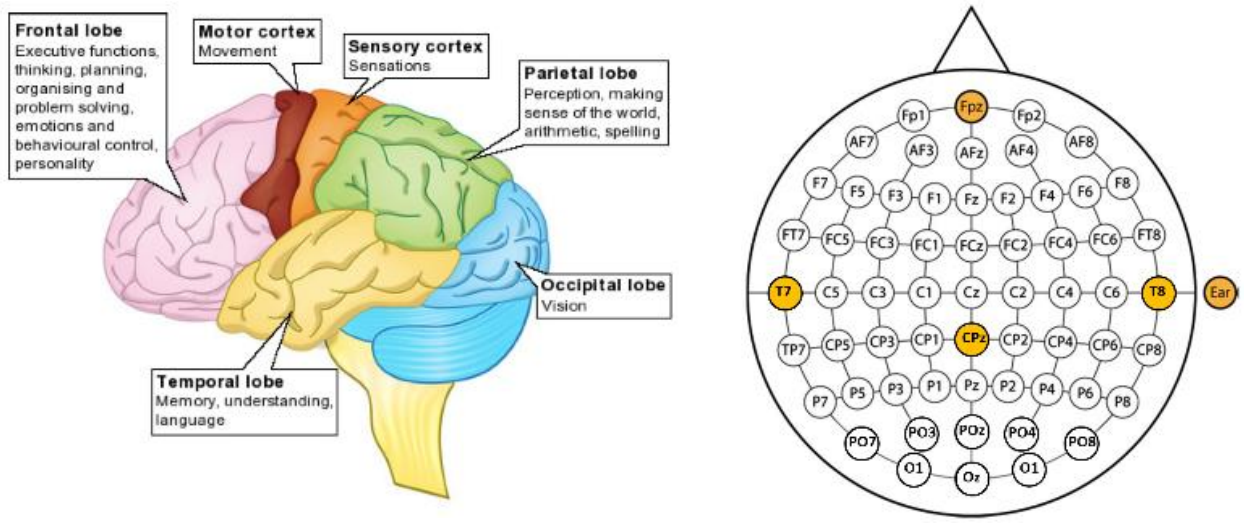

Appendix Figure A.4. Brain functional cortical areas and EEG electrode placements. (Left) Brain regions: The brain cortex subdivided into the frontal, temporal, parietal, and occipital lobes with different function correspondences. (Right) The interpretation of EEG 10-20 system: Our electrodes are attached on the left and right temporal lobe regions (T7) & (T8), central parietal lobe (CPz) and prefrontal lobe (Fpz).

The finite impulse response (FIR) band pass filter of 1~50 Hz, and notch filter of 50 Hz and 60 Hz, with Hamming window being utilized, are to remove DC offset, power line interference and electrocardiogram artifact. The signals were then transformed into frequency domain by short-time Fourier transformation (STFT), with sliding window 1s (250 data points) and 80% time window overlap. Afterwards, we divided frequency domain EEG power spectrum into 5 different bands, including: delta (0.5–4 Hz), theta (4-8 Hz), alpha (8-13 Hz), beta (13-30 Hz) and gamma (30-80 Hz). And the average power of each frequency band was extracted.

The affective touch induced EEG signals under different stimulation patterns were then compared at each electrode (4 aforementioned brain regions), by using STFT and average power analysis in each frequency band. Appendix Fig. A.5 shows the 3D representation of STFT spectrogram at central parietal cortex (CPz) during the entire 2 min experimental session. We

can observe that the slow human touch and slow brush stroke have obvious power attenuation, especially in the alpha and beta frequency bands, compared to other touch stimuli including stroke have relatively higher arousal. To be noticed, there are some ripples in STFT spectrogram during the human touch (corresponding to the touch intervals), because whenever the human touches the skin, the peripheral nervous system (Aβ fibers) will deliver somatic sensation signals to notify the parietal lobe cortex, which is just captured by our electrode at CPz.

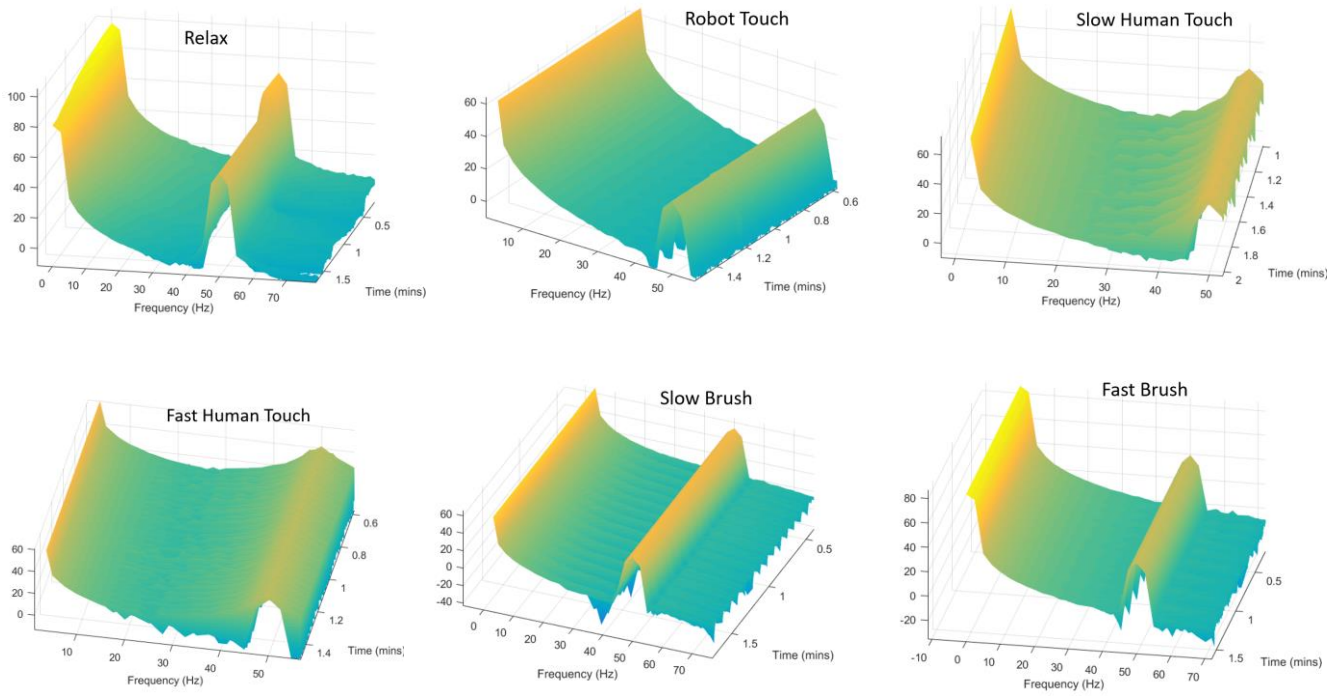

Appendix Figure A.5. The 3D diagram of Short-Time Fourier Transform (STFT) of EEG signals collected from Parietal Cortex (CPz). It shows the EEG power spectrum evolution for the two minutes tactile stimulation session under different affective touches.

Appendix Fig. A.6 and Appendix Fig. A.7 show the Comparison of average brainwave intensity in different frequency band under different touch stimulations, observed from electrode 3 (CPz) and 4 (Fpz). We can see that the average power distribution of robot simulated affective

touch and slow human touch are very similar, and lower than the other touch stimulations, which illustrates that our device can effectively replicate human affective touch sensations.

The data collected here at all 4 electrodes in the representation of power spectrum will be further utilized as training and testing dataset for our machine learning algorithm.

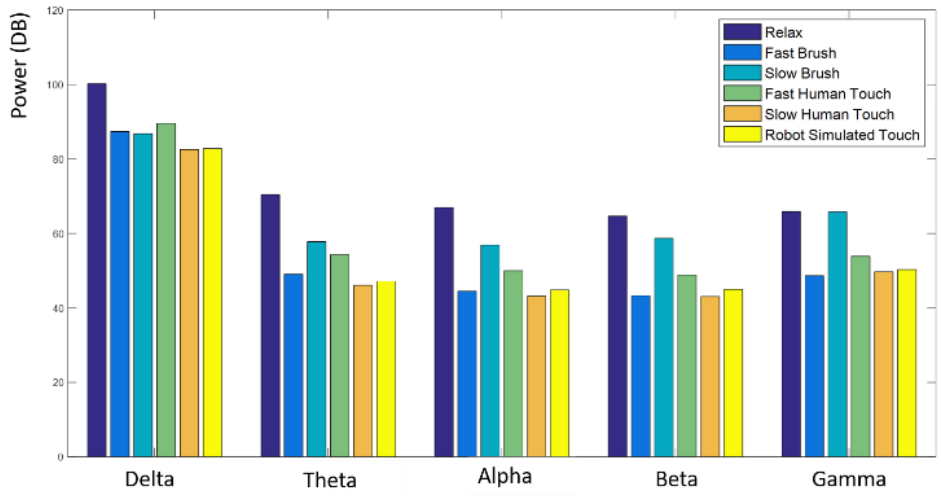

Appendix Figure A.6. Comparison of average brainwave intensity in different frequency band under affective touch in electrode 3 (CPz).

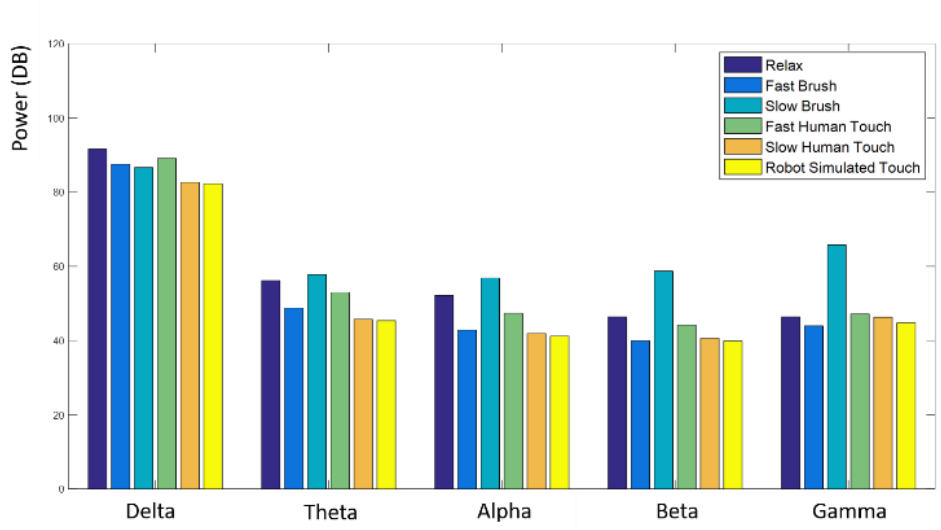

Appendix Figure A.7. Comparison of average brainwave intensity in different frequency band under affective touch in electrode 4 (Fpz).

Appendix A.4 Deep Multi-Spectrogram Convolutional Neural Network (Deep MS-CNN) for Emotion Recognition from Multiple Electrodes

To truly develop an intelligent wearable robot that can adapt to human's emotion and change the tactile patterns, we have to let the robot know what the human currently feels. As discussed above, a very important part of this paper is to develop an EEG-based emotion extractor for multiple electrodes that is trainable, producing informative representations for recognition and retrieval touch-stimulated emotions, and is efficient to compute.

The traditional way of using time-series data representation to identify EEG signals poses the problems of easily compromised by external and internal disturbances from the environment and body motions. As such, using frequency domain analysis has been demonstrated to be more reliable and have relatively stable quality in various brain activity identifications. In our approach, we used imaged- based frequency power spectrogram as the input features to our algorithm for the training and testing analysis.

Our spectrogram-based representations start from multiple views of STFT spectrogram, generated from time-series EEG data collected by sliding-windows at each electrode.

The mathematical description of the Discrete-time, short-time Fourier transformation (STFT) is:

$$X_m(\omega) = \sum_{n=-\infty}^{\infty} \mathrm{x(n)w(n-mR)}e^{-j\omega n}, \quad \text{(A.1)}$$

where

$x(n) =$ input time-series EEG signal at time n,

$w(n) =$ length m window function,

$X_m(\omega) =$ DTFT of windowed data centered about time mR,

$R =$ hop size, between successive DTFTs.

In our experimental settings, we pick $w(n)$ as Hamming window, with m = 250 data pts, R = 0.2 (80% overlap size between each window). After the STFT, each time-series data collected by Hamming window will be transformed into frequency domain with 250 frequency components, i.e., $X_m(\omega) \in R^{250\times 1}$ vector. We keep the Hamming window sliding through the time-series data with 80% overlap until we collect 250 $X_m(\omega)$ vectors, and obtain a spectrogram image with the size of 250×250 matrix. Notably, as long as we keep collecting the data using the sliding window strategy, we will get as many spectrogram images as possible. These spectrogram image will constitute the training and testing samples of our machine learning algorithm.

A simple way to use multiple spectrogram is to generate a 2D image emotion descriptor (please see the next **Section – Emotion Descriptor**) per each spectrum, and then use the individual descriptors directly for recognition tasks based on some voting or alignment scheme. For example, a naive approach would be to average the individual descriptors, treating all the spectrums as equally important.

Alternatively, if the spectrograms are rendered in a similar way, one could also pick one descriptor from all the views. Unfortunately, it is not always the case in our evaluation. In contrast to the above simple approaches, an aggregated representation combining features from multiple spectrograms is more desirable since it yields a single, compact descriptor representing the emotion. Our approach is to learn to combine information from multiple spectrograms using a unified CNN architecture that includes an emotion extraction layer (Appendix Fig. A.8). All

the parameters of our CNN architecture are learned discriminatively to produce a single compact descriptor for the emotion.

Emotion Descriptors:

The emotion descriptors we consider here is the CNN activation features. For our CNN features we use the VGG-M network from which consists of mainly five convolutional layers conv1,...,5 followed by three fully connected layers fc6,...,8 and a softmax classification layer. The penultimate layer fc7 (after ReLU non-linearity, 4096-dimensional) is used as emotion descriptor. The network is pre-trained on ImageNet, and then fine-tuned on all 2D spectrograms of the EEG signals in the training dataset.

Multi-spectrogram CNN:

Here, we focus on the problem of learning to aggregate multiple spectrogram in order to synthesize the information from all views into a single, compact emotion descriptor. We design the multi-spectrogram CNN (MS-CNN) on top of spectrogram-based CNNs (Appendix Fig. A.8). Each spectrogram observed from each electrode is passed through the first part of the network (CNN1) separately, aggregated at an emotion extraction layer, and then sent through the remaining part of the network (CNN2). All branches in the first part of the network share the same parameters in CNN1. We use element-wise maximum operation across the spectrogram in the emotion extraction layer. An alternative is element-wise mean operation, but it is not as effective in our experiments. The emotion extraction layer can be placed anywhere in the network. We show in our experiments that it should be placed close to the last convolutional

layer (conv5) for optimal classification and retrieval performance. Emotion extraction layers are closely related to max-pooling layers and maxout layers, with the only difference being the dimension that their pooling operations are carried out on. The MSCNN is a directed acyclic graphs and can be trained or fine-tuned using stochastic gradient descent with back-propagation.

Performance Evaluation:

We separate the training data sets into 3 categories: Affective touch, Non-affective touch and Relaxation (Neutral State). The affective touch constitutes all the touch stimuli which satisfy the affective touch condition (i.e., speed: 6 cm/s; normal force 0.5 N) (including slow human touch, slow brush stroke and robot slow touch), while non-affective touch comprises all the other touch stimuli not satisfying the conditions (including fast human touch and fast brush stroke). And we use the data collected in the relaxation session as the relaxation (neutral state) training datasets. All the datasets are separated into 5 folds as training and testing (validation) datasets for cross-validation.

The training progress diagram and confusion matrix can be seen in Appendix Fig. A.9 and Appendix Fig. A.10. It shows fast convergence rate when reaching to the stable classification accuracy, which is around 95%, to identify affective touch, non-affective touch and relaxation states. The true positive rate to identify each classified touch category is also significantly higher than the false positive rate.

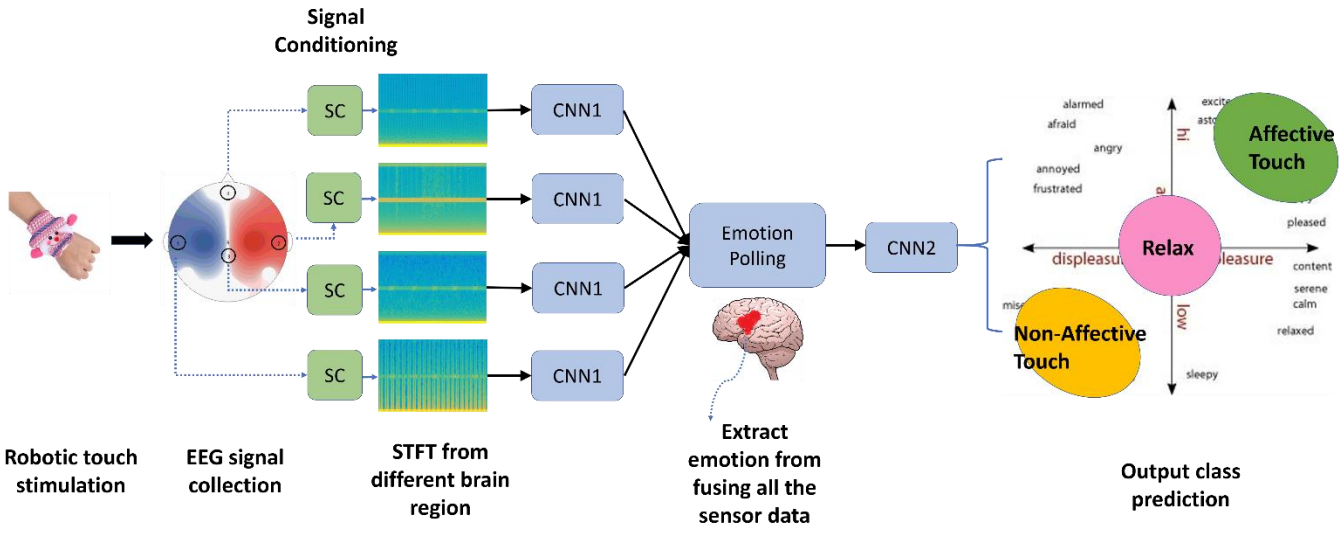

Appendix Figure A.8. Deep Multi-spectrogram Convolutional Neural Network (Deep MS-CNN) structure for touch-stimulated emotion extraction. The training and testing data sets collect from 4 electrodes (using STFT transformed into power spectrogram), are passed through CNN1 (emotion descriptor) to extract emotion-based features. These are then pooled across all emotion descriptors and passed through CNN2 to obtain identified human emotion.

In addition, we have compared our Deep MS-CNN classifier with the traditional KNN (K-nearest Neighbor) and SVM (Support Vector Machine) classification methods, where we extracted the features from frequency domain (i.e., 1-D vector containing 125 frequency components) transformed from time-series data using STFT sliding window technique. We used 3-nearest neighbors and Euclidean distance measurement to train the KNN model, while the Gaussian kernel function and One-vs-One multiclass classification method are applied on the SVM model. The classification results can be found in Appendix Table A.1. And our Deep MS-CNN also outperform the rest two classifiers.

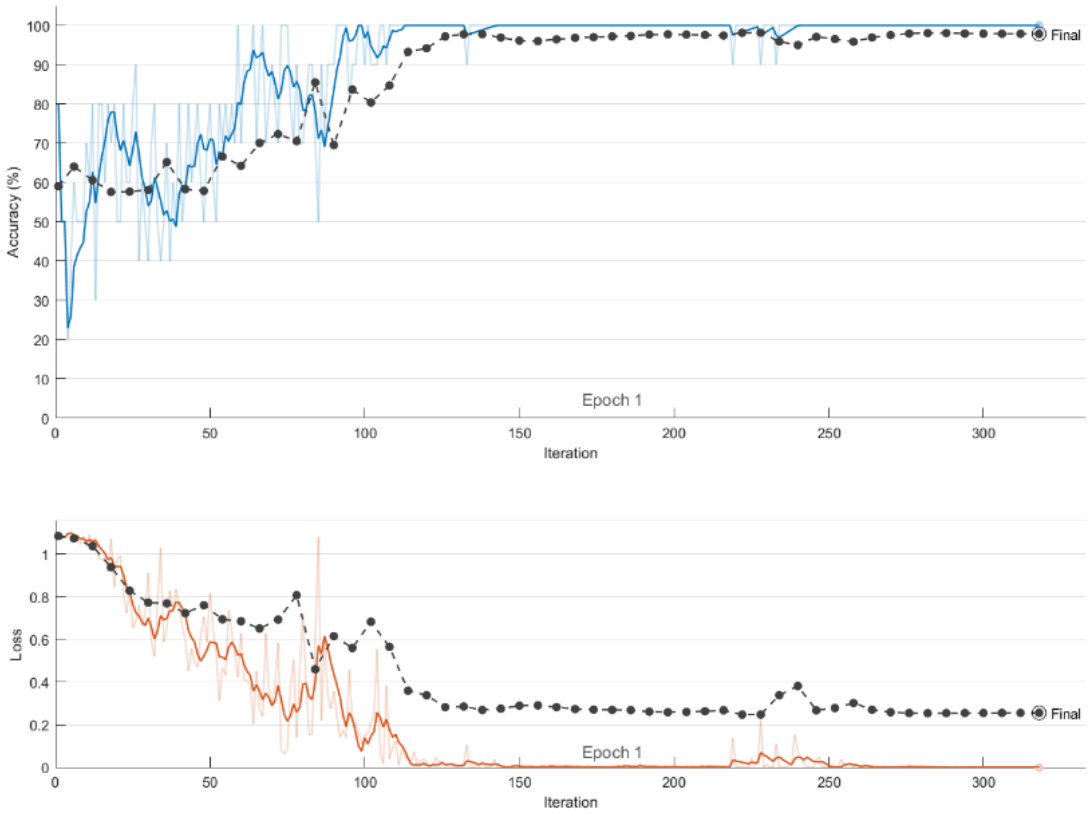

Appendix Figure A.9. Training progress diagram.

Appendix Table A.1. Classification Accuracy for Various Methods of Emotion Identification for EEG signals

	CLASSIFICATION (ACCURACY)	AUC
DEEP MS-CNN	95.3%	1.00
SVM	80.4%	0.94
KNN	60.5%	0.74

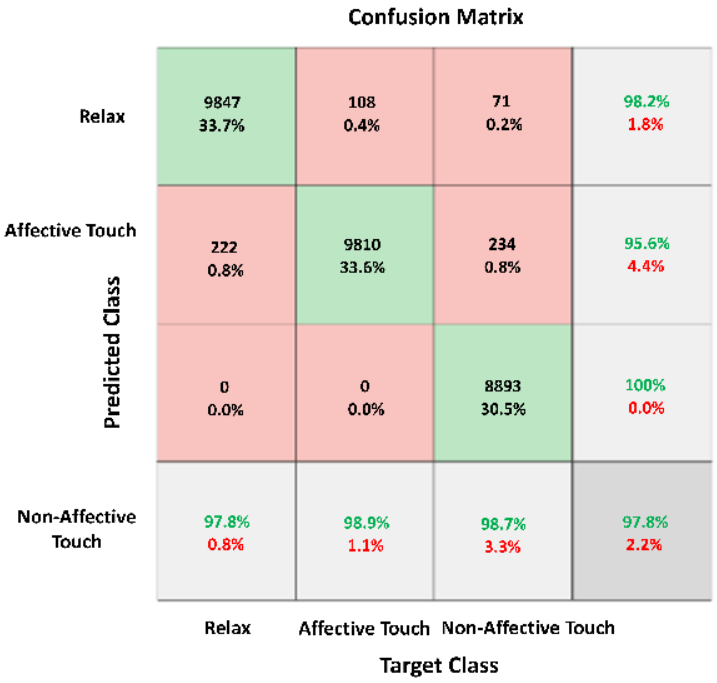

Appendix Figure A.10. Confusion matrix.

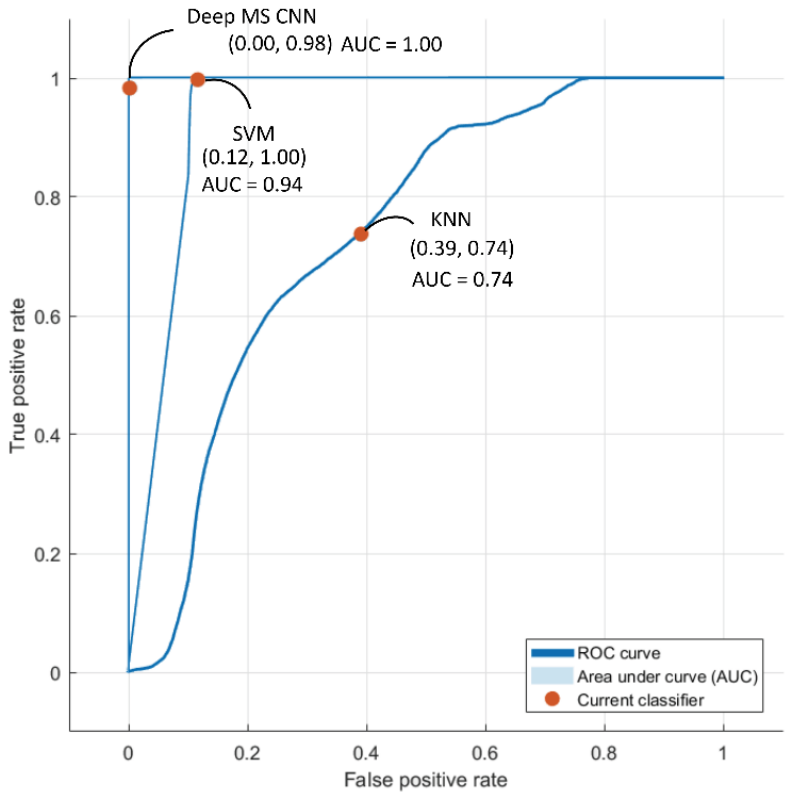

Appendix Figure A.11. ROC curve with different classification methods.

Appendix A.5 Findings and Future Works

The preliminary research work conducted in this paper is to establish a fundamental building bock to develop a high accuracy emotion states extractor based on EEG measurements to get feedback to the wearable robot. The developed learning framework can span to more electrodes attached on the head to identify different emotion or cognitive behaviors. The power spectrum frequency band analysis demonstrated that there are similarities of stimuli performed by robot tactile device and affective touch performed by slow brush and human hand. However, the sample size was small to draw conclusive insight. Some assumptions have been made in this preliminary machine learning model training, which is a limitation of this study: (1) the human subjects are restricted under the initial states in the relaxation, which could limit the possibility that human could have other emotion regulation consequences under the affective touch, if the initial states are different than the relaxation, e.g., “Happy”, “Sad” or “Excited”. (2) The model assumes every person will have the same emotional response under the same touch stimuli and individual difference hasn’t been taken into account.

Our future work includes expanding the sample size to collect more quantified emotion ratings/labels in order to provide more effective emotion mental states recognition under our Deep MS-CNN framework. And system identification of each individual person’s emotion regulation dynamics will be conducted. Also, the adaptive affective control algorithm will be investigated to change the stimulation patterns of the robot.

Bibliography

[1] D. T. McRuer and H. R. Jex, "A Review of Quasi-Linear Pilot Models, Human Factors in Electronics," IEEE Transactions on, vol.HFE-8, no.3, pp.231-249, 1967.

[2] E. Todorov, M. I. Jordan, "Optimal feedback control as a theory of motor coordination," Nature neuroscience 5 (11), pp.1226-1235, 2002.

[3] E. Todorov, "Stochastic optimal control and estimation methods adapted to the noise characteristics of the sensorimotor system," Neural computation, 17(5), pp.1084-1108, 2005.

[4] J. Diedrichsen, R. Shadmehr, R. B. Ivry, "The coordination of movement: optimal feedback control and beyond," Trends in Cognitive Sciences, v.4, i.1, pp.31-39, 2010.

[5] A. D. Kuo, "An optimal control model for analyzing human postural balance," Biomedical Engineering, IEEE Transactions on, vol.42, no.1, pp.87-101, 1995.

[6] M. Kawato, "Internal models for motor control and trajectory planning," Current opinion in neurobiology, 9(6), 718-727, 1999.

[7] M. Haruno, D. M. Wolpert, and M. Kawato, "Mosaic model for sensorimotor learning and control," Neural computation, 13(10), 2201-2220, 2001.

[8] J. M. P. Gunasekara, R. A. R. C Gopura, T. S. S. Jayawardane, S. W. H. M. T. Lalitharathne, "Control methodologies for upper limb exoskeleton robots," System Integration (SII), IEEE/SICE International Symposium on, pp.19-24, 2012.

[9] G. Ganesh, A. Takagi, R. Osu, T. Yoshioka, M. Kawato, and E. Burdet, "Two is better than one: Physical interactions improve motor performance in humans," Scientific Reports. 4, Article number: 3824, 2014.

[10] E. Baek, S. K. Song, S. Oh, S. Mohammed, D. Jeon and K. Kong, "A generalized control framework of assistive controllers for lower limb exoskeletons," IEEE International Conference on Robotics and Automation (ICRA), pp.1505-1509, 2014.

[11] A. Koenig, X. Omlin, D. Novak, and R. Riener, "A review on biocooperative control in gait rehabilitation," IEEE International Conference on Rehabilitation Robotics (ICORR), pp.1-6, 2011.

[12] J. Schaechter, "Motor rehabilitation and brain plasticity after hemiparetic stroke," Progress Neurobiol, 73:pp.61–72, 2004.

[13] R. Berjón, M. Mateos, A. Barriuso, I. Muriel, and G. Villarrubia, “Head tracking system for wheelchair movement control,” In Highlights in Practical Applications of Agents and Multiagent Systems, pp. 307-315. Springer, Berlin, Heidelberg, 2011.

[14] Origin Instruments, URL: http://www.orin.com/access/sip_puff/, 2018.

[15] A. L. S. Ferreira, L. C. de Miranda, E. E. C. de Miranda, and S. G. Sakamoto, "A survey of interactive systems based on brain-computer interfaces," SBC Journal on Interactive Systems, vol. 4, pp. 3-13, 2013.

[16] D. Vrabiea, O. Pastravanub, M. Abu-Khalafc, F. L. Lewis, “Adaptive optimal control for continuous-time linear systems based on policy iteration,” Automatica v.45, i.2, pp.477–484, 2009.

[17] Y. Jiang, Z. P. Jiang, “Computational adaptive optimal control for continuous-time linear systems with completely unknown dynamics,” Automatica v.48, i.10, pp.2699–2704, 2012.

[18] D. Mitrovic, S. Klanke, S. Vijayakumar, “Adaptive optimal feedback control with learned internal dynamics models,” From Motor Learning to Interaction Learning in Robots Studies in Computational Intelligence v.264, pp.65-84, 2010.

[19] V. L. Roger, A. S. Go, D. M. Lloyd-Jones, E. J. Benjamin, J. D. Berry, W. B. Borden, et al., "Heart disease and stroke statistics—2012 update a report from the American heart association," Circulation, vol. 125, pp. e2-e220, 2012.

[20] L. Mertz, "The Next Generation of Exoskeletons: Lighter, Cheaper Devices Are in the Works," Pulse, IEEE, vol. 3, pp. 56-61, 2012.

[21] H. Herr, "Exoskeletons and orthoses: classification, design challenges and future directions," Journal of neuroengineering and rehabilitation, vol. 6, p. 21, 2009.

[22] J. M. P. Gunasekara, R. A. R. C. Gopura, T. S. S. Jayawardane, and S. W. H. M. T. Lalitharathne, "Control methodologies for upper limb exoskeleton robots," in System Integration (SII), 2012 IEEE/SICE International Symposium on, pp. 19-24, 2012.

[23] E. Strickland, “Good-bye, Wheelchair, Hello Exoskeleton,” IEEE Spectrum, URL: http://spectrum.ieee.org/biomedical/bionics/goodbyewheelchair-hello-exoskeleton, Dec. 30, 2011.

[24] EKSO bionics website, URL: http://www.eksobionics.com/, 2016.

[25] ReWalk Robotics web site, URL: http://rewalk.com/, 2016.

[26] E. Guizzo, “UPDATE 2: Details on Sarcos exoskeleton's control system, power, and actuators,” IEEE Spectrum, URL: http://spectrum.ieee.org/automaton/robotics/ roboticssoftware/sarcos_robotic_exoskeleton, Nov.29, 2007.

[27] Cyberdine-HAL website, URL: http://www.cyberdyne.jp/english/products/HAL/index.html, 2016.

[28] G. Ganesh, A. Takagi, R. Osu, T. Yoshioka, M. Kawato, and E. Burdet, "Two is better than one: Physical interactions improve motor performance in humans," Scientific reports, vol. 4, 2014.

[29] L. A. Petrosjan, "Cooperative differential games," in Advances in Dynamic Games, vol. 7 of the series Annals of the International Society of Dynamic Games, Springer, pp. 183-200, 2005.

[30] N. Jarrassé, T. Charalambous, and E. Burdet, "A Framework to Describe, Analyze and Generate Interactive Motor Behaviors," PLoS ONE 7(11): e49945, 2012.

[31] M. C. Cheng, "Master Cheng's New Method of Tai Chi Chuan SelfCultivation," translated by Mark Hennessy, North Atlantic Books, Berkeley, CA., 1999.

[32] B. D. Anderson, "The inverse problem of optimal control," DTIC Document, Fort Belvoir, VA, USA, Tech. Rep. 6560-3, 1966.

[33] A. D. Santis, B. Siciliano, A. D. Luca, and A. Bicchi, "An atlas of physical human-robot interaction," Mech. Mach. Theory, vol. 43, no. 3, pp. 253–270, 2008. [Online]. Available: http://www.sciencedirect .com/science/article/pii/S0094114X07000547

[34] C. Passenberg, A. Peer, and M. Buss, "A survey of environment-, operator-, and task-adapted controllers for teleoperation systems," Mechatronics, vol. 20, no. 7, pp. 787–801, 2010.

[35] Y. Li and S. S. Ge, "Human-robot collaboration based on motion intention estimation," IEEE/ASME Trans. Mechatronics, vol. 19, no. 3, pp. 1007– 1014, Jun. 2014.

[36] Y. Li and S. S. Ge, "Force tracking control for motion synchronization in human-robot collaboration," Robotica, vol. 34, no. 6, pp. 1260-1281, 2016. [Online]. Available: http://journals.cambridge.org/article_S0263574714002240

[37] S. Hirche and M. Buss, "Human-oriented control for haptic teleoperation," Proc. IEEE, vol. 100, no. 3, pp. 623–647, Mar. 2012.

[38] C. Liu and M. Tomizuka, "Modeling and controller design of cooperative robots in workspace sharing human-robot assembly teams," in Proc. IEEE/RSJ Int. Conf. Intell. Robot. Syst., pp. 1386–1391, Sep. 2014.

[39] A. Mortl, M. Lawitzky, A. Kucukyilmaz, M. Sezgin, C. Basdogan, and S. Hirche, "The role of roles: Physical cooperation between humans and robots," Int. J. Robot. Res., vol. 31, no. 13, pp. 1656–1674, 2012.

[40] L. E. Parker, "Distributed intelligence: Overview of the field and its application in multi-robot systems," J. Phys. Agents, vol. 2, pp. 5–14, 2008.

[41] B. D. Argall, and A. G. Billard, “A survey of tactile human-robot interactions,” Robot. Auton. Syst., vol. 58, no. 10, pp. 1159–1176, 2010.

[42] T. Wojtara et al., “Human-robot collaboration in precise positioning of a three-dimensional object,” Automatica, vol. 45, no. 2, pp. 333– 342, 2009. [Online]. Available: http://www.sciencedirect.com/science/ article/pii/S000510980

[43] P. Evrard and A. Kheddar, “Homotopy switching model for dyad haptic interaction in physical collaborative tasks,” in Proc. 3rd Joint EuroHaptics Conf. Symp. Haptic Interfaces Virtual Environ. Teleoperator Syst., Salt Lake City, UT, USA, 2009, pp. 45–50.

[44] J. R. Medina, M. Lawitzky, A. Molin, and S. Hirche, “Dynamic strategy selection for physical robotic assistance in partially known tasks,” in Proc. IEEE Int. Conf. Robot. Autom., 2013, pp. 1180–1186.

[45] N. Hogan, “Impedance control: An approach to manipulation-Part I: Theory; Part II: Implementation; Part III: Applications,” J. Dyn. Syst., Meas., Control, vol. 107, no. 1, pp. 1–24, 1985.

[46] N. Jarrasse, V. Sanguineti, and E. Burdet, “Slaves no longer: Review on role assignment for human-robot joint motor action,” Adaptive Behavior, vol. 22, no. 1, pp. 70–82, 2014.

[47] T. Basar and G. J. Olsder, Dynamic Noncooperative Game Theory, 2nd ed. Philadelphia, PA, USA: SIAM, 1998. [Online]. Available: http://epubs.siam.org/doi/abs/10.1137/1.9781611971132

[48] R. Bellman, Dynamic Programming, 1st ed. Princeton, NJ, USA: Princeton Univ. Press, 1957.

[49] N. Jarrasse, T. Charalambous, and E. Burdet, “A framework to describe, analyze and generate interactive motor behaviors,” PLoS ONE, vol. 7, no. 11, 2013, Art. no. e49945, 2013.

[50] D. E. Kirk, Optimal Control Theory: An Introduction (ser. Dover Books on Electrical Engineering). New York, NY, USA: Dover, 2012. [Online]. Available: http://books.google.com.sg/books?id=onuH0PnZwV4C

[51] W. Gao, S. Emaminejad, H. Y. Nyein, S. Challa, K. Chen, A. Peck, H. M. Fahad, H. Ota, H. Shiraki, D. Kiriya, D. H. Lien, G. A. Brooks, R. W. Davis, A. Javey, Nature 2016, 529, 509.

[52] Y. Ai, Z. Lou, S. Chen, D. Chen, Z. M. Wang, K. Jiang and G. Shen, “All rGO-on-PVDF-nanofibers based self-powered electronic skins,” Nano Energy, 35, 121-127, 2017.

[53] D. Kim, D. Kim, H. Lee, Y. R. Jeong, S. J. Lee, G. Yang and J. Kim, “Body-attachable and stretchable multisensors integrated with wirelessly rechargeable energy storage devices,” Advanced Materials, 28(4), 748-756, 2016.

[54] J. Kim, M. Kim, M. S. Lee, K. Kim, S. Ji, Y. T. Kim, J. Park, K. Na, K. H. Bae, H. K. Kim and F. Bien, "Wearable smart sensor systems integrated on soft contact lenses for wireless ocular diagnostics," Nature communications, 8, p.14997, 2017.

[55] X. Wang, L. Dong, H. Zhang, R. Yu, C. Pan and Z. L. Wang, "Recent progress in electronic skin," Advanced Science, 2(10), 1500169, 2015.

[56] T. Q. Trung, S. Ramasundaram and N. E. Lee, "Transparent, stretchable, and rapid-response humidity sensor for body-attachable wearable electronics," Nano Research, 10(6), 2021-2033, 2017.

[57] M. F. El-Kady and R. B. Kaner, "Scalable fabrication of high-power graphene micro-supercapacitors for flexible and on-chip energy storage," Nature communications, 4, 1475, 2013.

[58] L. Li, Z. Lou, W. Han, D. Chen, K. Jiang, and G. Shen, "Highly Stretchable Micro-Supercapacitor Arrays with Hybrid MWCNT/PANI Electrodes," Advanced Materials Technologies, 2(3), 1600282, 2017.

[59] T. Wang, Y. Guo, P. Wan, H. Zhang, X. Chen, and X. Sun, "Flexible transparent electronic gas sensors," Small, 12(28), 3748-3756, 2016.

[60] Z. Q. Zheng, J. D. Yao, B. Wang and G. W. Yang, "Light-controlling, flexible and transparent ethanol gas sensor based on ZnO nanoparticles for wearable devices," Scientific reports, 5, 11070, 2015.

[61] B. Schazmann, D. Morris, C. Slater, S. Beirne, C. Fay, R. Reuveny, and D. Diamond, "A wearable electrochemical sensor for the real-time measurement of sweat sodium concentration," Analytical Methods, 2(4), 342-348, 2010.

[62] A. Spanu, S. Lai, P. Cosseddu, A. Bonfiglio, M. Tedesco, and S. Martinoia, "Organic FET device as a novel sensor for cell bioelectrical and metabolic activity recordings," In 2013 6th International IEEE/EMBS Conference on Neural Engineering (NER), pp. 937-940, 2013.

[63] X. Duan, T. M. Fu, J. Liu, and C. M. Lieber, "Nanoelectronics-biology frontier: From nanoscopic probes for action potential recording in live cells to three-dimensional cyborg tissues," Nano today, 8(4), 351-373, 2013.

[64] S. Imani, A. Bandodkar, A. Mohan, R. Kumar, S. Yu, J. Wang, and P. Mercier, "A wearable chemical–electrophysiological hybrid biosensing system for real-time health and fitness monitoring," Nature communications, 7, 11650, 2016.

[65] P. Ekman and W. Friesen, "Measuring facial movement with the facial action coding system," In Emotion in the human face (2nd ed.), New York: Cambridge University Press, 1982.

[66] R. W. Picard, "Affective computing," MIT Press, 1997.

[67] R. W. Picard, J. Healey, “Affective wearables,” vol. 1, Issue: 4, pp 231-240, 1997.

[68] M. Monajati, S.H. Abbasi, F. Shabaninia, “Emotions States Recognition Based on Physiological Parameters by Employing of Fuzzy-Adaptive Resonance Theory,” International Journal of Intelligence Science, 2, 166-175, 2012.

[69] C. Maaoui, A. Pruski, “Emotion Recognition through Physiological Signals for Human-Machine Communication,” Cutting Edge Robotics 2010, Vedran Kordic (Ed.), ISBN: 978-953-307-062-9, InTech, 2010.

[70] A. M. Khan, M. Lawo, “Wearable Recognition System for Emotional States Using Physiological Devices,” eTELEMED 2016 : The Eighth International Conference on eHealth, Telemedicine, and Social Medicine, ISBN: 978-1- 61208-470-1 131, 2016.

[71] P. Das, A. Khasnobish, D.N. Tibarewala, “Emotion Recognition employing ECG and GSR Signals as Markers of ANS,” Conference on Advances in Signal Processing (CASP), 2016.

[72] G. Wu, G. Liu, M. Hao, “The analysis of emotion recognition from GSR based on PSO,” In Intelligence Information Processing and Trusted Computing (IPTC) , 28-29 Oct. 2010

[73] K. H. Kim, S. W. Bang, S. R. Kim, “Emotion recognition system using short- term monitoring of physiological signals,” Med. Biol. Eng. Comput., 2004, 42, 419-427, 2004.

[74] N. Amour, A. Hersi, N. Alajlan, “Implementation of a Mobile Health System for Monitoring ECG signals,” BioMedCom 2014 Conference, Harvard University, December 14-16, 2014.

[75] E. Fortune, M. Tierney, C. Ni Scanaill, “Activity Level Classification Algorithm Using SHIMMERTM Wearable Sensors for Individuals with Rheumatoid Arthritis,” 33rd Annual International Conference of the IEEE EMBS Boston, Massachusetts USA, 2011.

[76] R. Richer, P. Blank and D. Schuldhaus, “Real-time ECG and EMG Analysis for Biking using Android-based Mobile Devices,” 11th International Conference on Wearable and Implantable Body Sensor Networks, 2014.

[77] A. Nakasone, H. Prendinger, M. Ishizuka, “Emotion recognition from electromyography and skin conductance,” In Proceeding. of the 5th International Workshop on Biosignal Interpretation, pp. 219-222, 2005.

[78] M. Soleymani, J. Lichtenauer,T. Pun, “A Multimodal Database for Affect Recognition and Implicit Tagging,” IEEE Transaction on Affective Computing, Vol. 3, No. 1, 2012.

[79] R. Subramanian, J. Wache and M. Abadi. “ASCERTAIN: Emotion and Personality Recognition using Commercial Sensors,” J. IEEE Transaction on affective computing, Vol. 3, No. 1, 2016.

[80] M. Ernst and M. Banks, “Humans integrate visual and haptic information in a statistically optimal fashion,” Nature, 415(6870), 429, 2002.

[81] D. Franklin, E. Burdet, K. Tee, R. Osu, C. Chew, T. Milner, and M. Kawato, “CNS learns stable, accurate, and efficient movements using a simple algorithm,” Journal of neuroscience, 28(44), pp.11165-11173, 2008.

[82] E. Todorov and M. Jordan, “Optimal feedback control as a theory of motor coordination,” Nature neuroscience, 5(11), 1226, 2002.

[83] E. Burdet, G. Ganesh, A. Albu-Schaeffer and C. Yang, “Interaction force, impedance and trajectory adaptation: by humans, for robots,” In: Proceedings of the International Symposium on Experimental Robotics, 2010.

[84] C. Yang , G. Ganesh, S. Haddadin, S. Parusel, A. Albu-Schaeffer, et al., “Human-like Adaptation of Force and Impedance in Stable and Unstable Interactions,” IEEE Transaction on Robotics 27: 1–12, 2011.

[85] I. O’Sullivan, E. Burdet, J. Diedrichsen, “Dissociating variability and effort as determinants of coordination,” Plos Computational Biology 5, 2009.

[86] J. Neumann, “Zur theorie der gesellschaftsspiele,” Mathematische annalen, 100(1), 295-320, 1928.

[87] J. Nash, “Equilibrium Points in N-Person Games,” In: Proceedings of the National Academy of Sciences of the United States of America. volume 36, pp. 48–49, 1950.

[88] J. Nash J, “Non-Cooperative Games,” The Annals of Mathematics 54: 286– 295, 1951.

[89] P. Dillenbourg, M. Baker and A. Blaye, “The evolution of research on collaborative learning,” In: Learning in Humans and Machines, London: Pergamon. pp. 189–211, 1996.

[90] J. Roschelle J, “The construction of shared knowledge in collaborative problem solving,” NATO ASI Series F Computer: 69–97, 1994.

[91] R. Trivers R, “The evolution of reciprocal altruism,” Quarterly Review of Biology 46: 35–57, 1971.

[92] R. Axelrod and W. Hamilton, “The evolution of cooperation,” Science 211: 1390, 1981.

[93] E. Todorov, “Stochastic optimal control and estimation methods adapted to the noise characteristics of the sensorimotor system,” Neural computation, 17(5), pp.1084-1108, 2005.

[94] J. Diedrichsen, R. Shadmehr, R.B. Ivry, “The coordination of movement: optimal feedback control and beyond,” Trends in Cognitive Sciences, v.4, i.1, pp.31-39, 2010.

[95] G. Liu, “A data-driven, piecewise linear approach to modeling human motions,” Doctoral dissertation, University of North Carolina at Chapel Hill, 2007.

[96] R. Shadmehr, “The equilibrium point hypothesis for control of movement,” Baltimore, MD: Department of Biomedical Engineering, Johns Hopkins University, 375., 1998.

[97] S. Baron, "Adaptive behavior in manual control and the optimal control model," in Adaptive control of ill-defined systems, vol. 16 of the series NATO Conference Series, Springer, pp. 51-73, 1984.

[98] S. Boyd, L. E. Ghaoul, E. Feron, and V. Balakrishnan, “Linear Matrix Inequalities in System and Control Theory,” vol. 15. Philadelphia, PA, USA: SIAM, 1987.

[99] S. Boyd and L. Vandenberghe, “Convex Optimization,” Cambridge, U.K.: Cambridge Univ. Press, 2004.

[100] E. Cheney and D. Kincaid, “Numerical Mathematics and Computing,” Stamford, CT, USA: Cengage Learning, 2012.

[101] M. C. Priess, R. Conway, C. Jongeun, J. M. Popovich, and C. Radcliffe, "Solutions to the Inverse LQR Problem With Application to Biological Systems Analysis," Control Systems Technology, IEEE Transactions on, vol. 23, pp. 770-777, 2015.

[102] F. L. Lewis, D. Vrabie, and V. L. Syrmos, Optimal control: John Wiley & Sons, 2012.

[103] A. E. Bryson and Y.-C. Ho, Applied Optimal Control, Optimization, Estimation, and Control. New York-London-Sydney-Toronto. John Wiley & Sons. 1975.

[104] M. Grant, S. Boyd, CVX: Matlab software for disciplined convex programming, version 2.0 beta, URL: http://cvxr.com/cvx, Sep. 2013.

[105] M. Grant, S. Boyd, “Graph implementations for nonsmooth convex programs,” Recent Advances in Learning and Control (a tribute to M. Vidyasagar), V. Blondel, S. Boyd, and H. Kimura, editors, pp. 95-110, Lecture Notes in Control and Information Sciences, Springer, http://stanford.edu/~boyd/graph_dcp.html, 2008.

[106] J. Chang, S. Chen, and J. Huang, “A Kinect-based system for physical rehabilitation: A pilot study for young adults with motor disabilities,” Research in developmental disabilities, 32(6), 2566-2570, 2011.

[107] A. L. S. Ferreira, L. C. de Miranda, E. E. C. de Miranda, and S. G. Sakamoto, "A survey of interactive systems based on brain-computer interfaces," SBC Journal on Interactive Systems, vol. 4, pp. 3-13, 2013.

[108] A. B. Schwartz, X. T. Cui, D. J. Weber, and D. W. Moran, "Brain-controlled interfaces: movement restoration with neural prosthetics," Neuron, vol. 52, pp. 205-220, 2006.

[109] J. P. Donoghue, "Bridging the brain to the world: a perspective on neural interface systems," Neuron, vol. 60, pp. 511-521, 2008.

[110] B. J. Fisch and R. Spehlmann, Fisch and Spehlmann's EEG primer: basic principles of digital and analog EEG: Elsevier Health Sciences, 1999.

[111] C. Vidaurre, C. Sannelli, K.-R. Müller, and B. Blankertz, "Machine-learning based co-adaptive calibration: a perspective to fight BCI illiteracy," in International Conference on Hybrid Artificial Intelligence Systems, 2010, pp. 413-420.

[112] O. AlZoubi, R. A. Calvo, and R. H. Stevens, "Classification of EEG for affect recognition: an adaptive approach," in Australasian Joint Conference on Artificial Intelligence, 2009, pp. 52-61.

[113] NeuroSky website, URL: http://neurosky.com/, 2017.

[114] EMOTIV website, URL: https://www.emotiv.com/, 2017.

[115] Laboratory of Miguel A.L. Nicolelis [Online]. Available: http://www.nicolelislab.net/?p=584, 2017

[116] W. Li, C. Jaramillo, and Y. Li, "Development of mind control system for humanoid robot through a brain computer interface," in Intelligent System Design and Engineering Application (ISDEA), 2012 Second International Conference on, 2012, pp. 679-682.

[117] Graz Brain-Computer Interface Lab [Online]. Available: https://www.tugraz.at/institute/ine/home/, 2017

[118] Puzzlebox Orbit [Online]. Available: https://puzzlebox.io/orbit/, 2017

[119] D. P. Subha, P. K. Joseph, R. Acharya, and C. M. Lim, "EEG signal analysis: a survey," Journal of medical systems, vol. 34, pp. 195-212, 2010.

[120] M. J. Bryan, S. A. Martin, W. Cheung, and R. P. Rao, "Probabilistic co-adaptive brain–computer interfacing," Journal of neural engineering, vol. 10, p. 066008, 2013.

[121] M. Plöchl, J. P. Ossandón, and P. König, "Combining EEG and eye tracking: identification, characterization, and correction of eye movement artifacts in electroencephalographic data," Frontiers in human neuroscience, vol. 6, p. 278, 2012.

[122] S. Meyberg, M. Werkle-Bergner, W. Sommer, and O. Dimigen, "Microsaccade-related brain potentials signal the focus of visuospatial attention," NeuroImage, vol. 104, pp. 79-88, 2015.

[123] P. Comon and C. Jutten, “Handbook of Blind Source Separation: Independent component analysis and applications,” Academic press, 2010.

[124] C. Bishop, “Pattern Recognition and Machine Learning (1st ed.),” New York, New York: Springer, 2006.

[125] E. Parvinnia, M. Sabeti, M. Z. Jahromi, and R. Boostani, "Classification of EEG Signals using adaptive weighted distance nearest neighbor algorithm," Journal of King Saud University-Computer and Information Sciences, vol. 26, pp. 1-6, 2014.

[126] C.-W. Hsu and C.-J. Lin, "A comparison of methods for multiclass support vector machines," IEEE transactions on Neural Networks, vol. 13, pp. 415-425, 2002.

[127] OpenBCI website, URL: http://openbci.com/, 2017.

[128] Hyvärinen, A., & Oja, E., “Independent component analysis: Algorithms and applications,” Neural Networks, 13(4-5), 2000, pp. 411-430.

[129] T. G. Dietterich, "Machine learning for sequential data: A review," in Joint IAPR International Workshops on Statistical Techniques in Pattern Recognition (SPR) and Structural and Syntactic Pattern Recognition (SSPR), 2002, pp. 15-30.

[130] Lab Streaming Layer [Online]. Available: https://github.com/sccn/labstreaminglayer, 2017.

[131] World Health Organization, “Depression and other common mental disorders: global health estimates,” No. WHO/MSD/MER/2017.2. World Health Organization, 2017.

[132] Mayo Clinic [Online]. Available: https://www.mayoclinic.org/, 2019.

[133] L. Zou, A. Yeung, C. Li, G.-X. Wei, K. Chen, P. Kinser, J. Chan, and Z. Ren, “Effects of meditative movements on major depressive disorder: A systematic review and meta-analysis of randomized controlled trials,” Journal of Clinical Medicine, vol. 7, no. 8, p. 195, 2018.

[134] G. Thornicroft, S. Chatterji, S. Evans-Lacko, M. Gruber, N. Sampson, S. Aguilar Gaxiola, A. Al-Hamzawi, J. Alonso, L. Andrade, G. Borges and R. Bruffaerts, “Undertreatment of people with major depressive disorder in 21 countries,” The British Journal of Psychiatry, 210(2), pp.119-124, 2017.

[135] A. Montagu, “Touching: The human significance of the skin,” Harper & Row, 1978.

[136] V. Marx and E. Nagy, “Fetal behavioral responses to the touch of the mother’s abdomen: A Frame-by-frame analysis,” Infant Behavior and Development, vol. 47, pp. 83–91, 2017.

[137] D. M. Stack, “The salience of touch and physical contact during infancy: Unraveling some of the mysteries of the somesthetic sense,” Blackwell Handbook of Infant Development, pp. 351–378.

[138] T. Field, “Touch for socioemotional and physical well-being: A review,” Developmental Review, vol. 30, no. 4, pp. 367–383, 2010.

[139] A. Montagu and F. W. Matson, “The human connection,” McGraw-Hill, 1979.

[140] F. Mcglone, J. Wessberg, and H. Olausson, “Discriminative and affective touch: Sensing and feeling,” Neuron, vol. 82, no. 4, pp. 737– 755, 2014.

[141] V. E. Abraira and D. D. Ginty, “The sensory neurons of touch,” Neuron, vol. 79, no. 4, pp. 618–639, 2013.

[142] H. Olausson, J. Cole, K. Rylander, F. Mcglone, Y. Lamarre, B. G. Wallin, H. Krämer, J. Wessberg, M. Elam, M. C. Bushnell, and Å. Vallbo, “Functional role of unmyelinated tactile afferents in human hairy skin: sympathetic response and perceptual localization,” Experimental Brain Research, vol. 184, no. 1, pp. 135–140, 2007.

[143] H. Olausson, J. Wessberg, I. Morrison, F. Mcglone, and Å. Vallbo, “The neurophysiology of unmyelinated tactile afferents,” Neuroscience & Biobehavioral Reviews, vol. 34, no. 2, pp. 185–191, 2010.

[144] R. Ackerley, H. B. Wasling, J. Liljencrantz, H. Olausson, R. D. Johnson, and J. Wessberg, “Human C-Tactile afferents are tuned to the temperature of a skin-stroking caress,” Journal of Neuroscience, vol. 34, no. 8, pp. 2879–2883, 2014.

[145] L. S. Löken, J. Wessberg, I. Morrison, F. Mcglone, and H. Olausson, “Coding of pleasant touch by unmyelinated afferents in humans,” Nature Neuroscience, vol. 12, no. 5, pp. 547–548, 2009.

[146] R. Picard, E. Vyzas, and J. Healey, “Toward machine emotional intelligence: analysis of affective physiological state,” IEEE Transactions on Pattern Analysis and Machine Intelligence, vol. 23, no. 10, pp. 1175–1191, 2001.

[147] R. Cowie, E. Douglas-Cowie, N. Tsapatsoulis, G. Votsis, S. Kollias, W. Fellenz, and J. Taylor, “Emotion recognition in human-computer interaction,” IEEE Signal Processing Magazine, vol. 18, no. 1, pp. 32–80, 2001.

[148] J. Kim and E. Andre, “Emotion-specific dichotomous classification and feature-level fusion of multichannel biosignals for automatic emotion recognition,” 2008 IEEE International Conference on Multisensor Fusion and Integration for Intelligent Systems, 2008.

[149] H. Lee, A. J. Shackman, D. C. Jackson, and R. J. Davidson, “Test-retest reliability of voluntary emotion regulation,” Psychophysiology, vol. 46, no. 4, pp. 874–879, 2009.

[150] I. C. Christie and B. H. Friedman, “Autonomic specificity of discrete emotion and dimensions of affective space: a multivariate approach,” International Journal of Psychophysiology, vol. 51, no. 2, pp. 143–153, 2004.

[151] G. Chanel, C. Rebetez, M. Bétrancourt, and T. Pun, “Emotion assessment from physiological signals for adaptation of game difficulty,” IEEE Transactions on Systems, Man, and Cybernetics - Part A: Systems and Humans, vol. 41, no. 6, pp. 1052–1063, 2011.

[152] O. Alzoubi, S. K. Dmello, and R. A. Calvo, “Detecting naturalistic expressions of nonbasic affect using physiological signals,” IEEE Transactions on Affective Computing, vol. 3, no. 3, pp. 298–310, 2012.

[153] L. Brown, B. Grundlehner, and J. Penders, “Towards wireless emotional valence detection from EEG,” 2011 Annual International Conference of the IEEE Engineering in Medicine and Biology Society, 2011.

[154] R. J. Davidson, “Affective neuroscience and psychophysiology: Toward a synthesis,” Psychophysiology, vol. 40, no. 5, pp. 655–665, 2003.

[155] Z. Yin and J. Zhang, “Identification of temporal variations in mental workload using locally-linear-embedding-based EEG feature reduction and support-vector-machine-based clustering and classification techniques,” Computer Methods and Programs in Biomedicine, vol. 115, no. 3, pp. 119–134, 2014.

[156] J. Russell, “A circumplex model of affect.” Journal of personality and social psychology, vol. 39, no. 6, p. 1161, 1980.

[157] G. Chanel, J. J. Kierkels, M. Soleymani, and T. Pun, “Short-term emotion assessment in a recall paradigm,” International Journal of Human-Computer Studies, vol. 67, no. 8, pp. 607–627, 2009.

[158] M. Balconi and G. Mazza, “Brain oscillations and BIS/BAS (behavioral inhibition/activation system) effects on processing masked emotional cues: ERS/ERD and coherence measures of alpha band,” International Journal of Psychophysiology, 2009.

[159] Y. Liu, O. Sourina, and M. K. Nguyen, “Real-Time EEG-based emotion recognition and its applications,” Lecture Notes in Computer Science Transactions on Computational Science XII, pp. 256–277, 2011.

[160] N. Jatupaiboon, S. Pan-Ngum, and P. Israsena, “Emotion classification using minimal EEG channels and frequency bands,” The 2013 10th International Joint Conference on Computer Science and Software Engineering (JCSSE), 2013.

[161] D. Huang, C. Guan, K. K. Ang, H. Zhang, and Y. Pan, “Asymmetric spatial pattern for EEG-based emotion detection,” The 2012 International Joint Conference on Neural Networks (IJCNN), 2012.

[162] M. Li and B.-L. Lu, “Emotion classification based on gamma-band EEG,” 2009 Annual International Conference of the IEEE Engineering in Medicine and Biology Society, 2009.

[163] K. S. Park, H. Choi, K. J. Lee, J. Y. Lee, K. O. An and E. J. Kim, “Emotion recognition based on the asymmetric left and right activation,” International Journal of Medicine and Medical Sciences, pp. 201–209, 2011.

[164] H. Singh, M. Bauer, W. Chowanski, Y. Sui, D. Atkinson, S. Baurley, M. Fry, J. Evans, and N. Bianchi-Berthouze, “The brain’s response to pleasant touch: an EEG investigation of tactile caressing,” Frontiers in Human Neuroscience, vol. 8, 2014.

[165] Y.-W. Park, S. Hwang, and T.-J. Nam, “Poke: Emotional touch delivery through an inflatable surface over interpersonal mobile communications,” Proceedings of the 24th annual ACM symposium adjunct on User interface software and technology - UIST 11 Adjunct, 2011.

[166] L. He, C. Xu, D. Xu and R. Brill, “PneuHaptic: Delivering haptic cues with a pneumatic armband,” In: Proceedings of the 2015 ACM International Symposium on Wearable Computers. pp. 47–48. ACM, New York, NY, USA, 2015.

[167] T. Kaaresoja, J. Linjama, “Perception of short tactile pulses generated by a vibration motor in a mobile phone,” In First Joint Eurohaptics Conference and Symposium on Haptic Interfaces for Virtual Environment and Teleoperator Systems, World Haptics Conference, pp. 471–472, 2005.

[168] C. Y. Zheng, “Affective touch with soft robotic actuators - A design toolkit for personalised affective communication,” in Workshop: Reshaping Touch Communication: An Interdisciplinary Research Agenda, ACM CHI Conference on Human Factors in Computing Systems, Montreal, 2018.